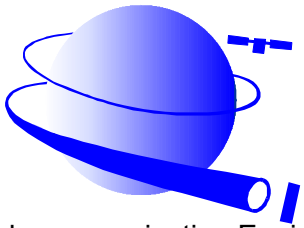

Telecommunication Engineering

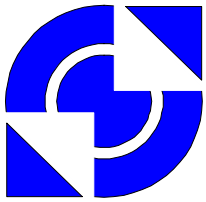

University of Twente

University of Twente
Faculty of Electrical Engineering
Chair for Telecommunication Engineering

# EMC STUDY OF AN AUTOMOTIVE APPLICATION

by

Dongsheng Zhao

Master thesis
Executed from August 2003 to April 2004

Supervisor: prof. dr. ir. F.B.J. Leferink, University of Twente
J. van Duijn, NEDAP
Advisor: prof. dr. ir. W.C. van Etten, University of Twente

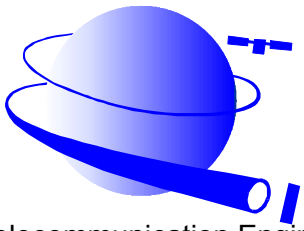

Telecommunication Engineering

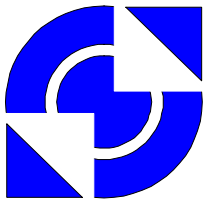

University of Twente

University of Twente
Faculty of Electrical Engineering
Chair for Telecommunication Engineering

# EMC STUDY OF AN AUTOMOTIVE APPLICATION

Dongsheng Zhao
Voortsweg 30
7523 CH, Enschede
Tel: 053-4362292
Email: d.zhao@student.utwente.nl
zds89@hotmail.com

# Summary

Electromagnetic compatibility (EMC) has become an important area of electrical engineering in automotive industry. Testing standards and regulations imposed by governments and other agencies have forced companies to pay close attention to the electromagnetic properties of their products.

Nedap Specials Automotive has developed and produced Sunroof Control Units (SCU) for more than 10 years. The SCU is assembled to build a sunroof system with a low-cost DC (Direct Current) motor and a sunroof structure, which are purchased from other suppliers. EMC is one of the most important concerns in the designing of SCU, because automotive products meet tighter EMC regulation, especially in the limitation for transient noise. On the other hand, with the adopting of Pulse Width Modulation (PWM) in a new product, additional electromagnetic interference (EMI) is gained, which even causes the EMI level of this product to go beyond the standard.

To reach electromagnetic compatibility it is important to consider EMC in an early stage of design. That is, try to prevent a noise from occurring by optimizing crucial designable parameters.

In this report, models of switch, relay, cable, motor and SCU are firstly developed in PSPICE so that the potential noise sources can be pointed out. Some models are validated by experiments. Our experience and the analysis and experiments described in this report show that the EMI is unwanted oscillatory current or voltage noise sources originated by transient. The transient may be opening and closure of switch, bouncing of relay, switching of MOSFET or commutation of motor, etc., and potential noise sources produced by transient will conduct and radiate interference to surrounding. Radiation models are constructed to find correlation between noise source and radiated emission. One model used in predicting radiated emission in low frequency has been presented and the condition for use is described.

Experiences from former designs show that many designable parameters can determine how severely a transient causes EMI. Base on these validated models, the evaluation of designable parameters becomes feasibly. Unfortunately, changing some parameters makes benefit and disadvantage simultaneously in suppressing EMI which generated by different causes. Therefore, a compromise has to be found, and some configuration parameters that do not significantly affect EMI behavior can be discarded. Synthesis is done at last to get optimized configuration for designable parameters.

# Contents

# Chapter 1

# Introduction

In this chapter, the background of this master assignment is described, preceded with an introduction of Electromagnetic compatibility (EMC) concept and requirements. After that, this chapter presents objectives and approaches of the research as well as the structure of this thesis.

## 1.1 Project background

The accelerating growth in the needs for a perfect driving experience leads to an ever-increasing demand for professionals in automotive manufacturing. Future vehicle electronic systems will provide many more functions to aid the driver. For this purpose, more electrical devices are installed at a concentrated area in the vehicle. The increased working ability of these equipments increases strength and frequency range of noise emission as well.

Nedap Specials Automotive has been involved in developing and producing Sunroof Control Units (SCU) for more than 10 years. The SCU is assembled to build a sunroof system with a low-cost DC (Direct Current) motor and a sunroof structure. In the past sunroof systems, SCU, motor and sunroof structure were considered to be separate units and developed more or less separately by the three parties involved (Nedap, motor supplier and sunroof builder).

In one application a Pulse Width Modulation (PWM) based motor speed controller was built. The adoption of PWM technique brings additional Electromagnetic Interference (EMI), which made the development of this kind of unit very difficult, both in reducing development time and reduction of component costs.

In the second place, all kinds of products meet tighter restriction of popping noise for the reputation of the automotive manufacturers and the satisfaction of their customers. Transient noise occurs when a switching event happens. They are undesirable as they couple to other devices and make malfunction or audible noises.

An updated study of system EMI issues should be made to achieve a successful handling of these problems. We need a systematic solution to treat three parts together. A standard guideline document for component manufacture, system design, and device installation should be provided to make EMI controllable or predictable.

This report is a master thesis on the subject "EMC Study of an automotive application" and is written by the order of the University of Twente, Telecommunication Engineering group (TEL). This group is part of the faculty of Electrical Engineering, Mathematics & Computer Science (EEMCS).
Most of the research was carried out at NEDAP in Groenlo. NEDAP is an abbreviation of "N.V. Nederlandsche Apparatenfabriek". Although established in 1929, this company has a young spirit of innovative and creative corporate culture focusing on added value for customers. Main areas involved are security system, management info system, election system and electronic devices. This research was carried out at the specials division.

## 1.2 EMC concept

Electromagnetic Interference (EMI) noise is defined as an unwanted electrical signal that produces undesirable effects in a system. In modern vehicles, for instance, EMI will cause the popping noise heard in radio, malfunction of controller which even can lead to hazardous accidents. The term EMC refers to an electronics system that is able to function compatible with other electronic systems and does not produce or is not susceptible to interference.
If a system is EMC, three criteria should be satisfied:

- It does not cause interference with other systems.
- It is not susceptible to emission from other systems.
- It does not cause interference with itself.

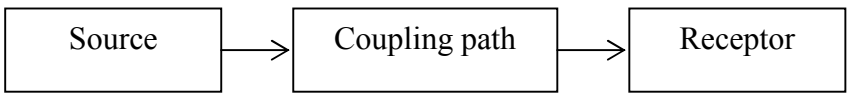


**Figure 1-1: Three elements in EMI scenarios**

Summarized, aspects of EMC are concerned with the generation, transmission and reception of electromagnetic energy. Figure 1-1 illustrates three elements of an EMC problem: source produces the emission, and a coupling path provides emission energy transferred from source to receptor, and so unwanted electromagnetic energy is converted into some undesired behavior. By breaking the coupling paths into two classes, we get two subgroups of EMC problems: radiated and conducted.
From the point of receptor and emitter, EMC issues can be catalogued to Electromagnetic Emission (EME) and Electromagnetic Susceptibility (EMS). We will focus how to reduce emission in this research.
Three ways should be applied to reduce radiated and conducted interference:

- Suppress the emission at the source.
- Make the coupling path as ineffective as possible.
- Make the receptor immune to the emission.

## 1.3 EMC requirements

In automotive industry, there are several EMC requirements imposed on electronic products installed in a vehicle. Requirements are mandatory by governmental agencies. These regulations are compulsory legal requirements, which mean equipment under regulation cannot be sold without compliance with these EMC regulations.
In automotive industry, most of EMC concerned rules and regulations are listed at the Table 1-1. Some of them are worldwide and some of them are regional.

**Table 1-1: International and regional standards used in automotive industry**

| Body | Standard | Content |
|---|---|---|
| IEC | CISPR-12 | Vehicles, motorboats and spark-ignited engine-driven devices — Radio disturbance characteristics — Limits and methods of measurement |
| IEC | CISPR-25 | Radio disturbance characteristics for the protection of receivers used on board vehicles, boats, and on devices — Limits and methods of measurement |
| SAE | SAE-J551 | Electromagnetic Compatibility Measurement Procedures and Limits for Vehicles and devices |
| SAE | SAE-J1113 | Electromagnetic Compatibility Measurement Procedures and Limits for Vehicle Components. |
| ISO | ISO 7637 | Electrical disturbance by conduction and coupling |
| ISO | ISO 10605 | Road vehicles — Test methods for electrical disturbances from electrostatic discharge |
| EU | 95/54/EC | Automotive EMC Directive |
| JASO | JASO 7637 | Automotive Electromagnetic Susceptibility Requirement |
| ISO | ISO 11451 | Electrical disturbances by narrow-band radiated electromagnetic energy—Vehicle test methods |
| ISO | ISO 11452 | Electrical disturbances by narrow-band radiated electromagnetic energy—Component test methods |

Some more requirements are imposed by product manufacturers themselves for customer satisfaction. It is also called automotive Original Equipment Maker (OEM) standards. These standards are not easily accessible because they are classified. They are imposed for the purpose of insuring a reliable, quantity product. These stricter regulations are used to obtain a good reputation from the standpoint of quality control of its product. Almost each automotive manufacturer has his own additional regulation.
In NEDAP, a test handbook summarized from variant standards is used for validation test. Configurations, specifications, and procedures are abstracted so that the test items and criteria are fixed during the test. The reason is that some regulations give several options for the same measurement items, and some organizations give regulations on

the same issue. Because configuration will take effect as a result, a relative firm setup is needed.

## 1.4 Objectives and expected results

The topic of this investigation is to study the generation mechanism, mitigation techniques of EMI in sunroof system. We know from Section 1.2, in order to suppress radiated and conducted interference, we have 3 choices. The first 2 choices is what we can do in source side, that is:

- Suppress the emission at the source.
- Make the coupling path as ineffective as possible.

In the final analysis, transient is the root of noise sources. This time, we consider the three parts of sunroof system as a whole, because from former design experiences we know that the manner to assemble three parts affects EMC performance of the whole system. Therefore, we have at least the following designable parameters:

- Wiring configuration, includes grounding plan, connection interface, etc.
- Components value, includes the components in SCU and motor.
- Circuit topology, includes the circuit inside SCU and motor.
- Shield plan

These designable parameters determine how severely a transient contributes to noise source, and it also determines how efficiently a noise source contributes to EMI.
We illustrate their relationship in Figure 1-2.

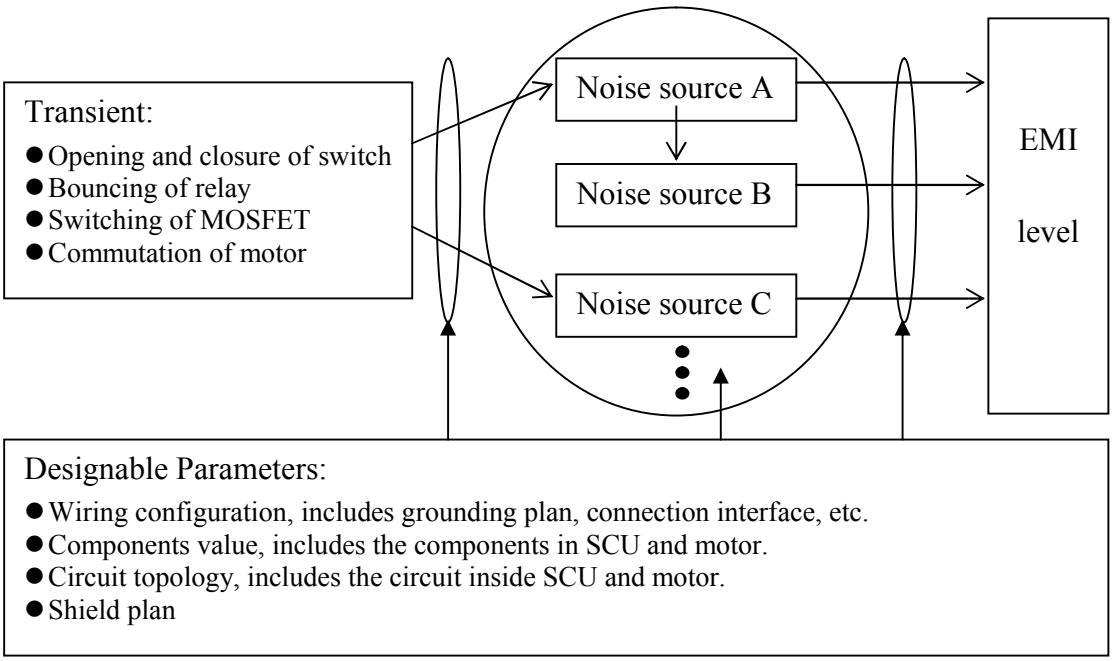


**Figure 1-2: Designable Parameters determine EMI level**

Designable parameters affect the generation of noise source from transient. Here, transient may be opening and closure of switch, bouncing of relay, switching of

MOSFET or commutation of motor, etc. It brings a variation in circuit connection. It leads to variations in voltage and current. This transient can be periodic or aperiodic. we call the noise produced by periodic transient as running noise, and produced by aperiodic transient as transient noise.

We also classify noise source into 3 sorts. Noise source A represents a Differential Mode (DM) noise source, which is also called normal mode noise or functional noise. Noise source B represents a Common Mode (CM) noise which is converted from a DM noise, and the conversion efficiency is determined by designable parameters. Noise source C represents another type of CM noise, which is excited directly by transient. We also call it DCM (Common Mode noise in Differential format) noise, if we want to distinct it from CM noise.

In [5], a number of paths are summarized in the coupling of noise from a source to surrounding. They include:

- Common wiring
- Capacitance between devices
- Mutual inductance between devices
- Radiation via air link

The efficiencies of these paths can also be changed with designable parameters. Therefore, the assignment can be summarized as "Get a optimized configuration of crucial designable parameters which can be used in future design. This configuration should be realistic and cost-efficiently, and the results should include quantified values".

To approach objective, these questions should be answered during the research:

- Where are these noise sources located?
- What are their mechanisms?
- How much these noise sources contribute to EMI?
- Which noise sources are predominant in a particular situation?
- How to suppress or predict them?

At last, the research should result in a standard guideline document for component manufacture, SCU design, and device installation, with instructions to achieve a controllable and predictable EMI emission.

## 1.5 Methodology

Firstly, several models are built in PSPICE. We use the method called "back-annotation". That is to say, we keep on evolving the models until the simulation results get satisfying match with measurement results. Since these models are sufficiently validated, we can easily locate potential noise sources and find mechanisms of these noises. We can use models to evaluate the influence of designable parameters.

Besides validation measurement for model, many comparison measurements are performed to provide evidence for our hypothesis of noise source.

Synthesis is applied at last to find a compromise between conflictive configurations. We take the realization values and cost factor into account to make a decision.
With these methods, furthermore, the EMC performance of SCU can be partly determined before the construction of the first prototype.

## 1.6 Organization of this report

This report is organized as follows.
It starts with some brief introduction about this project and EMC knowledge. The chapter 2 will give a description of the sunroof system which is used as prototype in our research.
In Chapter 3, some general models especially radiated emission, which will be useful in later chapters, is introduced. In the next 4 chapters, investigations of four transients, which cause noise, are presented respectively.
Next, Chapter 8 will give a presentation of all comparison measurements. Short explanations are given to validate our conclusions drawn by models. Synthesis is done base on models and measurement results to unveil the dominant noise source.
Following the conclusion of this thesis in chapter 9, two tables list the radiated emission measurement result with different wiring configurations and potential noise sources, they are included in Appendix A and Appendix B respectively.

# Chapter 2

# Vehicle sunroof system

In this chapter, we will give some introduction about the structure of a sunroof firstly. After that, we provide some background information on how the roof system is working. Finally, we give a brief introduction to the main issue we will encounter.

## 2.1 Structure of sunroof system

The vehicle sunroof system normally consists of three main parts. That is, the sunroof structure, SCU and the motor. In most situations, they are purchased from separate suppliers, and the SCU designer is responsible for designing most effective SCU to opening, closing the glass panel and meeting the requirements of sunroof system vendor. Roof systems exist in many shapes for different cars. The most popular type is the tilt vent slide sunroof. The glass panel has two opening modes, lift-up and sliding mode; the former one provides extra ventilation in the rain without getting wet, and the sliding mode will give the largest direct access to the open air.
A typical sunroof system is shown in Figure 2-1.


**Figure 2-1: A typical sunroof system**

The SCU and the motor are firmly installed in the sunroof structure. The gear in the motor axis drives two driving cables via cogs to convert rotation into linear movement of the glass panel. The sunroof structure is fixed in the car body for safety reason.

SCU, motor and sunroof are assembled with the car body. The battery negative pole is connected to car body, but electric connection between motor housing and car body is not determined. It is an important EMC factor, and can be designed in such a manner to achieve lowest EMI level.

A switch is installed for comfortable operation. Switch cable connects the switch to SCU and battery positive pole. Motor is connected to SCU via motor cable. In most products, the motor cable use unshielded two-wires cable. SCU is also powered by unshielded two-wires cable, which is named as battery-SCU cable in the coming discussion. A diagram of electric connection in a sunroof system is shown at Figure 2-2. The range of cable length is also labeled.

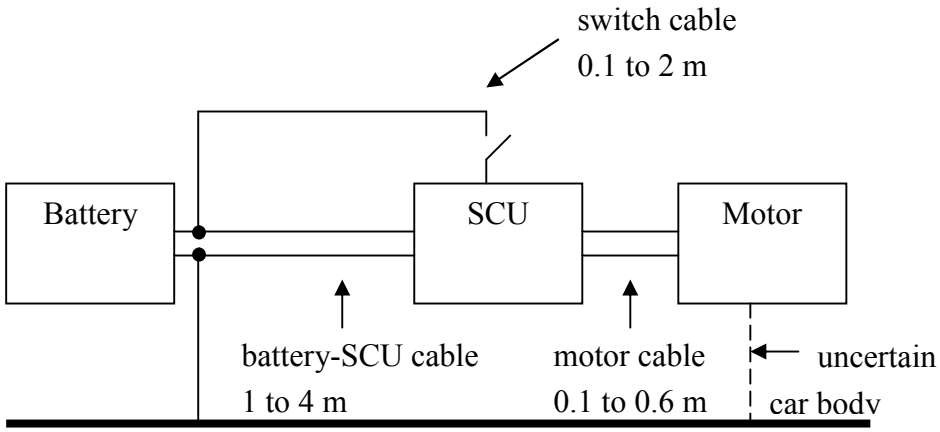


**Figure 2-2: Electrical connection of a typical sunroof system**

## 2.2 Operation

To operate sunroof, two modes are available. The first mode is by switch. There are three positions in the switch, two sliding positions represent slide open and close, the pushing position means stop. Resistors with different values are shunted with the switch to identify three positions. The second mode is by Controller Area Network (CAN). A CAN bus is connected to SCU to transfer information from the central controller. The roof will be closed automatically for safety when the engine stops, here the “close it” command is directly sent by CAN bus.

When the switch slides to open or close position, SCU detects this and drives a FET to operate relay. The relay is connected to drive DC motors as an H-bridge circuit. It is called H-bridge because it looks like the capital letter “H” on classic schematics. The great advantage of an H-bridge circuit is that the motor can be driven forward or backward. Most kinds of SCU drive motors in this way. When relay is operated or released, the motor is connected or disconnected to power immediately. We call this event fast start or fast stop. This kind of SCU is called traditional SCU in coming discussions.

In recent years, a new SCU product utilizes PWM to control a power MOSFET placed in series in the main loop of the motor to get a variable speed control. By changing the

duty cycle smoothly from 0% to 100% and from 100% to 0%, the motor can be started and stopped softly. We call this procedure soft start and soft stop with PWM. Whereas there is only one product belongs to this type of structure, PWM will be used wider in the future. We call such SCU as PWM SCU.

A small magnetic ring is fixed around the axis of the motor, which is illustrated in Figure 5-2. With the running of motor, the magnetic field polarity produced by this ring is varying. With a Hall sensor IC in SCU, the rotation of motor axis is counted. After calibrating in the factory, the SCU remembers the fully opened and fully closed position. By this method, SCU will softly stop the motor when the glass panel is fully opened and closed.

Because the sunroof system works with the "one-touch close" feature, the demand for Anti-Pinch Protection (APP) has become one of necessity rather than choice. In certain countries, integration of APP technology into production vehicles is imposed by law. A sensor to measure working current is placed in the main loop of SCU, the voltage dropped in that resistor is monitored continuously to detect pinch event. If a pinch occurs, the motor will be stopped immediately. This procedure is also fast stop event.

## 2.3 Main EMC issues

According to the response from the roof system vendor and what we met during designing and testing, we have the following main EMC issues.

- When we push the switch on, a popping noise occurs.
- When with the motor running in always-on mode, noise will occur because of the commutation noise.
- In a fast stop event of PWM SCU, or in a fast start or fast stop event of traditional SCU, a popping noise is heard in the AM radio.
- When motor is running in PWM mode, and duty cycle is varying between 0% and 100%, EMI is excessive in some frequency bands. It happens in a soft start or soft stop event.

We will analyse the above issues in our study to see which factors are mostly related to these issues, and in which way they can be solved effectively.

# Chapter 3

# General models

In this chapter we will review models which are related to the remainder parts of this report. Cable model is summarized firstly. It can be simplified with the condition of "electrical short". After that, the method to calculate Per-Unit-Length (PUL) parameters of cable is given. Then signal spectra are given for some typical waveforms we will meet in future. At last, radiation model is established which is needed to evaluate contribution of noise source to EMI.

## 3.1 Cable model

Cables are used in a sunroof system to connect SCU to the motor as well as SCU to power supplier. They are closely spaced and parallel to each other. If we ignore the higher-order modes and assume that TEM mode is only a propagation mode on the line, we can divide the cable into the cascade of small sections of the line, and each section can be replaced with a lumped-circuit model which is related to per-unit-length parameters.

Figure 3-1 shows how one line segment with the length $\Delta z$ is approximated with an electric circuit.

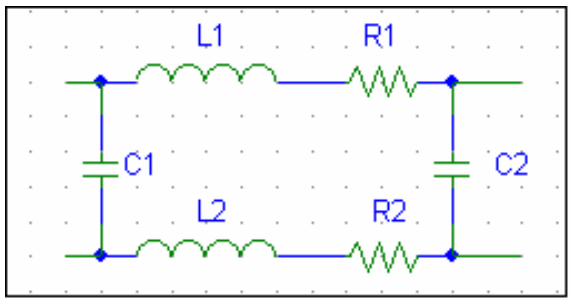


**Figure 3-1: The equivalent circuit of one line segment of two-conductor line**

Here, $R_1$ and $R_2$ represent the resistances in both conductors, $L_1$ and $L_2$ are the inductances in both conductors, and $C_1$ and $C_2$ are the capacitances between the conductors. The conductance of the dielectric media is ignored here.

The reason why we break parameters into two conductors is that the cable normally consists of two balance wires and without shield.
This approximation can be used to predict differential mode signal, which is dominant below 2 MHz.
In high frequency range, CM current becomes dominant, and the influence of reference must be taken into consideration. Because connection wires are fixed adjacently to the car body in most cases, it causes the parasitic parameter to take effect at high frequency. The equivalent circuit evolves like Figure 3-2 shows.

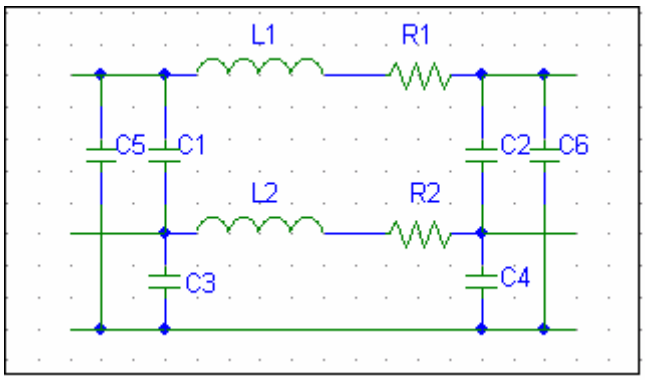


**Figure 3-2: Motor cable representation**

Here, $C_3$ and $C_4$ are added to represent the capacitances between one conductor and the reference, and $C_5$ and $C_6$ are the capacitances between another conductor and reference. The inductance of the reference is ignored here. The mutual inductance between two conductors is also not considered, because the main issue is how DM current between two conductors introduces CM current in reference.
If the wavelength of the highest frequency component from signal source is much longer than the largest dimension of transmission line, we say that the line is "electrically short". In such a situation, the current distribution is nearly uniform on the line. The cable can be replaced with one segment of electric circuit, which is an adequate representation for frequencies up to a few megahertz.

## 3.2 Per-Unit-Length (PUL) parameters of cable

In sunroof system, battery-SCU cable and motor cable are unshielded non-twisted wire pair for price factor. The formula of PUL parameter can be found in [3].

### 3.2.1 Resistance

For solid copper slab, resistance is given by:

$$R = \frac{l}{\sigma \times S}[\Omega] \tag{3.1}$$

Where, $\sigma = 5.8\times10^7$ S/m equals the conductivity of copper.
$S$ is the area of cross section of slab, unit in $m^2$
$l$ is the length of the slab, unit in m

Due to the phenomena of skin effect, the current will crowd closer to the outer periphery in high frequency. The skin depth is defined by,

$$\delta = \frac{1}{\sqrt{\pi f \mu_0 \sigma}} [\text{m}] \tag{3.2}$$

Therefore, the unit length resistance of wire will change with frequency, which follows this equation,

$$R = \begin{cases} \dfrac{l}{\sigma \pi r_w^{\,2}} [\Omega] & \text{for } r_w << \delta \\ \dfrac{l}{2 r_w} \sqrt{\dfrac{\mu_0 f}{\pi \sigma}} [\Omega] & \text{for } r_w >> \delta \end{cases} \tag{3.3}$$

For a typical cable used in SCU, with a wire gauge of AWG18 (AWG means American Wire Gauge), it is a stranded wire composed of 19 strands of solid wires of radii 0.127mm, which can be approximated to compute external inductance and capacitance by replacing it with a solid wire of diameter 1.02mm.

Figure 3-3 shows the wire resistance versus frequency of a sample motor cable.

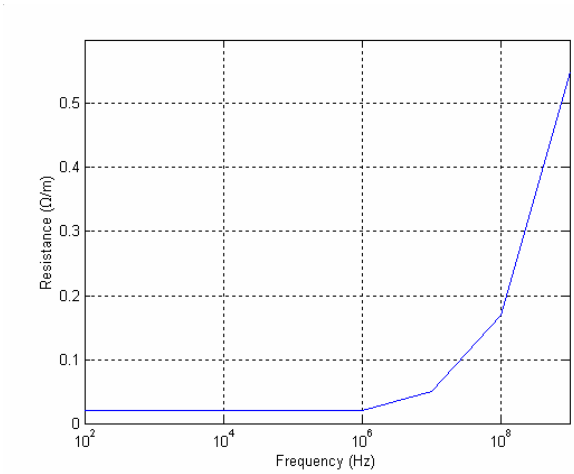


**Figure 3-3: A sample motor cable resistance versus frequency**

## 3.2.2 Inductance

The wire inductance plays a crucial role in determining the specification of circuit in high frequency [3]. Figure 3-4 shows two wires where one wire carries power current and the other wire carries power return current.

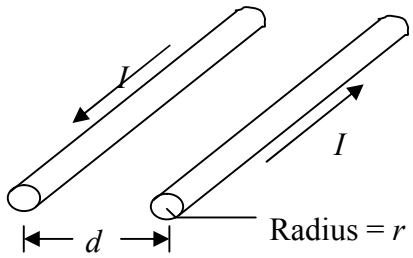


**Figure 3-4: Inductance between two parallel wires**

Equation 3.4 gives the self-inductance in two cables with the same radius,

$$L = l \times 4 \times 10^{-7} \times \ln\left(\frac{d}{r}\right)[\mathrm{H}] \tag{3.4}$$

Also with the cable of AWG18 we assume the separate distance of two cables is 2 cm and the length is 1 m. Its inductance is 1.47μH.

Because the cables are normally laid on a surface of the car body, we should consider the influence of the ground plane.

In Figure 3-5, a wire is put over a ground plane at height *h*. The wire carries power current and the plane carries power return current.

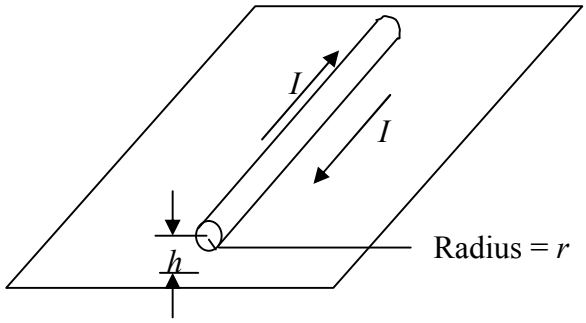


**Figure 3-5: Inductance between wire and metal plane**

Equation 3.5 gives the self-inductance for a wire over a ground plane.

$$L = l \times 2 \times 10^{-7} \times \ln\left(\frac{2h}{r}\right)[\mathrm{H}] \tag{3.5}$$

Because of the proximity effect, the frequency affects the self-inductance as well. Figure 3-6 shows the inductance measurement result of a sample motor cable versus frequency.

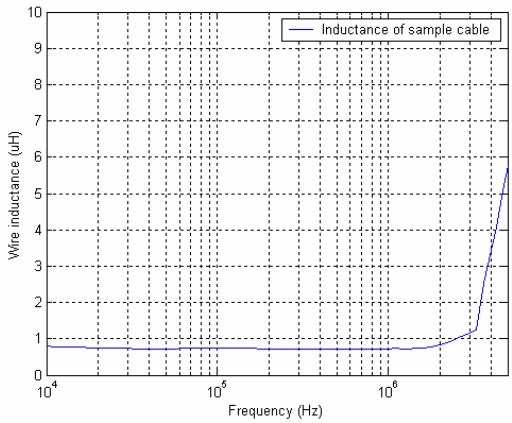


**Figure 3-6: Wire inductance of a sample cable versus frequency**

The above figure shows that a wire inductance can be estimated as 1μH/m below 1MHz, and 6μH/m in 5MHz.

We did an additional inductance measurement for a wire when it is passing through a current probe. It makes the wire inductance increase about 1.5 times. A ratio versus frequency is shown at Figure 3-7.

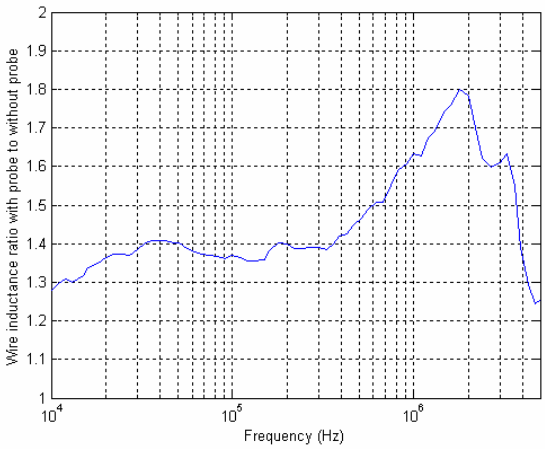


**Figure 3-7: The Ratio of wire inductance with a current probe to without a probe**

These two experiments explain why there exists a deviation between prediction and measurement result, the influence of measurement equipment and high frequency effect should be taken into account.

### 3.2.3 Capacitance

Capacitance is another important PUL parameter. In high frequency, parasitic capacitance may become a resonance path leading to oscillation.
Equation 3.6 gives the capacitance in two cables with the same radius,

$$C = l \times \frac{2.778 \times 10^{-11}}{\ln\left(\frac{d}{r}\right)} [\mathrm{F}] \tag{3.6}$$

Also with the cable of AWG18 we assume that the separate distance of two cables is 2 cm and cable length is 1 m. The capacitance between them is 7.5pF.
Equation 3.7 gives the capacitance between a wire and a ground plane.

$$C = l \times \frac{5.556 \times 10^{-11}}{\ln\left(\frac{2h}{r}\right)} [\mathrm{F}] \tag{3.7}$$

With the cable of AWG18 we assume that the separate distance between cable and ground plane is 5 cm and length is 1 m. The capacitance between them is about 10.5pF.

## 3.3 Signal spectra

Spectra of some common periodic signal we will meet in this project are listed below.

The PWM signal is a periodic trapezoidal wave as Figure 3-8 shows.

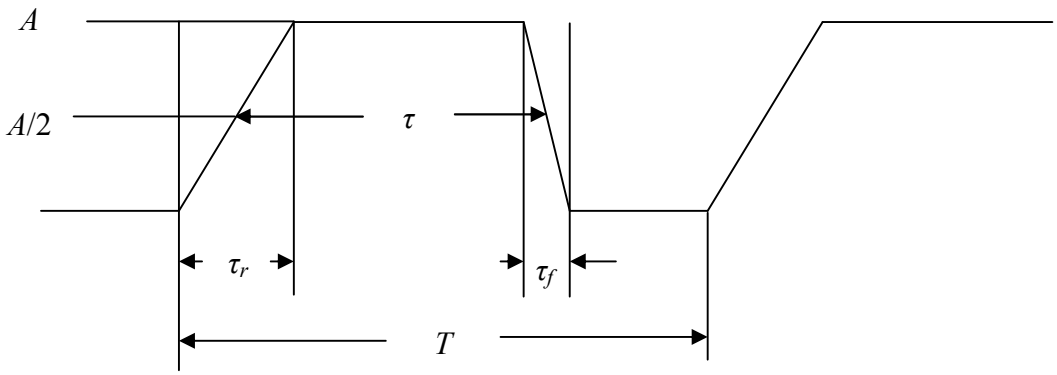


**Figure 3-8: One element of a periodic trapezoidal waveform**

Here, $\tau_r$ represents the rise time, $\tau_f$ is fall time, $T$ is the period of this waveform, $\tau$ is the time that amplitude above one-half of the maximum amplitude. Another important parameter is duty cycle defined as $\tau/T$.

As a result of complex-exponential Fourier series obtained in [3], two asymptotes can be used to outline the bounds for the magnitude spectrum of this periodic signal.

$$M = \begin{cases} 20\log_{10}(\frac{2A\tau}{T}) & when \quad f < f_1 \\ 20\log_{10}(\frac{2A\tau}{T}) - 20\log 10(\frac{f}{f_1}) & when \quad f_1 < f < f_2 \\ 20\log_{10}(\frac{2A\tau}{T}) - 20\log 10(\frac{f_2}{f_1}) - 40\log 10(\frac{f}{f_2}) & when \quad f > f_2 \end{cases} \tag{3.8}$$

Figure 3-9 shows two asymptotes of signal spectrum for a trapezoidal wave.

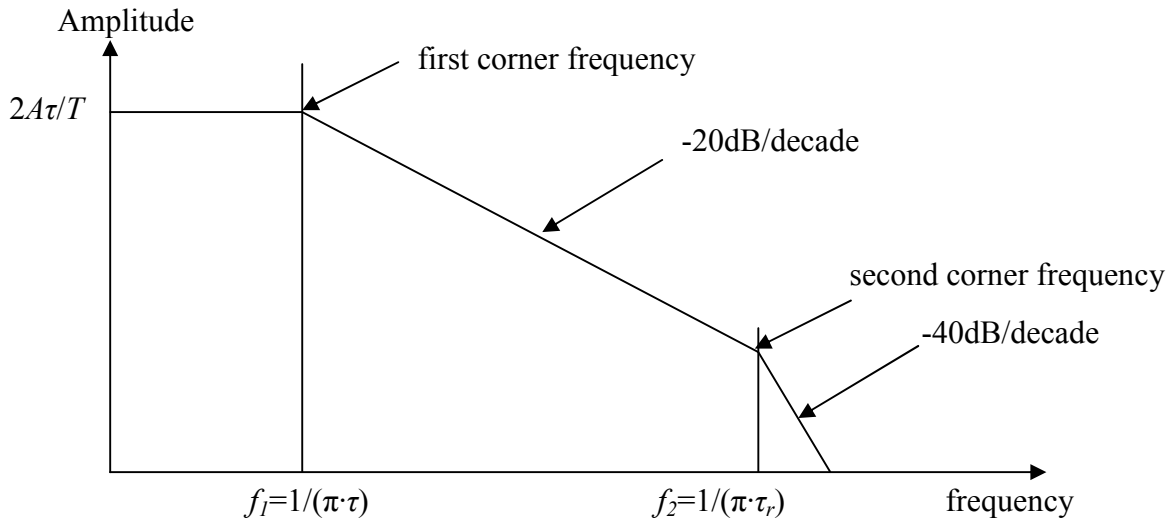


**Figure 3-9: Asymptotes for Spectrum of trapezoidal waveform**

By changing some designable parameters, we know the effects of these parameters.

- By decreasing rise and fall time, the second corner frequency will move to a low frequency with the same duty cycle.

- The first corner frequency will move to low frequency by reducing the repetition rate with the same duty cycle.
- Reducing the duty cycle decreases the low-frequency spectral content of waveform, but it does not have any effects on high frequency.

Another special waveform we discussed here is the triangular waveform, which is very common in switch current ripple. A typical triangular wave is shown in Figure 3-10.

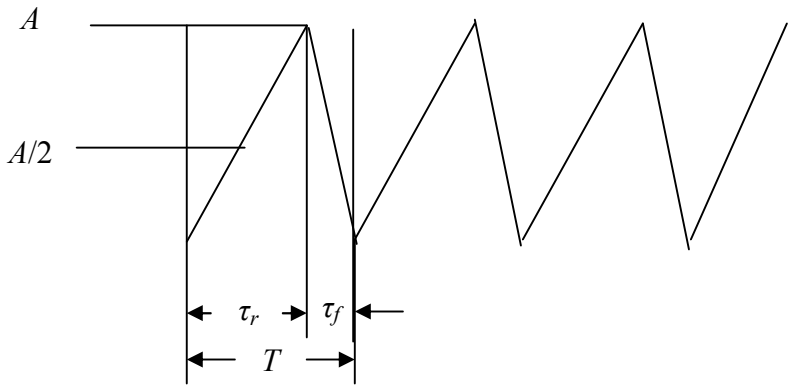


**Figure 3-10: One element of a periodic triangular waveform**

A triangular waveform can be regarded as a special case of trapezoidal wave, where the duty cycle is 50%. According to the effects of parameters we discussed before, the duty cycle does not have essential influence at high frequency, and the crucial parameter is still the rise time and fall time, which determines the second corner frequency.

The last special waveform occurs mostly in a current of flywheel diode. The rise time of front edge is extremely short, normally 100ns. The fall edge follows an exponential curve.

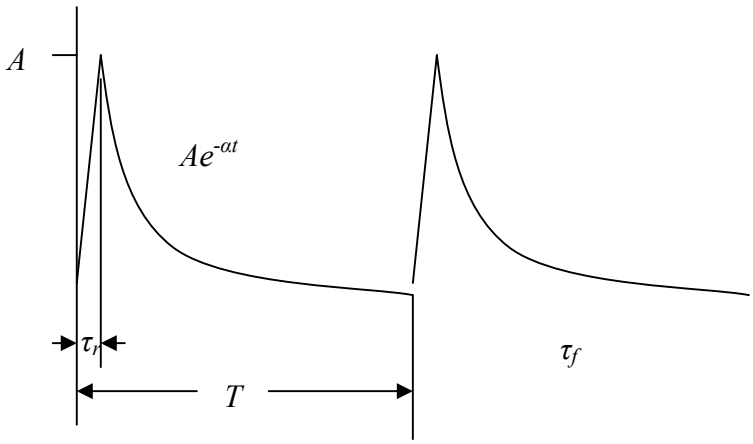


**Figure 3-11: One element of a periodic waveform**

For Fourier series, we have the expansion coefficient as

$$C_n = \frac{A}{\alpha T + j2\pi n}\left(1 - e^{-\alpha T}\right) \tag{3.9}$$

When $\tau_r << T$

## 3.4 Radiated emission model

In next 4 chapters, this report will deal with the topic of noise source produced by transient. However, base on PSPICE model, we only get the result of conducted emissions. In the field of EMC, radiated emission is also very important. This section discusses radiated emission and models which will be used in coming chapters.
By multiplying the calibration factor, we can arrive at the predictions of the radiated emissions via prediction result under far-field assumption, although this is just an approximation.

### 3.4.1 Radiated emissions requirement

Radiated emissions are the electric and magnetic fields radiated by one device that may be received by other devices. Although radiated emissions include both electric and magnetic fields, regulatory agencies only require that electric fields be measured for certification. According to the standards [22], [23] and [24] of automotive industry, the concerned frequency range starts from 150kHz to 1GHz. A radiated emission limit is shown in Table 3-1.

**Table 3-1 Requirement for radiated emission**

| Frequency range (MHz) | Allowed disturbance level (dBµV) | |
|---|---|---|
| | Narrow Band | Broad Band |
| | Peak | Peak |
| 0.15 – 0.45 | No requirements *) | No requirements*) |
| 0.45 – 2 | 20 | No requirements*) |
| 2 – 30 | 20 | No requirements*) |
| 30 – 400 | 10 | 25 |
| 400 – 1000 | 22 – 32 | 40 – 50 |

According to the experiences of former design, there is no problem found beyond 30MHz for narrow band noise. Therefore, we put our focus on 450kHz to 30MHz and set 20dBµV/m as baseline for narrowband noise. The toughest band for broadband noise is 30MHz to 400MHz, with a limitation of 25dBµV/m.

### 3.4.2 The near field and far field

Field region is divided into near field and far field. The boundary depends on the frequency and physical distance to source. In a physical viewpoint, the wavefront propagates cylindrically in near field and propagates spherically in far field. In near field, reactive energy is dominant to radiating energy [2].
These regions are conventionally divided at a radius $R$ given by

$$R = \frac{\lambda}{2\pi} \tag{3.10}$$

Within radius $R$, it is the near field, while beyond it lies the far field.

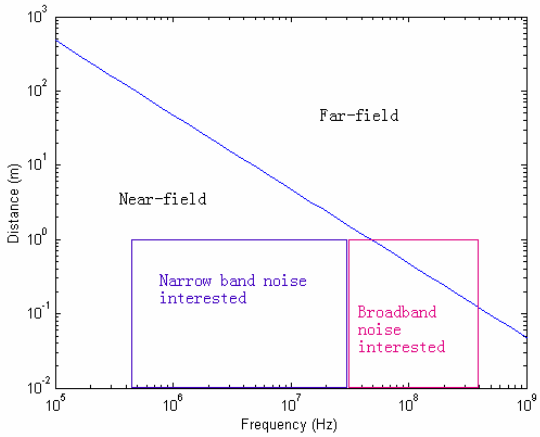


**Figure 3-7: The predominant contribution of near-field and far-field component**

Figure 3-7 shows that the boundary between the near-field region and far-field region is relevant to frequency.

For this project, antenna is placed 1 m away from DUT (Device Under Test) in radiation emission measurement. We draw blocks to indicate our interesting frequency ranges in Figure 3-7. It is clearly pointed out that all the narrow band noise and main part of broadband noise from DUT are in the near-field radiation mode.

### 3.4.3 Radiated emissions model

To build up a practical antenna model, two simplest models, namely the short wire and the small loop, are considered firstly.

For an elemental electric dipole, the field intensity vector is [27],

$$E_\theta = \frac{\hat{I}dl}{4\pi}\eta_0\beta_0 \sin\theta\left(j\frac{1}{r}+\frac{1}{\beta_0 r^2}-j\frac{1}{\beta_0{}^2 r^3}\right) \tag{3.11}$$

$$E_r = \frac{\hat{I}dl}{4\pi}\eta_0 \cos\theta\left(\frac{2}{r^2}-j\frac{2}{\beta_0 r^3}\right) \tag{3.12}$$

$$H_\phi = \frac{\hat{I}dl}{4\pi}\eta_0\beta_0 \sin\theta\left(\frac{j}{r}-j\frac{j}{\beta_0 r^2}\right) \tag{3.13}$$

Here, $\beta_0=2\pi/\lambda$, $\theta$ is the zenith angle to radial distance $r$, and the length of the short wire $dl << \lambda$.

For an elemental magnetic dipole, the field intensity vector is [27],

$$H_\theta = \frac{j\hat{I}dS}{4\pi}\beta_0{}^2 \sin\theta\left(j\frac{1}{r}+\frac{1}{\beta_0 r^2}-j\frac{1}{\beta_0{}^2 r^3}\right) \tag{3.14}$$

$$H_r = \frac{j\hat{I}dS}{4\pi}\beta_0 \cos\theta\left(\frac{2}{r^2}-j\frac{2}{\beta_0 r^3}\right) \tag{3.15}$$

$$E_\phi = \frac{j\hat{I}dS}{4\pi}\beta_0{}^2 \sin\theta\left(\frac{j}{r}-j\frac{j}{\beta_0 r^2}\right) \tag{3.16}$$

By assuming that the current at all points along the wire is the same, the maximum magnitude of radiated emission due to differential-mode currents is [3]:

$$E_{DM} = 20\log_{10}\left(1.316\times10^{-8}\times\frac{A\times f_n^{\,2}\times I_n}{r}\right)\ [\text{dB}\mu\text{V/m}] \qquad (3.17)$$

Here, $A$ = the area of loop, in $m^2$.
$f_n$ = spectral signal frequency, in Hz.
$I_n$ = spectral signal current, in A.
$r$ = distance from victim to source, in m.
This formula is only valid under the condition of far field because the second and third terms in Equation 3.11 can be ignored.
To predict the maximum electric field in the near field, which is true in low frequency, a factor should be used:

$$Factor = \sqrt{\left(\frac{\lambda}{2\pi r}\right)^2 + \left(\left(\frac{\lambda}{2\pi r}\right)^2 - 1\right)^2} \qquad (3.18)$$

By the same assumption, the maximum radiated emission due to common-mode currents is:

$$E_{CM} = 20\log_{10}\left(1.257\times\frac{L\times f_n\times I_n}{r}\right)\ [\text{dB}\mu\text{V/m}] \qquad (3.19)$$

Here, $L$ = the length of wire, in m.
$f_n$ = spectral signal frequency, in Hz.
$I_n$ = spectral signal current, in A.
$r$ = distance from victim to source, in m.

# Chapter 4

# Switch

Switch is a basic but important device [1]. They are widely distributed in most electronic equipment as well as in SCU systems. A push-slide-button switch is used to operate SCU.

The switch is the first object we will study, because it is a source of abrupt current or voltage change. We need to know how to model switches without loss of their main characteristics.

In this chapter, firstly, we look at an ideal switch. After that we will take into account more non-ideal effects. By "back-annotation" method, we get a satisfying model. At last, some suggestions to avoid transient noise caused by switch are given.

## 4.1 Ideal switches

A model of an ideal switch is obtained by assuming:

- The transient time for the switch opening or closing is as short as possible.
- The transients of opening and closing are solid and without bouncing.
- When the switch is closed, the contact resistance is null.
- The parasitic inductance in the lead of the switch can be ignored.

Figure 4-1 shows a simplified equivalent circuit of SCU. Here switches are used to simulate the scenario of the closing and opening event of a relay, and the motor is represented by $R_1$ and $L_1$.

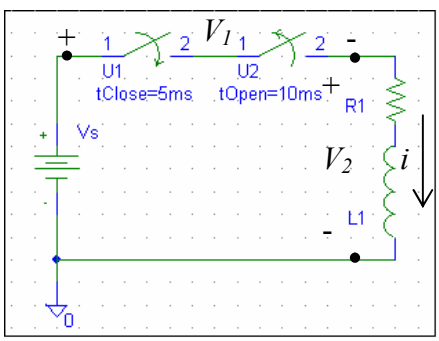


**Figure 4-1: An ideal switch model**

Applying Kirchhoff's Voltage Law (KVL) and Kirchhoff's Current Law (KCL) to Figure 4-1, we get this equation,

$$V_s = V_1 + L_1 \frac{di}{dt} + R_1 i \tag{4.1}$$

Here, $V_1$ is the voltage between two terminals of the switch, and $i$ is the current flowing along the loop. When switch $U_1$ is closing, the current will exponentially rise up to $V_s/R_1$ with a time constant of $L_1/R_1$. In another transient, when the switch is opened with the assumption that transient time is zero, the loop current $i$ abruptly changes to 0. At that moment, voltage over inductance $L_1(\mathrm{d}i/\mathrm{d}t)$ is infinitely large, and voltage $V_1$ over the switch is also infinitely large to make Equation 4.1 balance. No component in real life can sustain infinite voltage, so it must be a different case for real circuit.

## 4.2 Real switch modeling

In a real circuit, stray capacitance between two terminators of load needs to be considered. Figure 4-2 shows the improved model.

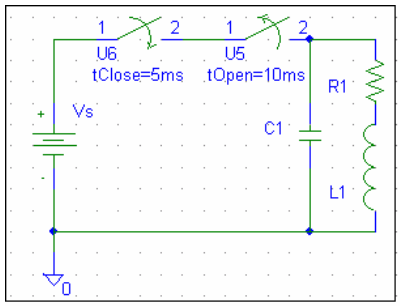


**Figure 4-2: Improved model of switch (1)**

By adding this capacitor, the energy stored in coils will not create infinite voltage when a switch is opened, but charge capacitor $C_1$. This energy will transfer back and forth between capacitor $C_1$ and inductor $L_1$ after peak voltage, and consumed by $R_1$. This oscillation is damped and decreased to zero in the end.

By solving a two-order differential equation, we know that the frequency of this oscillation is

$$f_1 = \frac{1}{2\pi\sqrt{L_1 C_1}} \tag{4.2}$$

The maximum voltage between load terminals is

$$V_{2\max} = -i_0\sqrt{\frac{L_1}{C_1}} \tag{4.3}$$

Here $i_0$ is the current just before the switch opens and the minus sign is due to Back electromotive force (EMF) of inductance.

The above circuit seems perfect, but when we look through the source side of this circuit, the inductance of the power supply cable cannot be ignored. The same problem arises when a switch is opened, energy stored in the wire inductance needs a way out;

otherwise there is an infinite voltage generated in the wire. Then, the model evolves as figure 4-3 shows.

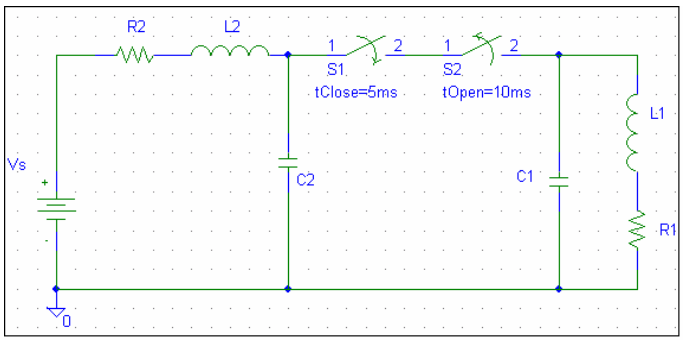


**Figure 4-3: Improved model of switch (2)**

As a matter of fact, it is consistent with the method to model a cable via transmission theory. When the cable is electrically short, that is

$$l << \frac{\lambda}{2\pi} \tag{4.4}$$

the cable can be replaced by lumped circuit components.

Let us consider what will happen in a switch closing and opening.

When the switch is closed, *Vs* charges $C_1$ through $R_2$, $L_2$, $C_2$, the current is built up to a peak very rapidly and then decays to the ultimate DC current. In most situations, this decay is accompanying an oscillation with a frequency approximately

$$f_2 = \frac{1}{2\pi\sqrt{L_2 C_1}} \tag{4.5}$$

The opening transient of switch $S_1$ involves two oscillations that occur at the source side and the load side of this circuit. One oscillation is produced at the load side, which we have discussed before. The other oscillation comes with loop of $R_2$, $C_2$, $L_2$, and its frequency is

$$f_3 = \frac{1}{2\pi\sqrt{L_2 C_2}} \tag{4.6}$$

Since $R_2$, $C_2$, $L_2$ is much smaller than $R_1$, $L_1$ and $C_1$, and thus ring frequency $f_3$ at the source side is much higher than frequency $f_1$ produced at the load side.

We know that the wire inductance and stray capacitance must be considered from the above analysis. In an extreme situation, when both the stray capacitance and wire inductance are very small, a very high frequency resonance predicted by the above formula does not appear in measurement result. The reason is that some more factors are dominant in forming an oscillation.

By computer simulations, we know that oscillation will be generated only if the switch time is short enough. We define the following parameter,

$$P_1 = \frac{\tau}{2\pi\sqrt{LC}} \tag{4.7}$$

It is a ratio of switch transient time to the period of an assumed oscillation. By applying variable parameter in simulation, we got the following results.
Figure 4-4 shows the waveform of oscillation when $P_1$=1.

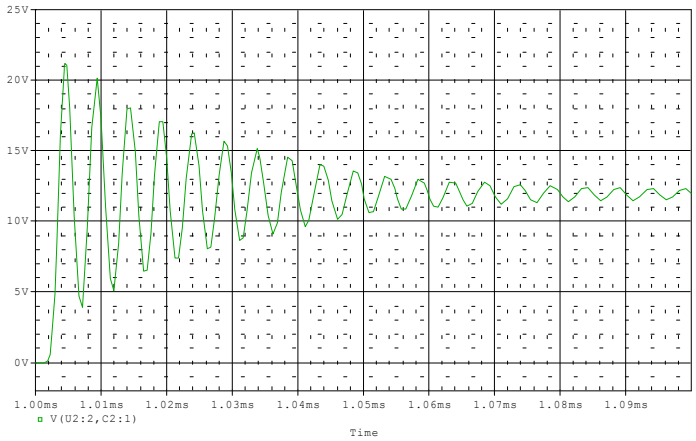


**Figure 4-4: The waveform of oscillation when $P_1$=1**

Figure 4-5 shows the waveform of oscillation when $P_1$=10.

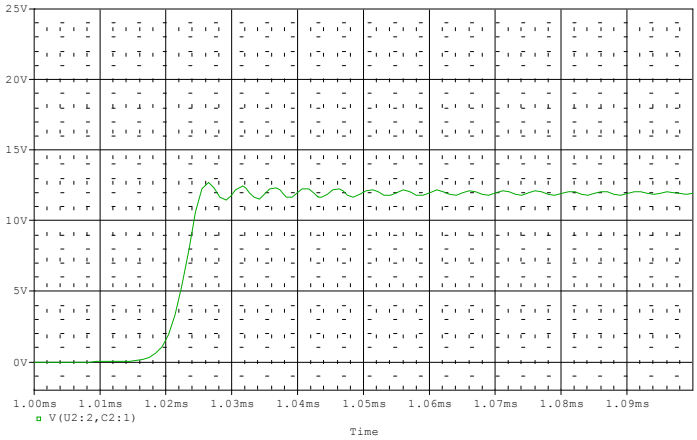


**Figure 4-5: The waveform of oscillation when $P_1$=10**

When the following condition is satisfied, oscillation will become a smooth transient in RLC loop.

$$P_1 > 25 \tag{4.8}$$

That is a criterion to avoid an oscillation. We must select $P_1$ to be above 25. This transient waveform can be seen in Figure 4-6.

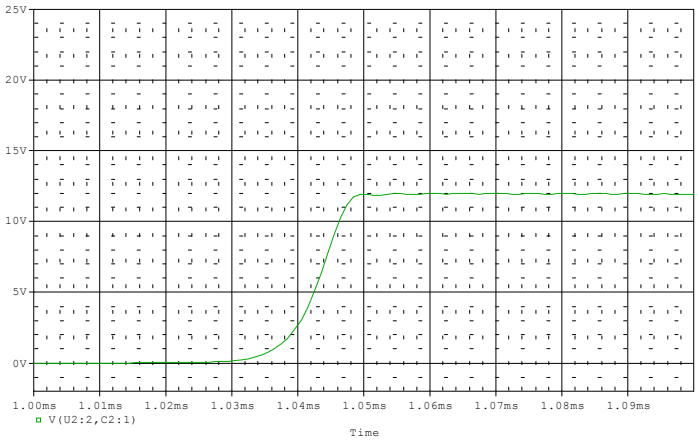


**Figure 4-6: The waveform of oscillation when $P_1$=25**

The impedance will determine the decay time for oscillation. The oscillation will attenuate rapidly if the resistance is large enough. Figure 4-7 shows a comparison between two configurations when $R_2$=0.5 Ω and $R_2$=5Ω.

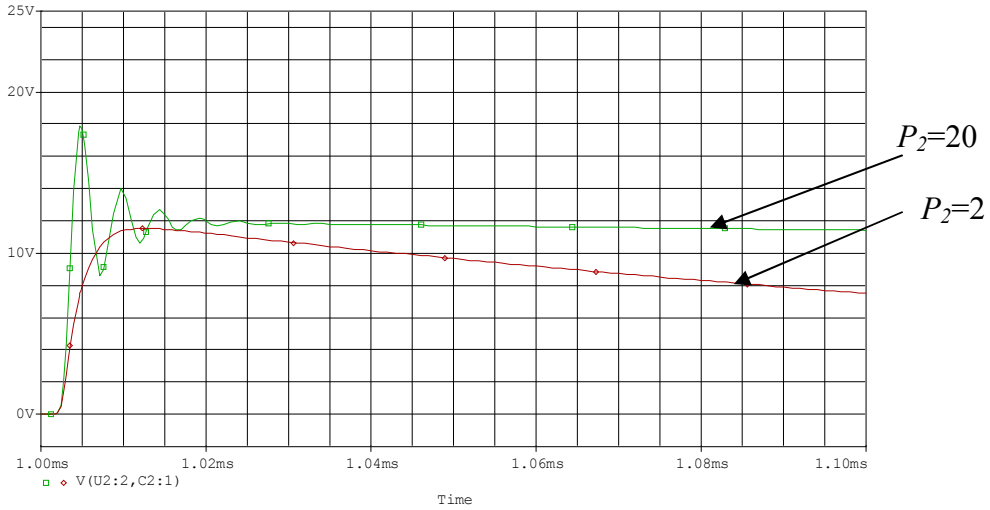


**Figure 4-7: Comparison of the waveform of oscillation when $P_2$=20 and 2**

Similar criterion can be achieved by simulation. We define $P_2$ as

$$P_2 = \frac{\tau}{RC} \tag{4.9}$$

$P_2$ must be selected below 2 to avoid an oscillation.

Sudden current change is also a factor to determine amplitude of oscillation. Figure 4-8 shows the comparison between different current variations.

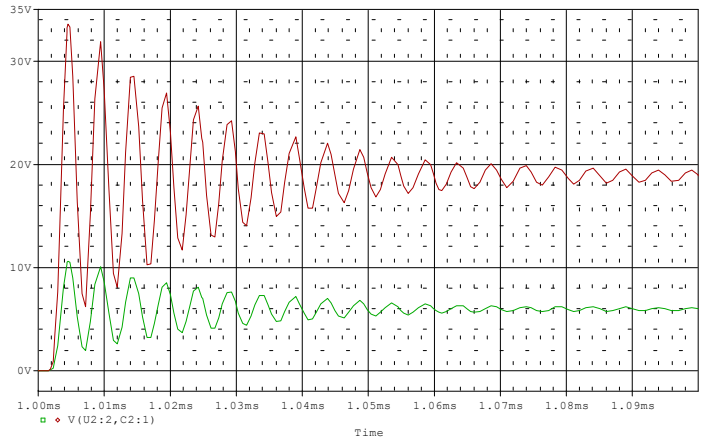


**Figure 4-8: Comparison of the waveform of oscillation with different current variation**

As a conclusion, oscillation can be blocked by the following procedure.

- Increasing the switch transient time.
- Adding enough attenuation to damp oscillation.
- Reducing the sudden current variation by selecting a good topology.

## 4.3 Evaluations

We set up an experiment for verification. It is done with a real Printed Circuit Board (PCB) board. A LISN is inserted to make impedance stable, and a relay driver is controlled by switch. We only consider the voltage ripple introduced by a switch. The mechanical characteristic makes the rotor inside the motor start rotating 7-8 ms after the relay is closed. Therefore, the influence of the motor can be ignored at the switch transient time. The input resistance of relay driver is replaced with a resistor.
The setup of the experiment is shown as Figure 4-9 below.

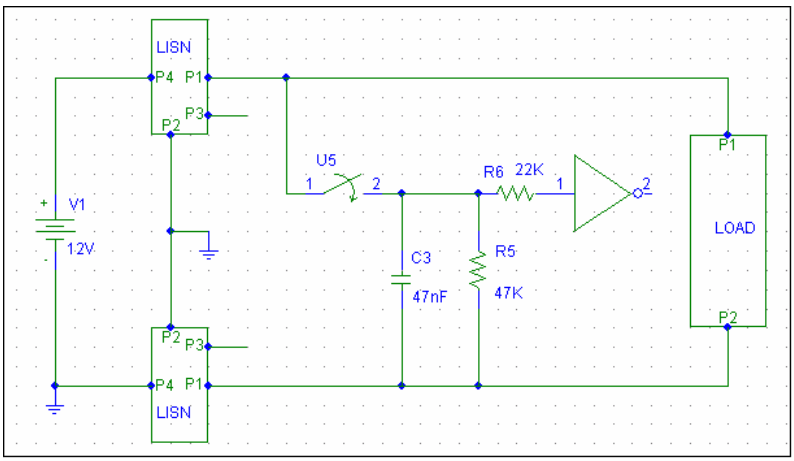


**Figure 4-9: Experiment setup to verify switch model**

The schematic circuit diagram of the simulation is given at Figure 4-10 below.

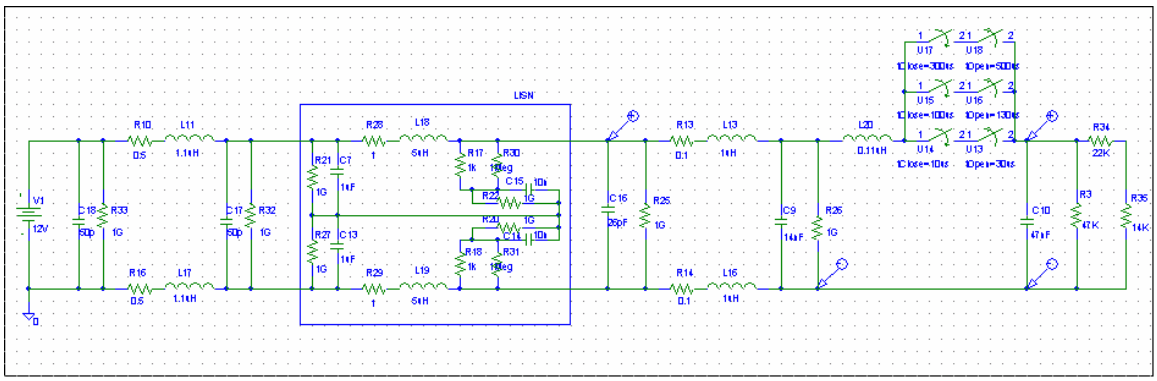


**Figure 4-10: Simulation diagram for a switch model**

We model bouncing with three ideal switches. The attach impedance and switch time are set in switch parameters. We also consider the wire inductance and stray capacitance, and model them as lumped circuit components.

Transient happens when the switch is closed. At that time, capacitor $C_{10}$ and inductance $L_{11}$, $L_{18}$, $L_{13}$, $L_{20}$, $L_{16}$, $L_{19}$, $L_{17}$ forms a RLC series circuit. The resonance frequency is approximately

$$f_L = \frac{1}{2\pi\sqrt{L_x C_{10}}} \tag{4.10}$$

Here, $L_x$ is the sum of $L_{11}$, $L_{18}$, $L_{13}$, $L_{20}$, $L_{16}$, $L_{19}$ and $L_{17}$.

An important note has to be mentioned here, this resonance frequency is shifted to low frequency in measurement, because the inductance of LISN is inserted.

Another loop is found in $L_{20}$, $C_9$, and $C_{10}$. Because $L_{20}$ is far smaller than $L_{18}$ or $L_{19}$, this ring frequency is much higher than the first one, and it is represented as one ring frequency overlapping another one. The high frequency component could be a main source of interference in radio frequency although with less amplitude. The resonance frequency is determined by

$$f_H = \frac{1}{2\pi\sqrt{L_y C_y}} \tag{4.11}$$

Here, $L_y$ is the wire inductance from the switch to SCU PCB.

$C_y$ represents the equivalent capacitance of $C_9$ series with $C_{10}$.

If the stray capacitance of the cable from switch to SCU is taken into account, another resonance frequency arises,

$$f_S = \frac{1}{2\pi\sqrt{L_y C_{cable}}} \tag{4.12}$$

Here, $L_y$ is the wire inductance from the switch to SCU PCB.

$C_{cable}$ represents the stray capacitance of the cable from switch to SCU.

The simulation results and measure results are shown below. In simulation result, bias is added to one trace to separate two traces.

Two voltage differences are observed, the first one is a voltage drop between switches, and another one is a DM voltage in LISN.

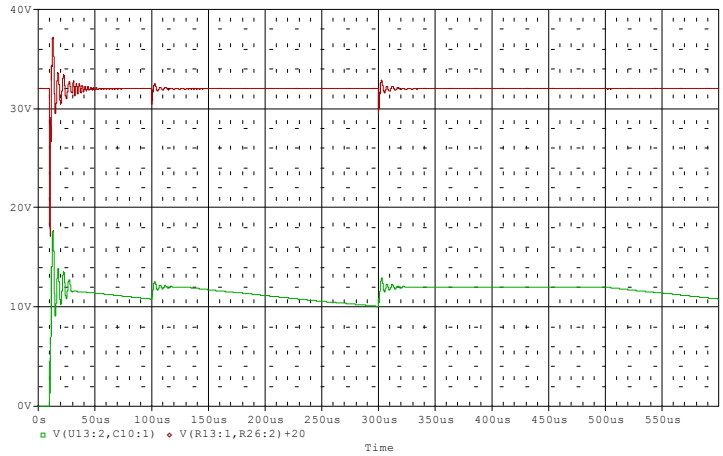


**Figure 4-11: Switch model verification simulation result (100μs/div)**

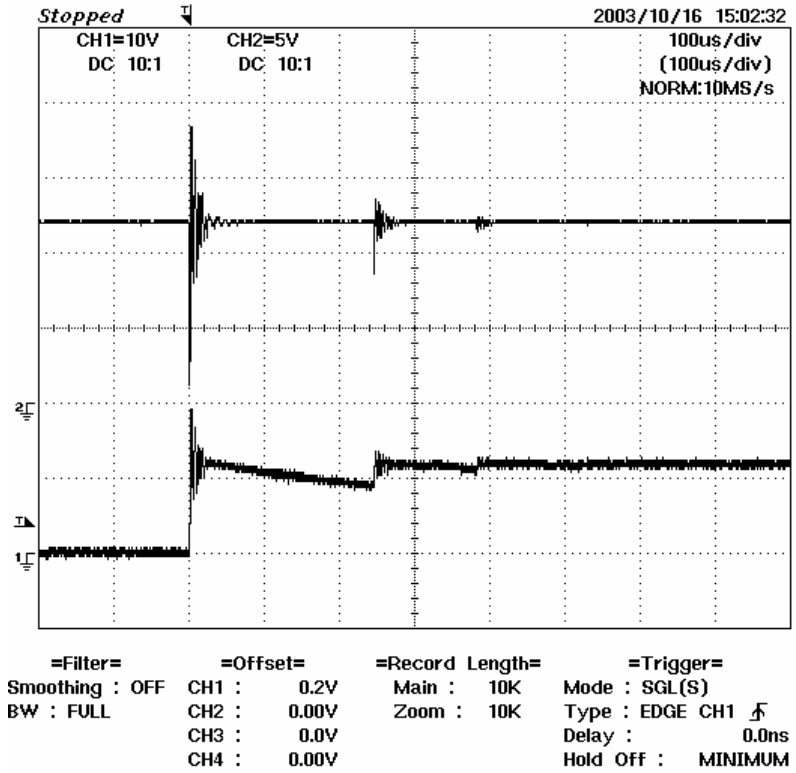


**Figure 4-12: Switch model verification measurement result (100μs/div)**

Via experiments, we know that a switch produces 3-5 bounces mostly, and it comes stable after 500μs. The contact time in a prior bounce event is quite short. The selection of $C_{10}$ should satisfied this equation,

$$C_{10} > \frac{5\times10^{-4}}{R_C} \tag{4.13}$$

Here $R_C$ represents the equivalent resistance parallel to $C_{10}$. Otherwise the relay driver will produce a flip-flop signal to the microprocessor.

If this signal is pre-processed via software filtering in a microprocessor, we can remove the restriction (4.13). Therefore, $C_{10}$ is only represented by parasitic capacitance, and two resonant modes will disappear because the criterion (4.8) is satisfied.

By expanding the time scale, we get more details.

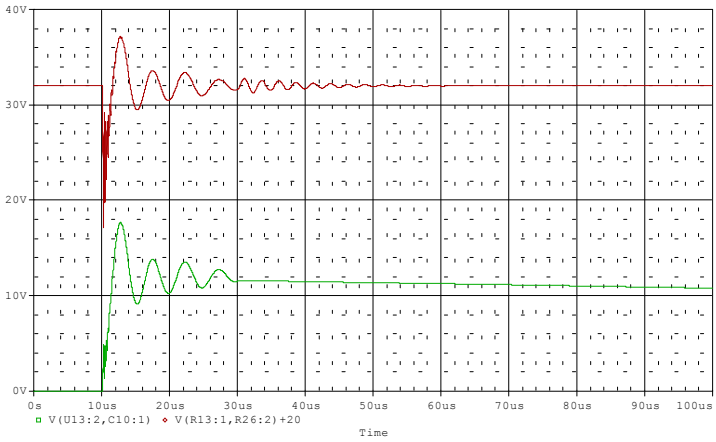


**Figure 4-13: Switch model verification simulation result (10µs/div)**

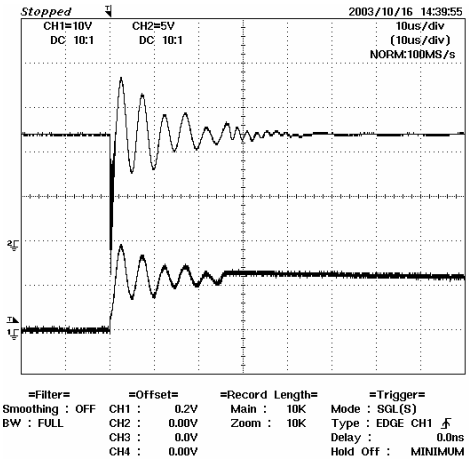


**Figure 4-14: Switch model verification measurement result (10µs/div)**

We found the frequency components $f_L$ in above plot. The shape and frequency are quite similar between simulation and measurement. Let us expand the time scale further.

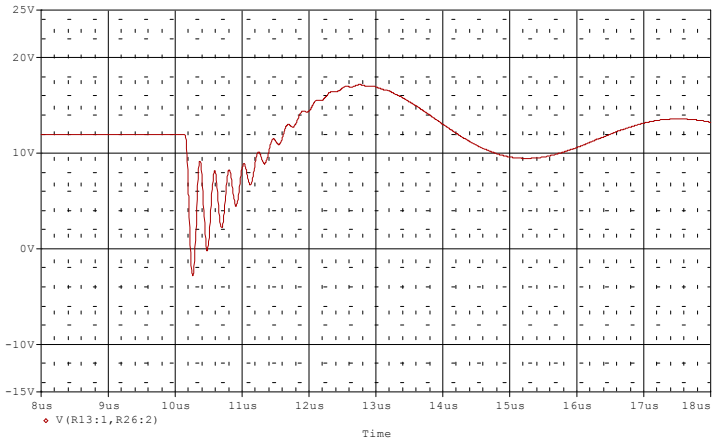


**Figure 4-15: Switch model verification simulation result (1µs/div)**

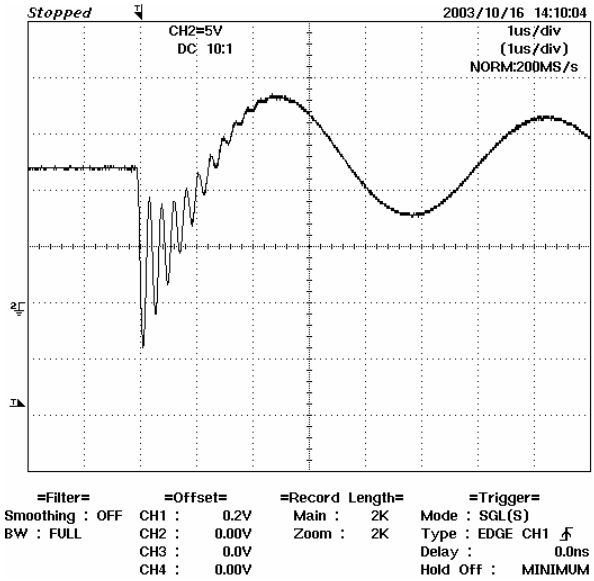


**Figure 4-16: Switch model verification measurement result (1μs/div)**

From above figures, we found the high frequency component $f_H$ appears as predicted. Doing FFT transform upon the signal, we got the spectrum of the noise source which is shown below. Two resonance frequencies can be found easily. They are 200 kHz and 4.5 MHz.

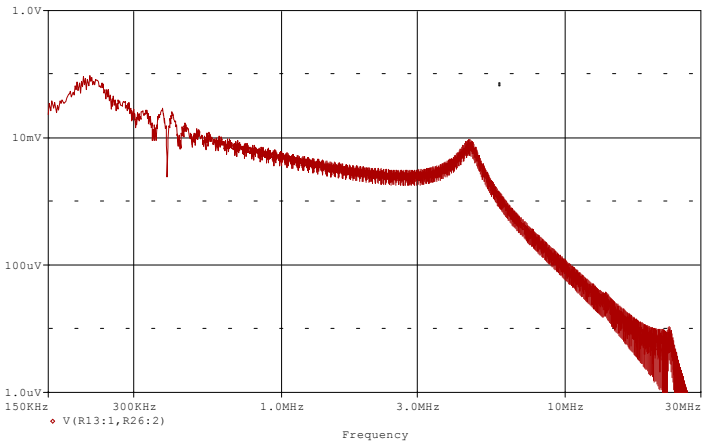


**Figure 4-17: Switch model verification simulation result in frequency domain**

## 4.4 Conclusion

The good agreement between simulation and measurement proves our model. We know that some factors are necessary prerequisite to generate oscillation along the loop. That is to say, EMI resonance loop can be blocked by destroying prerequisite.

The below EMC design guides are concluded from this chapter,

1. Resonant mode can be blocked with enough impedance in the loop. An experimental criterion is (4.14) to avoid oscillation. But we need an extra component here.

$$R > \frac{3\times10^{-7}}{C} \tag{4.14}$$

2. The wire inductance of the cable from the switch to SCU will create oscillation. Try to shorten this cable if the arrangement of the switch is allowed.
3. By removing $C_{10}$, we can eliminate resonance, but software filtering is needed.
4. If we must keep $C_{10}$, by selecting value of $C_9$ and $C_{10}$, we can avoid resonance frequency falling into radio band. Increasing $C_9$ and $C_{10}$ will make the resonance frequency lower, but the minor one is dominant factor.

It has to be noted here, however, that any real life design is always a compromise between numerous design requirements. Thus, the proposed notes to avoid EMI may be considered at the same time with other design rules.

# Chapter 5

# Motor

In automotive industry, mechanically commutated DC motors are most widely used for price factor. The principle of DC motor is known as the predominant source in causing electromagnetic interference. When it is in commutation between two brushes, an excitation voltage generates broadband noise with frequency covering tens of kHz through tens of MHz. This interference can conduct to other components or radiate to generate EMI.
In this chapter, we will describe the structure of the motor. Terminology used is clearly defined. By modeling a single coil inside the motor, we encapsulate it as a macro model. Upon the coil model and switch model, we establish a model for the whole motor. Transient noise when motor is powered off is also discussed. The influence of designable parameters is discussed in conclusion.

## 5.1 Structure of the motor

When describing a specific motor, some terminology used in connection with the motor should be clearly defined first. We use the following terminology in this paper,

- Turn: is one complete loop of a conductive wire. Normally, each turn in DC Permanent Magnetic (PM) motor consists of a single strand of conductor, and a conductor is coated with isolator to separate each wire from the others.
- Coil: Each coil consists of multiple turns, and the ends of the coils are soldered to the commutator. It is also referred to as armature winding.
- Rotor: it is the rotating part inside the stator. Slot cut lengthwise into the surface of the rotor contains the armature windings. A rotor is also called armature.
- Commutator: it is a mechanical switch made up of a ring of copper segments, which is called bar. When the rotator rotates between poles and passes at a special angle, inertia will let the brush come into contact with the next bar, so the electromagnetic force added on the rotator keeps the same direction.
- Axis: it is used to transfer rotation to load via a thread. A magnetic ring is fixed in the axis. Thus, a Hall sensor IC in SCU can detect the rotation of axis.

- Brush: Usually, it is made up of graphite, which has a low resistance ratio. By a spring pushing behind, it keeps contact with the commutator when sliding on its surface.
- Housing: it is made up of a hollow metal cylinder and a lid. It is also called frame or case. In most motor, suppression capacitors and inductors are integrated in the inside lid face.
- Stator: it is the cylindrical part around a rotor to set up magnetic field. A magnetic field may be produced by a current in stator winding or by a permanent magnet, but we refer to a stator using permanent magnets here. The poles alternate between north and south around the stator. If there is only one pair of north and south poles for stator, we call it a 2 poles motor. The stator is attached to the inner wall of the motor housing.

Figure 5-1 to 5-3 shows pictures for each part of a motor.

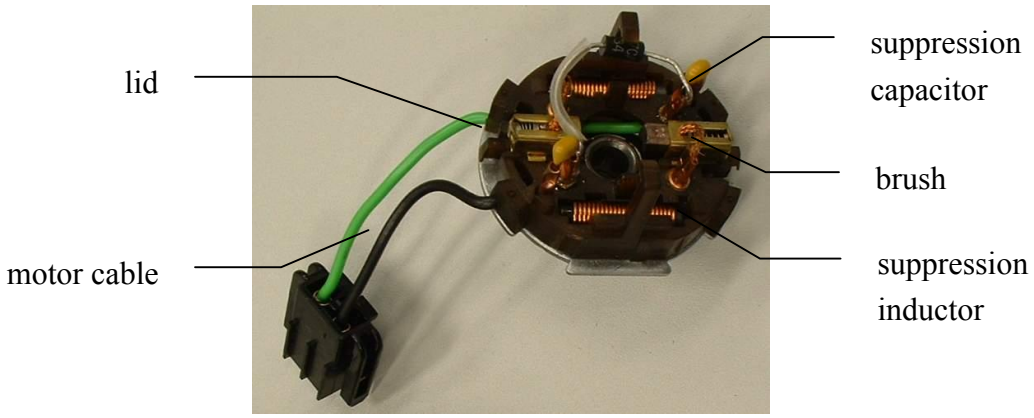


**Figure 5-1: A motor lid includes brushes and suppression circuit**

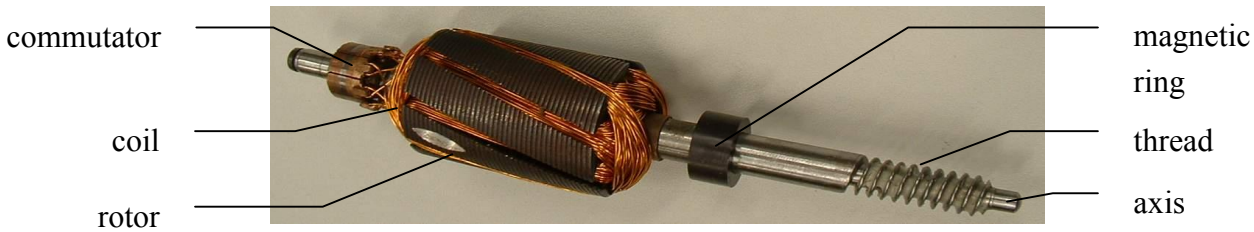


**Figure 5-2: A motor rotor**


**Figure 5-3: A motor housing and stator**

The motor we will study is a two poles, 8 armature windings permanent magnet motor. In this motor, suppression circuit is also included. One capacitor is shunt to the terminals of the motor while the other two capacitors connect terminals to the motor housing. Here we call the shunt one as shunt suppression capacitor, the other two as grounding suppression capacitors. A typical suppression circuit is illustrated in Figure 5-4.

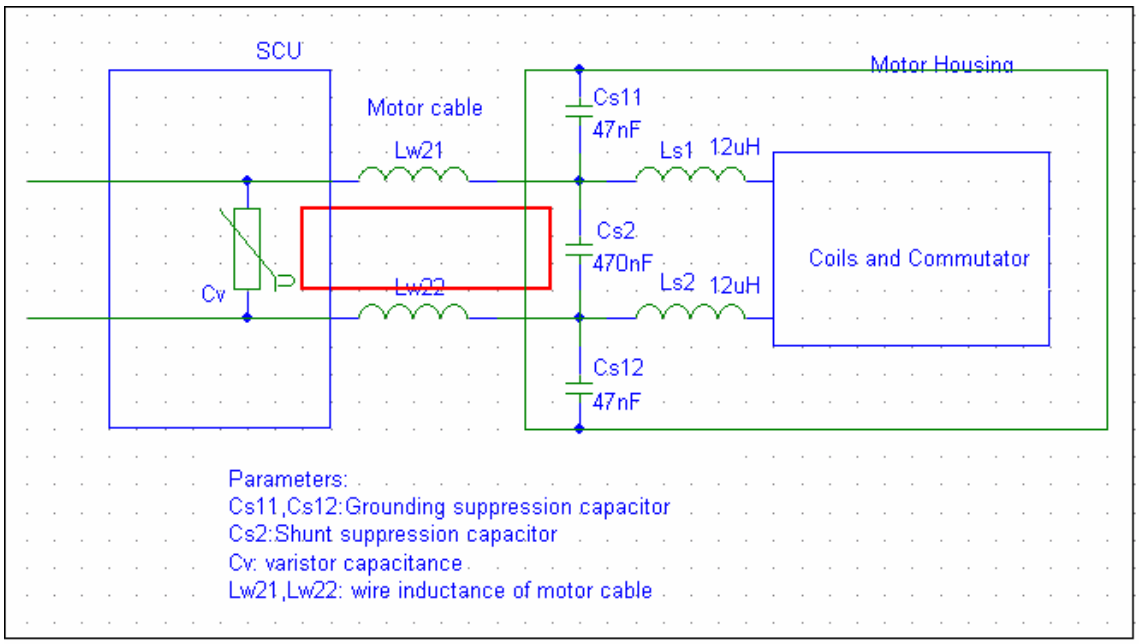


**Figure 5-4: The suppression circuit and its location**

## 5.2 Coil model

Of course, primary modeling should be based on coils, but not on turns. Some references [15] deduce a model by assuming coil made of turns connected in series, and each turn is represented by an equivalent circuit including mutual effects between turns. However, when a motor with a different structure and coil geometry is adopted at SCU, it is a really hard approach to do it respectively. Analysis starting with coils is not too insignificant and will include enough phenomena we need to concern. Another advantage of dividing a motor into coils is that the running time for simulation is far shorter with a high turn number motor.

The theory to model a coil is based on the assumption that a coil is a 4-terminal black box. This method is found in some literature [7], [14] and [21] which state coil model in AC motor. Coil is treated as a combination of resistors, inductors and capacitors. The connection of these components is arranged in such a way that both the real part and imaginary part of the impedance look into terminals is the same as the measurement result of a real coil over the frequency we are interested in.

We use HIOKI 3532-50 LCR HiTESTER to measure impedance. It has a wide frequency range from 42Hz to 5MHz. Test probes are connected to the commutation bar

by very short wires. Data achieved by measurement are recorded and drawn by MATLAB.

Firstly, we measured the impedance between two terminals of motor winding. The measurement is done in a frequency range from 42Hz to 5MHz. The relationship between equivalent inductance and frequency is shown in Figure 5-5. The equivalent inductance of one coil in 1MHz is 1/8 of the value measured at 42Hz. This result makes clear that the model of a winding in high frequency (HF) is far more complicated than a series RL circuit model in low frequency (LF).

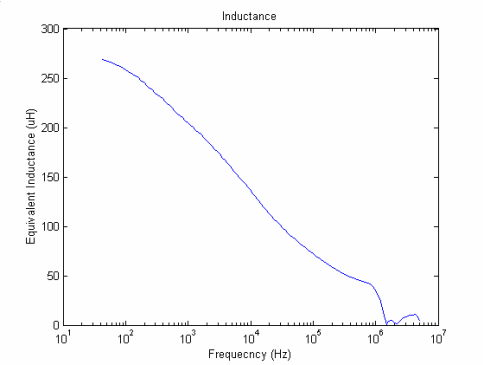


**Figure 5-5: Equivalent inductance versus frequency of one coil in DC motor**

The basis of a coil model is a series RL circuit. An inductor represents the self and mutual coupling inductance among a set of winding. A resistor is introduced to model the wire resistance. Although the value will change for the skin effect and the proximity effect at different frequencies, it is treated as a fixed average value here.

The reason why inductance decreases in high frequency is that inter-turn capacitance takes effect with frequency increasing. Damp resistance of parasitic capacitor also needs to be considered. By adding a series RC circuit parallel to original RL circuit, we got a primary version of a coil model.

In the next procedure, we take AC iron loss into account. A resistor is paralleled to RC circuit to represent this loss. It makes the terminal-to-terminal impedance below a reasonable value.

After that, turns to frame parasitic capacitance is considered. It forms between the coil and the iron core as well as between coil and housing. By adding a series RC circuit between terminal and ground, parasitic capacitance and dielectric losses in the path to ground are considered.

We got the first model for a coil in high frequency as Figure 5-6 shows.

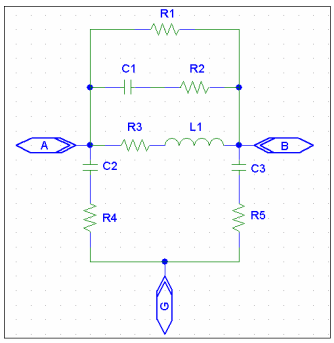


**Figure 5-6: High frequency equivalent circuit of a coil (1)**

This proposed model is validated by impedance measurement of terminal-to-terminal and terminal to ground performed on a test motor. The suppression circuit has been removed for accuracy.

Choosing the value of these components for model obviously is important and difficult. MATLAB is used to compare the calculated impedance value to measurement result. By a curve fitting, we update the coil model with adjusted values. This procedure is called "back-annotation" method. It can also be done by numerical techniques. We increase the density of frequency points around resonance frequency to get a more detail. Because winding of the coils and distribution of parasitic capacitance are not totally the same, resonance frequency is not exactly the same between impedance test results. The deviation is within 10%. Here we use a typical test result to model the coil.

The curves of impedance we measured are shown at Figure 5-7.

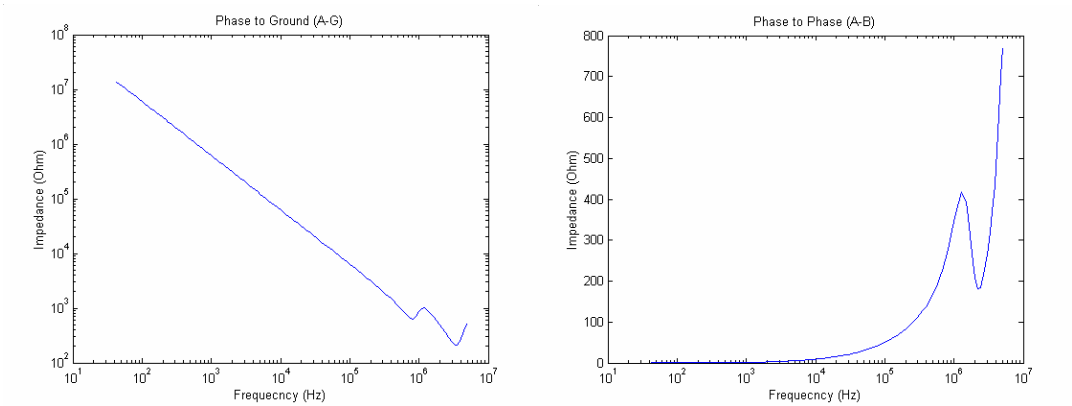


(a) Terminal to Ground (b) Terminal to Terminal

**Figure 5-7: Impedance characteristic curve (measured)**

Resonance frequencies can be easily observed in the measurement. There exist two resonance frequencies under observation. We evolve the model by two parallel LC circuits which are connected in series. It is shown at Figure 5-8.

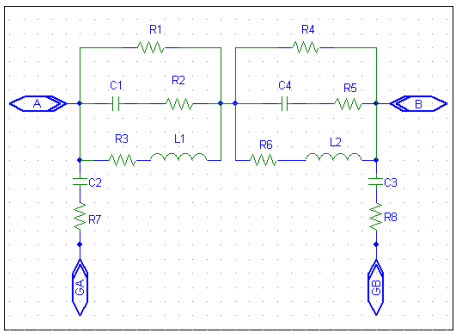


**Figure 5-8: High frequency equivalent circuit of a coil (2)**

By measuring, an initial estimate of resistive and reactive parameters can be obtained.

- At frequency range from DC to 100Hz, we got $R_{DC} = 0.45\Omega$, $L_{LF} = 260\mu H$.
- Because resonance frequencies lies at 1.2MHz and 6MHz (by extrapolation), we get an initial estimation of reactive parameters, $L_1$, $C_1$, $L_2$, and $C_4$. They can be determined by solving the following equation

$$f_1 = \frac{1}{2\pi\sqrt{L_1 C_1}} \tag{5.1}$$

$$f_2 = \frac{1}{2\pi\sqrt{L_2 C_4}} \tag{5.2}$$

$$L = L_1 + L_2 \tag{5.3}$$

  Here, $L$ represents inductance in HF, which can be guessed as 1/3 of $L_{LF}$.
- The value of $R_3$ and $R_6$ are guessed by this equation

$$R = R_3 + R_6 \tag{5.4}$$

  Here, $R$ is wire resistance in high frequency. It can be guessed as 2 times $R_{DC}$.
- The value of $R_1$ and $R_4$ are initialized as peak impedance at two resonant frequencies.
- Using the impedance measurement result of terminal to ground, we can determine the coil-frame capacitance $C_2$ and $C_3$.

These values are initial values for "back-annotation" method. We keep on modifying them in every trial cycle until the calculated result matches well with measurement.

The ultimate model of a motor coil is shown in Figure 5-9.

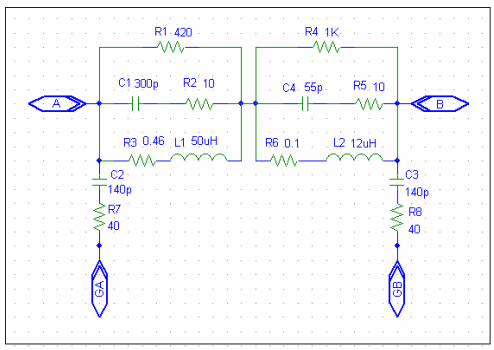


**Figure 5-9: High frequency model of one coil in DC motor**

For this model, the calculated impedance of terminal-to-terminal and terminal to ground versus frequency is illustrated below.

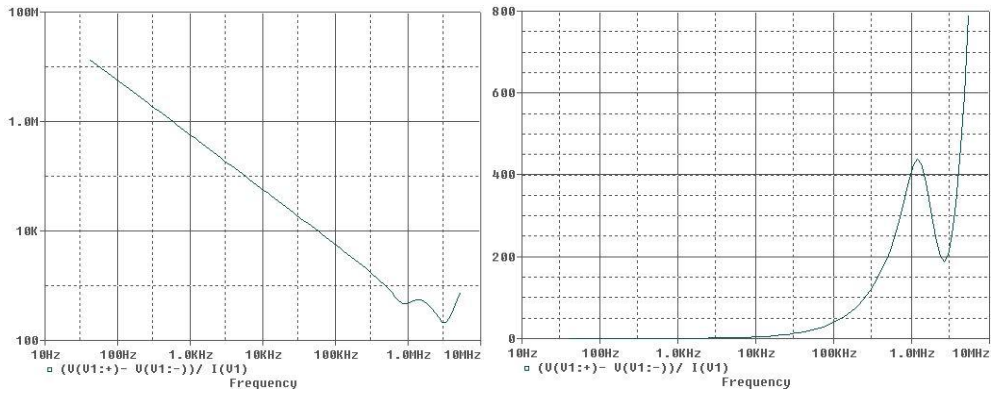


(a) Terminal to Ground (b) Terminal to Terminal

**Figure 5-10: Impedance characteristic curve (simulated)**

This model shows very good agreement with the experimental result. This circuit is encapsulated into a macro model which can be used in the coming application.

## 5.3 Modelling of Commutation

When a motor gets enough torque, the rotor begins to rotate and commutation happens. Four phases of DC motor commutation are shown in Figure 5-11. After phase (d), motor is in phase (a) again and leads to another new cycle.

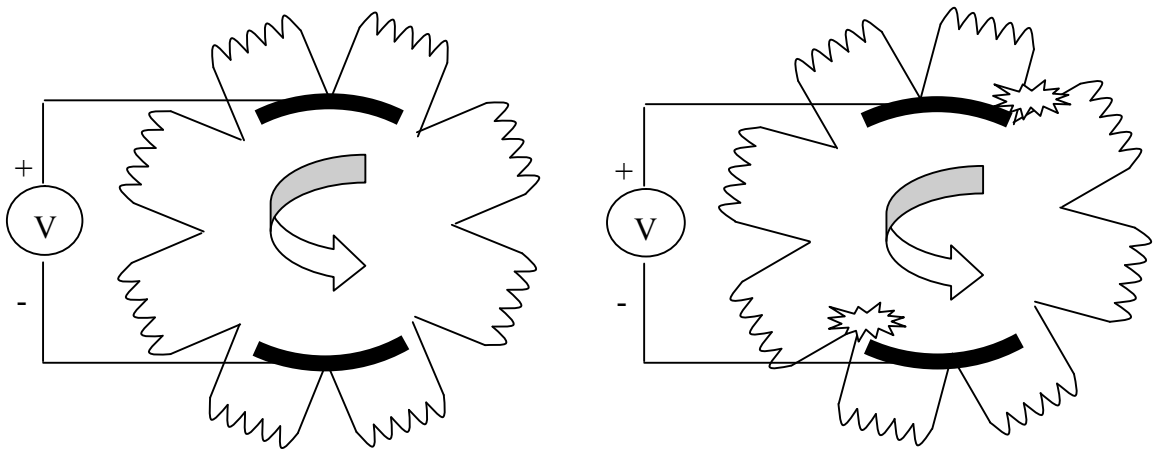


(a) Prior to Commutation (b) Entering Commutation

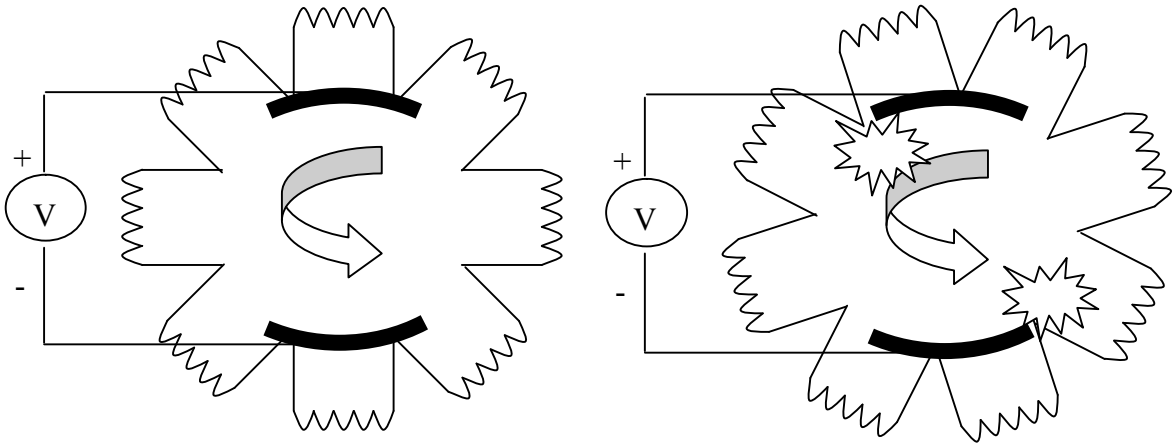


(c) In Commutation (d) Leaving Commutation

**Figure 5-11: Four phases in DC motor commutation**

Before commutation the current splits between parallel paths in the motor winding as in Figure 5-11(a). When entering commutation, one of the coils in each series in the motor is shortened prior to reversal of the current in that coil. Energy stored in the coil will generate a voltage spike between commutation ends.

Another more severe situation happens when leaving commutation. There are three coils in two parallel paths when the motor is in commutation. One more coil joins a parallel path in phase (d). Sudden change of the coil current leads an excitation voltage as is shown in Figure 5-11(d).

These noise sources excite the motor cable via a high frequency path as Figure 5-12 shows. This common mode current will be a broadband noise and efficiently radiated from motor cable.

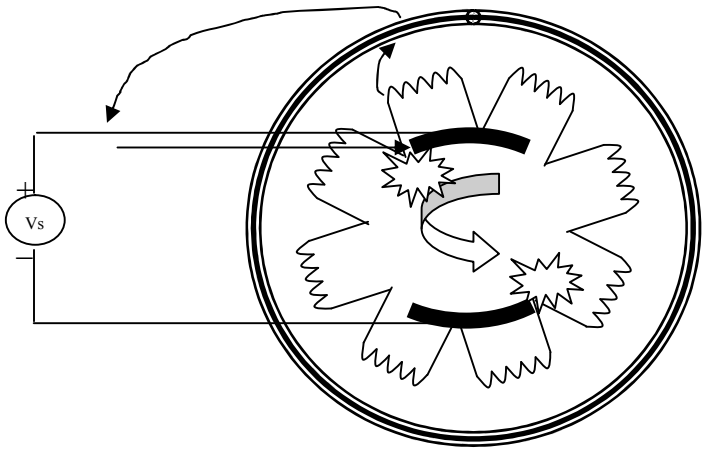


**Figure 5-12: How common mode current is generated**

We use a simple circuit to simulate abrupt changing of current flowing in a power line that happens in commutation. A derivation of a mathematic way is also given to explain the generation of EMI from a viewpoint of energy.

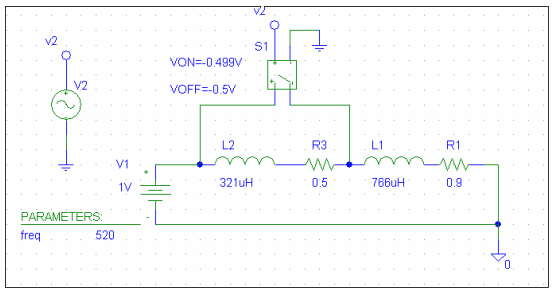


**Figure 5-13: A simplified commutation model**

Each commutation is modeled as opening and closure of switch shown in figure above, $S_1$ is opened and closed by a voltage source. When $L_2$ is shortened, it is the same scenario of entering commutation. The opening of $S_1$ represents the scenario of leaving commutation.

Here we get the prediction of the current flowing into $L_1$ and $L_2$.

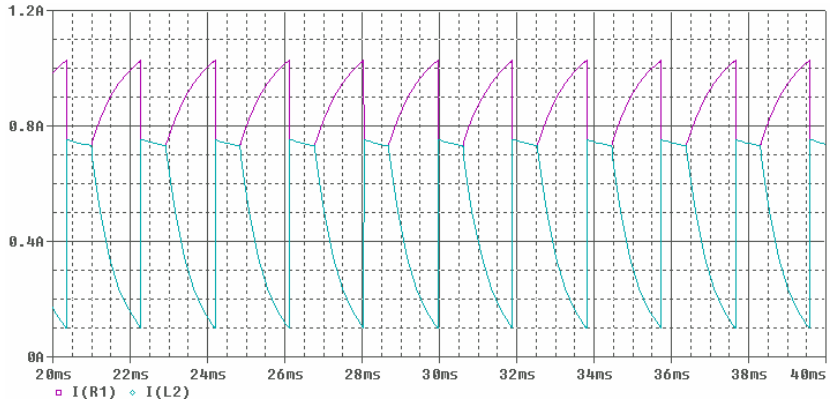


**Figure 5-14: Simulation result of coil current**

Now, we give a derivation using circuit theory. We also split the waveform into 4 phases: in phase (a), current of $L_1$ is increasing; in phase (b), current starts to decrease; in phase (c), current keeps on decreasing; in phase (d), current is suddenly changed. We expand it in time axis to make it better visible.

Two asymptotes illustrated by a dashed line represent two ultimate current values if the period is long enough.

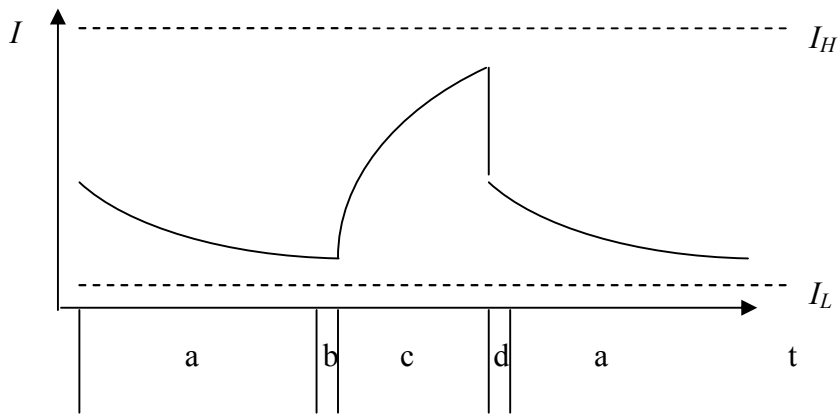


**Figure 5-15: Phases of Current transient**

These four phases of current change are correspondent to four phases of commutation illustrated in Figure 5-11.

In phase (a), the current decreases from $I_H$ to $I_L$, the ultimate value is not reachable because the cycle starts again after the interval. The time constant of exponential decreasing is $\tau_1$, where

$$I_L = \frac{V_1}{R_1 + R_3} \tag{5.5}$$

$$I_H = \frac{V_1}{R_1} \tag{5.6}$$

$$\tau_1 = \frac{L_1 + L_2}{R_1 + R_2} \tag{5.7}$$

In phase (b), the current starts to increase.

In phase (c), the current increases from $I_L$ to $I_H$, the ultimate value is also never reached. The time constant of exponential increasing of is $\tau_2$, where

$$\tau_2 = \frac{L_1}{R_1} \tag{5.8}$$

In phase (d), when $S_1$ is opened, the current has a sudden change. Suppose current in $L_1$ and $L_2$ is $I_1$ and $I_2$ respectively, and the moment right before and after transient is $t_{0-}$ and $t_{0+}$.

At time $t_{0+}$, to obey KCL law,

$$I_1(t_{0+}) = I_2(t_{0+}) \tag{5.9}$$

This equation exists according to KVL law,

$$L_1 \frac{dI_1}{dt} + R_1 I_1 + L_2 \frac{dI_2}{dt} + R_2 I_2 = V_1 \tag{5.10}$$

Integrate above equation from $t_{0-}$ to $t_{0+}$ and consider that the current in inductor cannot be infinite, thus,

$$L_1\left(I_1(t_{0+}) - I_1(t_{0-})\right) + L_2\left(I_2(t_{0+}) - I_2(t_{0-})\right) = 0 \tag{5.11}$$

We can get current value at $t_{0+}$, using the setup shown in Figure 5-13,

$$I_1(t_{0+}) = I_2(t_{0+}) = \left(\frac{L_1 \times I_1(t_{0-}) + L_2 \times I_2(t_{0-})}{L_1 + L_2}\right) = \frac{766 \times 1.02 + 321 \times 0.1}{766 + 321} = 0.75(\text{A}) \tag{5.12}$$

Here a question arises, as we know, the inductor is an energy storing component, the energy is stored in the magnetic field set up by the current. The potential energy is,

$$U = \frac{1}{2} L I^2 \tag{5.13}$$

We find that the energies that are stored in $L_1$ and $L_2$ are not equal before and after $t_0$. Is the energy conservation law broken? The answer is: a huge voltage (if the switch is ideal, the voltage is infinite) is added to the inductor at that moment so that the current is forced to change. This energy is consumed by other components in the circuit or transformed into emissions. The rear part is an unwanted signal, in other words, it is always a source of EMI.

## 5.4 Running analysis

We know from the former section, commutation is a switch instead, and the model for the coil is available. After that, we set up a model for a motor running in always-on mode, that is, a constant voltage is supplied to motor. By ignoring the mechanical dynamics, the rotor speed is set to a fixed value for each simulation.

Because inductance varies with frequency, we establish models for low frequency and for high frequency respectively.

Figure 5-16 gives a motor model in low frequency. EMF is considered in model, because it affects the amplitude of current significantly.

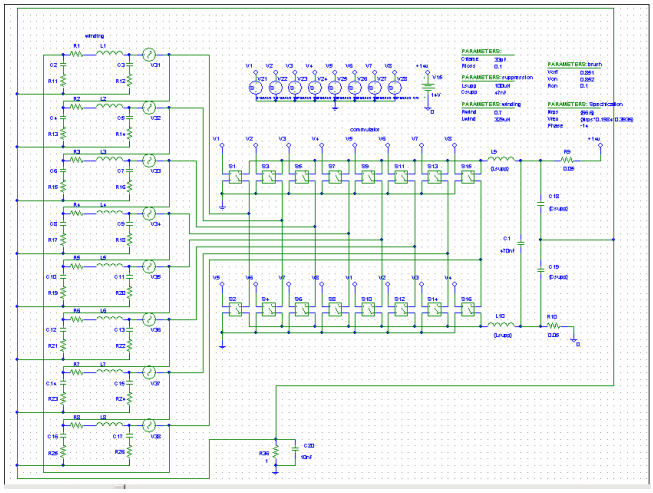

**Figure 5-16: Low frequency model of a motor**

The simulation results of a current in the motor cable are shown at Figure 5-17.

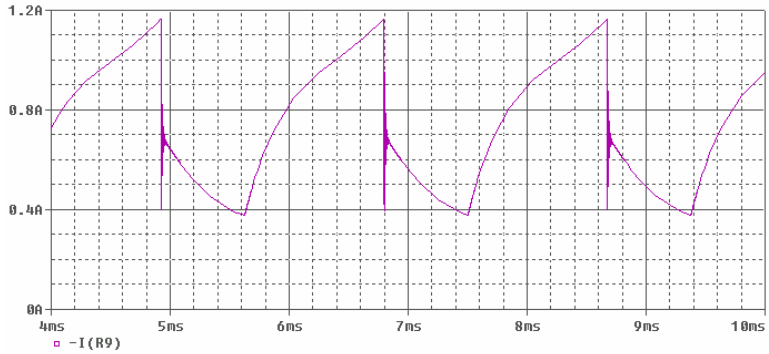


**Figure 5-17: Simulation result of Differential Mode current**

Using current probe (Tektronix A6302), current amplifier (Tektronix AM503B) and oscilloscope (YOKOGAWA DL1540), we get a measurement result of the current given in Figure 5-18. We can find a good agreement between measurement and simulation.

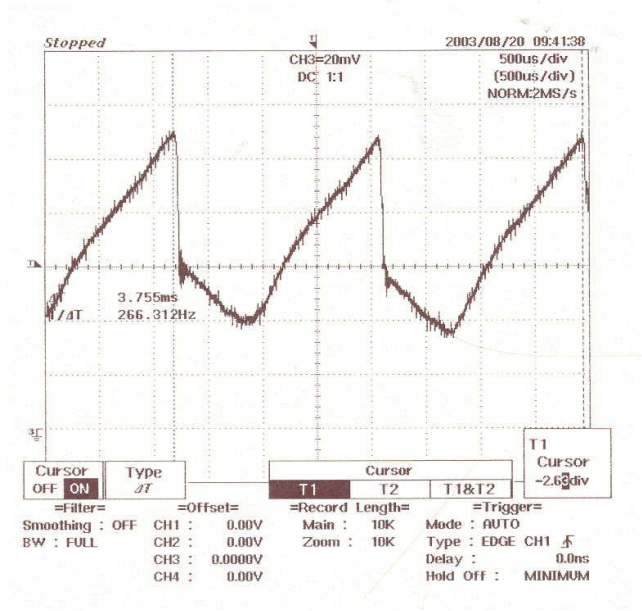


**Figure 5-18: Measured DM Current with 3m cable (0.2A/div 0.5ms/div)**

The prediction of high frequency behaviour for motor running continuously bases on our high frequency coil model established before. At high frequency, the commutation frequency is relatively much lower. We assume that the commutation is always happening in one coil, which does not make any difference and the back EMF is considered as a fixed value.

Figure 5-19 shows a model of a motor in high frequency.

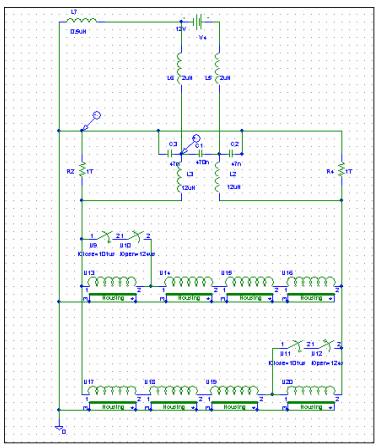

**Figure 5-19: High frequency model of a motor**

We use switch to represent commutation. In simulation, we mark the housing of the motor as reference, and every coil inside the motor is floating to reference. In time domain, the highest peak of voltage in the coil terminal appears when motor leaving commutation. The spectrum of commutation noise is shown at Figure 5-20.

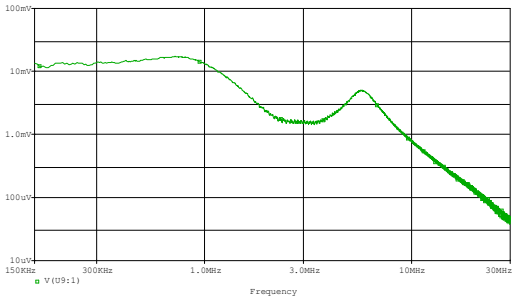


**Figure 5-20: Commutation noise spectrum without suppression (simulation)**

We find a peak around 5MHz in the spectrum of motor commutation noise. It is consistent with measurement result of motor CM current because a 4.6MHz oscillation is also found. The amplitude of oscillation is about 3mA.

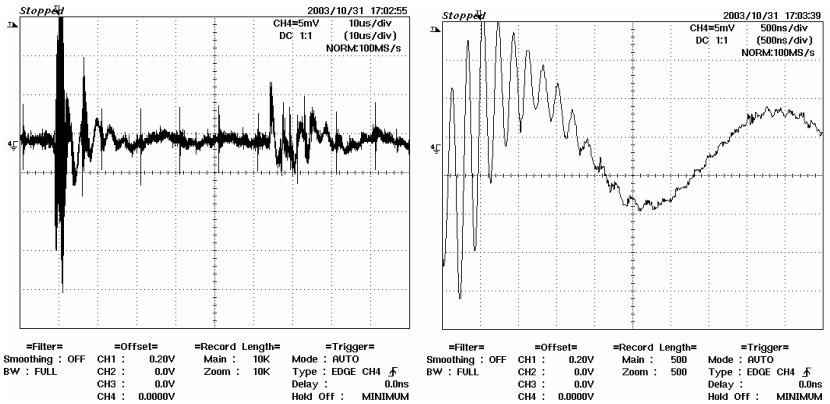


(a) (1.1mA/div 10μs/div) (b) (1.1mA/div 0.5μs/div)

**Figure 5-21: Commutation noise converts to CM current (measured)**

This peak in spectrum represents a resonant mode, which is established along suppression inductor, grounding suppression capacitor and coil. Increasing grounding suppression capacitor will shift this peak towards a lower frequency.

Another resonant mode is observed in the DM current of motor, we find the resonant mode with frequency of 3.1MHz and amplitude around 3mA.

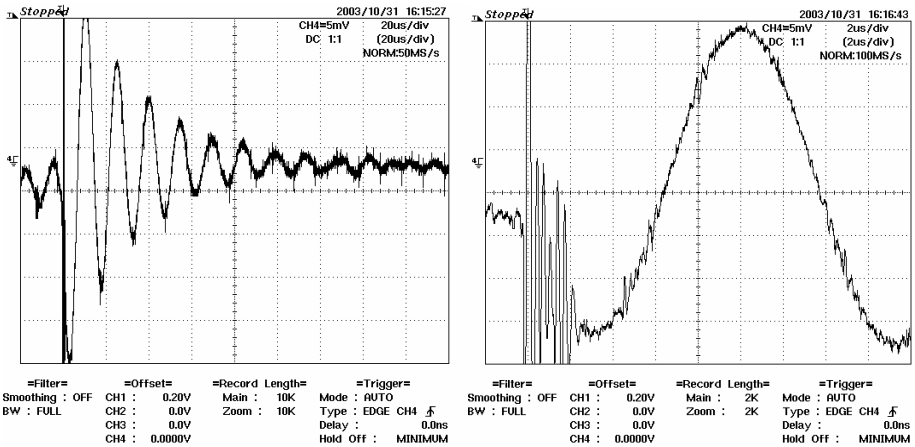


(a) (1.1mA/div 20μs/div) (b) (1.1mA/div 2μs/div)

**Figure 5-22: Commutation noise converts to DM current (measured)**

This resonance is caused by motor cable inductance, shunt suppression capacitor in motor and varistor in SCU. Compare to CM current, DM current has a much smaller loop area which makes it radiates inefficiently. Noise caused by DM current is ignored, but DCM current which is converted from this DM current has significant effect. The conversion efficiency determines the level. We leave the discussion of this noise source at Section 7.3.

The suppression circuit reduces noise effectively. This conclusion is verified by simulation. The spectrum of noise before and after suppression is shown at Figure 5-21.

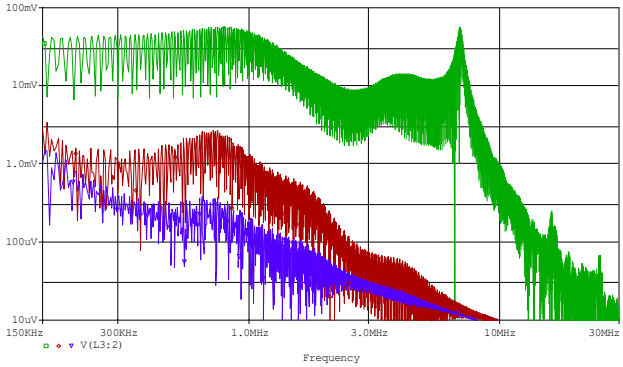


**Figure 5-23: Commutation noise spectrum with different ground suppression capacitor (simulation)**

Figure 5-23 shows three curves, the highest one is the noise level with 47pF grounding suppression capacitance and the second highest one is obtained with 47nF grounding suppression. The lowest one is simulation result with 470nF grounding suppression capacitor.

Therefore, for a satisfying suppression, 47nF of grounding suppression capacitor is necessary.

Effect of increasing shunt suppression capacitor is also evaluated. Figure 5-24 shows two curves, the higher one is the noise level with 470nF, and the lower one is simulation result with 4700nF.

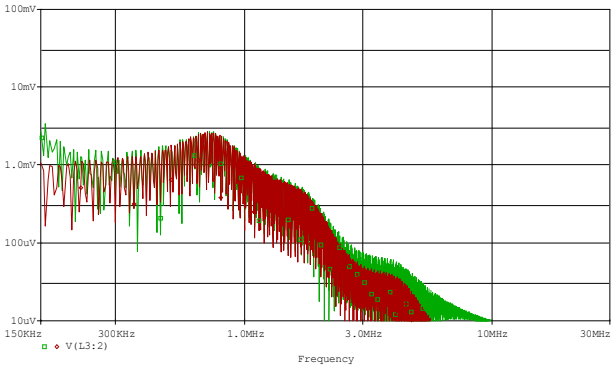


**Figure 5-24: Commutation noise spectrum with different shunt suppression capacitor (simulation)**

By comparing the spectrum of noise voltage before and after suppression, we know that suppression circuit works effectively above 1MHz. The ripple below 500kHz does not change significantly before and after suppression. Figure 5-25 confirms this conclusion in time domain.

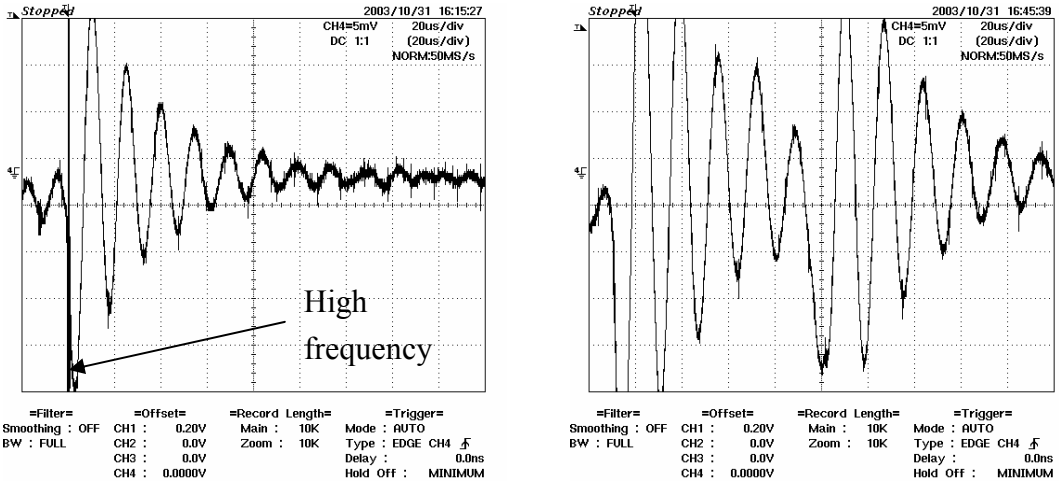


(a) DM current without suppression (1.1mA/div 20μs/div)

(b) DM current with suppression (1.1mA/div 20μs/div)

**Figure 5-25: Comparison of DM current with and without suppression capacitor**

When motor is running, commutation becomes a main noise source. We really find a resonant mode in measurement. This is a potential noise source. The motor case, although limited in size, acts as a ground plane. The motor cable acts as an antenna. Thus, a monopole antenna is formed. The antenna impedance of monopole can be calculated by [25]. In [13], it proves the way to simplify the radiation model by monopole antenna is feasible.

This noise can be eliminated by shorting both ends of noise source, that is to say, with good connection to ground plane at both motor housing and battery negative pole, the lump produced at 5MHz will disappear. The wiring configuration has influence for this noise. In this thesis, we use the word "lump" to present a broadband increased level. Lump is distinct from narrow band peak, while peak is a single increased level.

One more mechanism of noise source is introduced here. It is caused by commutation noise and the resonance is built along the loop illustrated in Figure 5-26.

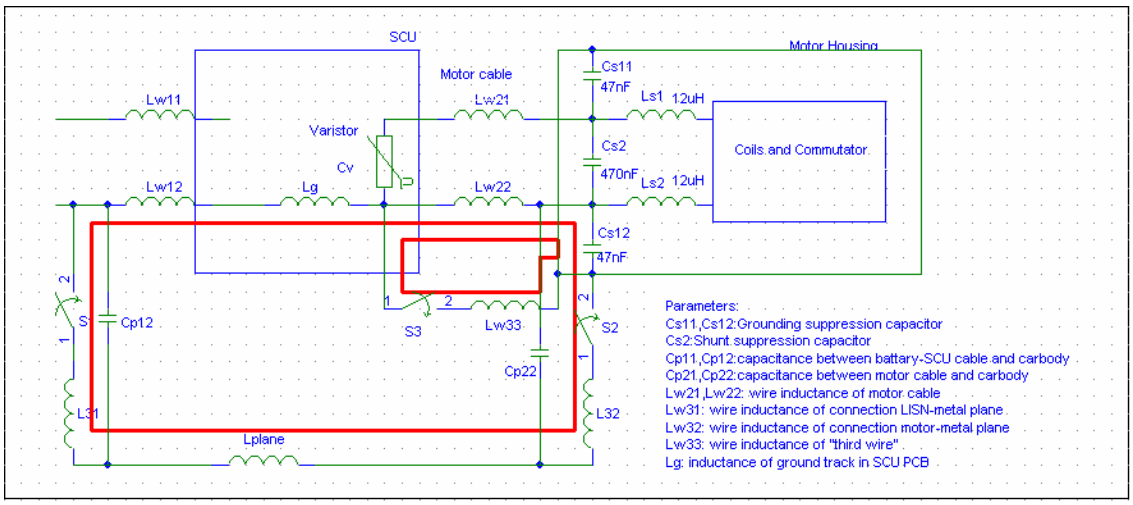


**Figure 5-26: Mechanism of CM current in grounding network**

Resonance is formed via inductance $L_{plane}$ in metal plane, inductance $L_g$ in ground track, inductance $L_{w12}$, $L_{w22}$ in ground track, and capacitance in this loop.

Because the cable between SCU and the motor is much shorter than the cable between LISN and SCU, therefore, we have $C_{p22}<<C_{p12}$ and $L_{w22}<<L_{w12}$. We estimate the value of these parasitic parameters for resonance frequency:

$L_{w11}=L_{w12}$ =2μH, $L_{w22}=L_{w22}$ =0.06μH, $L_g+ L_{plane}$=0.2μH, $C_{p11}=C_{p12}$ =14pF, $C_{p21}= C_{p22}$ =1.4pF.

According to these estimate value, we predict the lump produced in different wiring configuration.

When motor housing or battery negative pole is not connected to car body, capacitance in this loop is in the order of 1pF. That makes the assumed resonance frequency equal to 45MHz. The noise source in this frequency is too weak to excite a resonance.

When motor housing or battery negative pole is both connected to car body, the calculated resonance frequency is around 350kHz.

If “third wire” between motor housing and SCU ground is presented, the calculated resonance frequency is around 800kHz.

This peak changes its resonance frequency with the wiring configuration, because elements along the resonant loop are changed with wiring configuration.

## 5.5 Transient analysis

Compare to commutation, a more severe situation happened when motor is disconnected to power. The reason is the energy stored in all coils will release to surrounding, while commutation involves one coil at one time.

In [26], this transient is carefully studied in detail. A test setup is used in measuring the currents exciting the wire harness from a motor when it is switched off. A typical conducted emission voltage is measured and shown below.

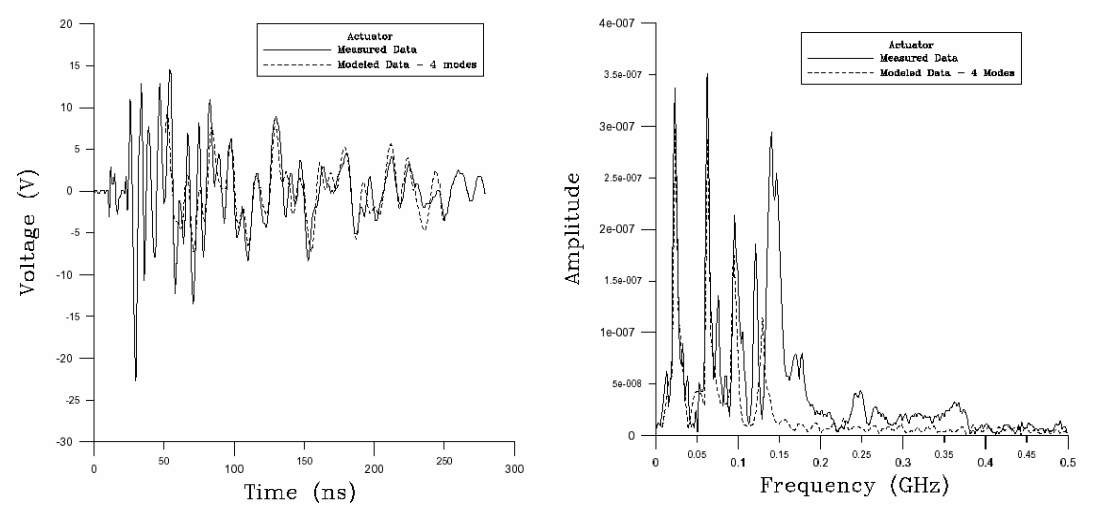


(a) In time domain (b) In frequency domain

**Figure 5-27: Conducted Emission Transient when motor is switch off suddenly**

The transient noise when motor is switch off has a much more frequency content than commutation noise. The main frequency components are extent to 200MHz. These transient pulses can be decomposed to extinction pulses, which are called E-pulse in [26]. These pulses appear as DM current in motor cable, and the highest level of these pulses is 110mA. An empirical estimation is transient noise when motor is switch off produces 20dB higher EMI than commutation noise.

The prediction of this noise is extremely difficult, because it involves the parasitic parameter of motor up to very high frequency. These peaks varies with different motor like fingerprint of motor, it is also called natural modes [26]. To suppress this noise, we should make the motor cable shorter and the shunt suppression capacitor larger since it is a DM current noise. Wiring configuration seems has no influence for this noise.

Decreasing current variation in transient will bring great benefits in suppressing transient noise.

## 5.6 Conclusion

Since the prediction of EMI depends on an accurate prediction of both differential- and common mode HF current, the motor model is particularly useful and crucial. We start the model from coil and end with a complete model for low frequency and high frequency.

The below EMC design guides are concluded from this chapter,

- The commutation noise comes from the voltage spark between the coil and brush when the coil is leaving commutation. Suppression circuit can reduce the noise level. The grounding suppression capacitor has dominant effect.
- Radiated emission from commutation noise can be eliminated by short both ends of noise source, that is to say, with good connection to ground plane at both motor housing and battery negative pole.

- The commutation noise between the terminal and motor housing will radiate to air while the cable acting as an effective antenna. Therefore, we should keep the motor cable as short as possible. This provision is also helpful to suppress transient noise when motor is switch off.
- Shunt suppression capacitor has effect on suppressing transient noise.

# Chapter 6

# Relay

Transient noise occurs when we switch on or switch off SCU. Besides the transient caused by the switch, the opening and closing of a relay also leads to abrupt current change or voltage change. Because its inductive load leads larger current variation, it is more harmful. It may result in sparks between lines and a popping noise is heard in the radio. These situations need transient analysis. In ISO7637-1 and ISO/WD 7637-2, transient noise is already adopted as specification in automotive industry.
Recently, requirements of transient noises are becoming stricter than before. We need to learn more about its characteristics and its cause; transient processes should be carefully studied. It is also helpful for component selection and determining suppression methods. In this chapter, we will establish a model for a relay. By an experiment setup, we will do transient analysis at relay opening and closing respectively. This experiment is used to validate the relay model and to study transient noise caused relay. We will discuss the influence of some designable factors. We give some strategies for EMI suppression at last.

## 6.1 Model of relay and setup for validation

Component library in PSPICE gives a macro model for the relay, which takes the mechanical specification into account. But in EMC view of point, the switch-on and switch-off are of primary interest, particularly during closing and opening of electrical contacts. Therefore we ignore the behavior of relay coil. Being quite similar to a switch, relay is modeled by parallel switches which represents the bounces event. The lead inductance is included.
Like in the previous chapter, a setup is established for validation which is shown at Figure 6-1.

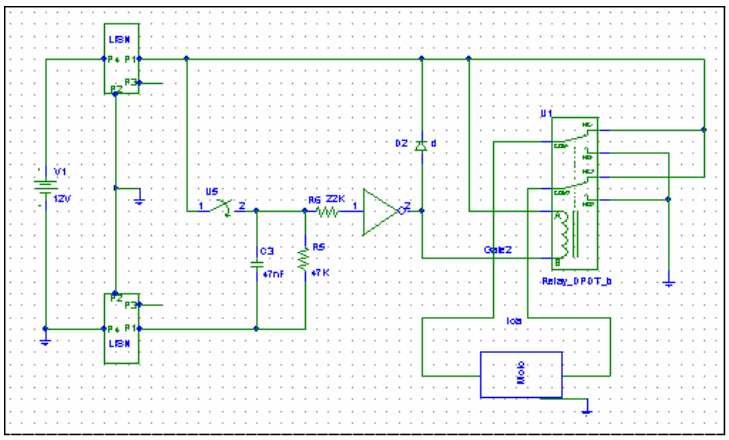


**Figure 6-1: Setup to validate behaviour of the relay**

The PCB for our experiment is a real product called P138. We construct the corresponding circuit in a simulation environment. Some models come from the PSPICE component library, while the model of the motor is the result of previous chapter.

The connection between motor housing to battery negative pole is represented by a series RL circuit. Battery-SCU cable is modeled according to transmission line theory, whose model values are determined by the length and dimension of the wires.

The connection from the motor housing to ground is not definite. We will consider three possibilities in this chapter, one is a very good connection, another is floating to ground, and the last one is connected with certain resistance.

## 6.2 Transient analysis for relay closing

We start our discussion by assuming that the housing of the motor is connected well to the ground. In this situation, both differential mode current and common mode current are present.

When the relay operates, three series resonant modes are established. Loop1 consists of the wire inductance and the shunt suppression capacitor inside the motor; loop2 consists of the battery input capacitor, the lead inductance of the relay, the inductance of the motor cable and the shunt suppression capacitor of the motor.

Because two grounding suppression capacitors which are connected to the housing of the motor have low impedance in high frequency, the third loop is established via this path. Loop3 consists of the battery input capacitor, the lead inductance of the relay, the inductance of the motor cable, the shunt suppression capacitor of the motor, the ground suppression capacitor and the grounding network. The current in loop3 is the main component of common mode current.

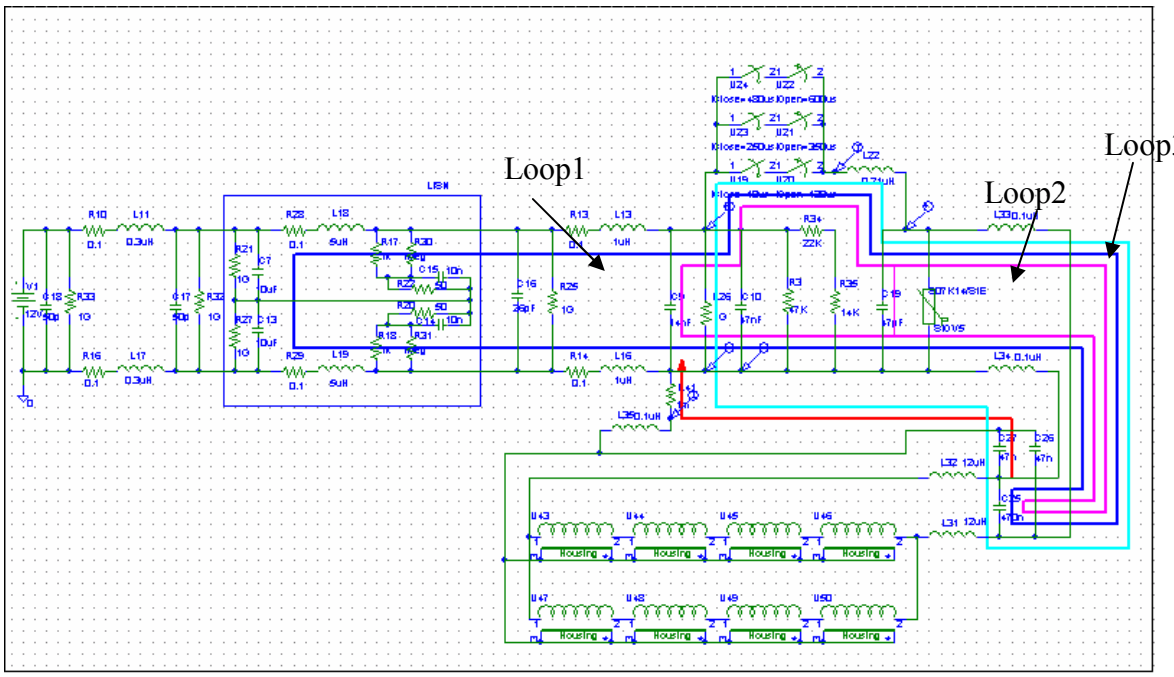


**Figure 6-2: Three resonant modes established with relay closing**

It has been found that the resonant frequency of loop1 is quite low, and only the shunt suppression capacitor affects this frequency. In fact, the small capacitor and MOV parallel to shunt suppression capacitor will not bypass the current in this loop.

Resonant frequencies that generated by loop2 and loop3 are relatively high and in the order of MHz. Both of them will have an effect on the common mode current. Here the resonant frequency is determined by the minor one of shunt suppression capacitor and battery input capacitors. Another factor is the parasitic inductance of the relay and the inductance of the motor cable.

Loop3 will not be constructed if the housing of the motor is not connected to the ground because the current path to the ground is blocked.

## 6.3 Transient analysis for relay opening

When the relay operates, the closure is typically a rapid series of closing events and opening events resulting from bouncing, sliding, rocking and surface contaminants. What happens when the relay is opening is also studied.

Figure 6-3 shows three series resonant loops to release energy stored in coils. These loops will contribute to common mode current.

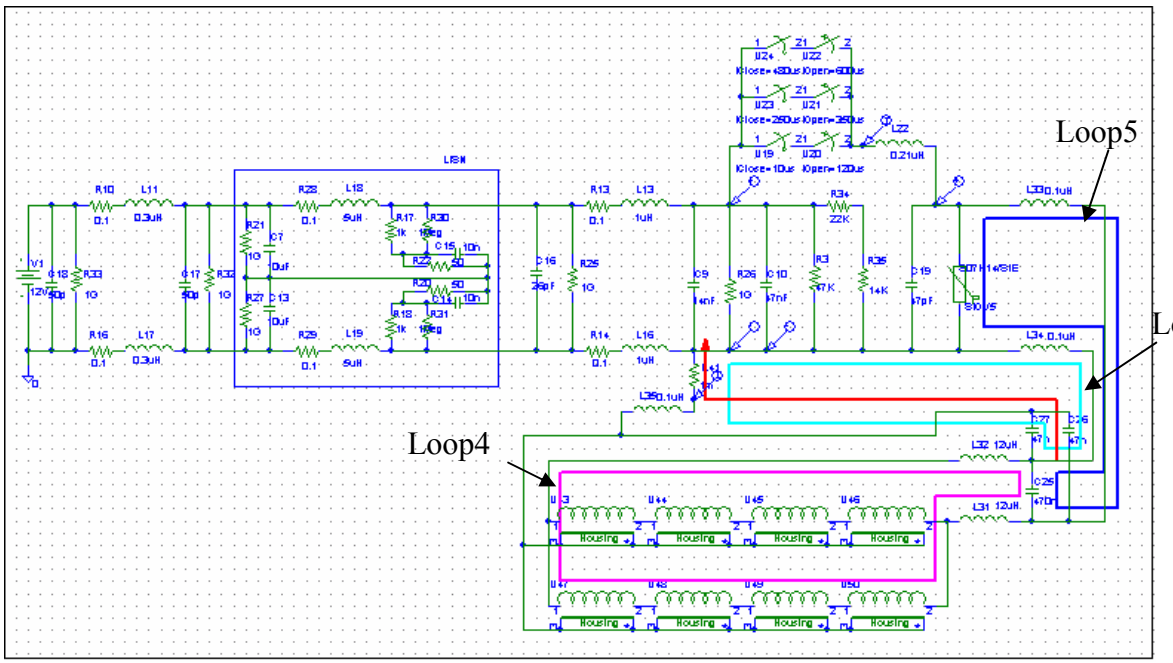


**Figure 6-3: Motor circuit with resonant loop when relay opening**

Loop4 consists of all coils in the motor and the shunt suppression capacitor; Loop5 is made up of the series connection of the line inductance and the shunt suppress capacitor inside the motor; Loop6 consists of the series of line inductance, grounding suppression capacitor and the grounding network.

The oscillation in loop4 will be constrained by a breakdown of Metal Oxide Varistor (MOV). Energy is dissipated by MOV if the amplitude between terminals of the motor is above 33V. It also provides a path for high frequency current with its capacitance of 2500pF.

Although shunt suppression capacitor is included in Loop5, capacitance of MOV is the main factor to determine the resonance frequency, because capacitance of MOV is normally in the order of nF, it is far smaller than the shunt suppression capacitor. Wire inductance of the motor cable determines the resonance frequency of loop5 also.

The impedance of grounding network is the main element to determine the characteristic of loop6. High impedance will make the resonance decay faster.

Figure 6-4 shows the simulation result of CM current when the motor housing is well connected to the ground. Figure 6-5 shows the conducted emission in frequency domain.

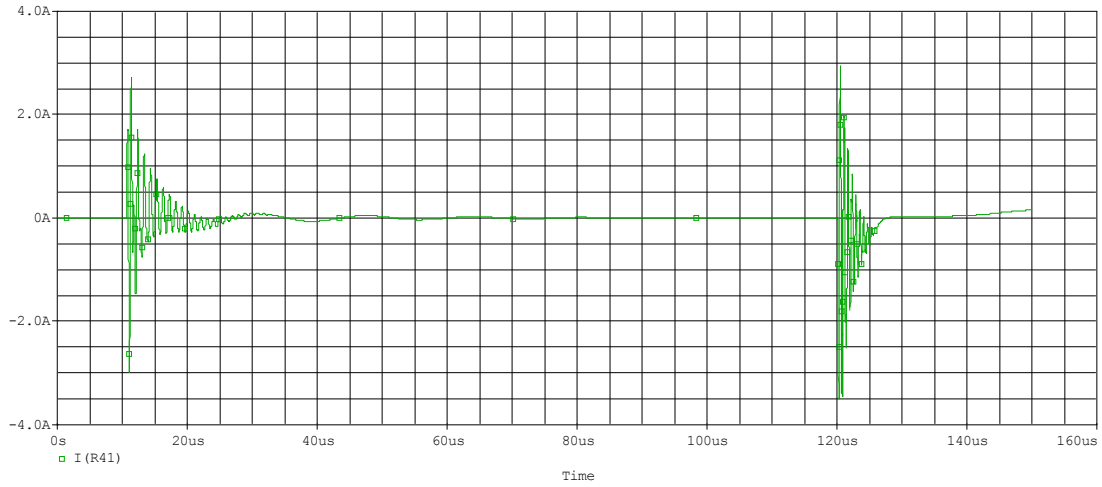


**Figure 6-4: Simulated time domain transient of CM current**

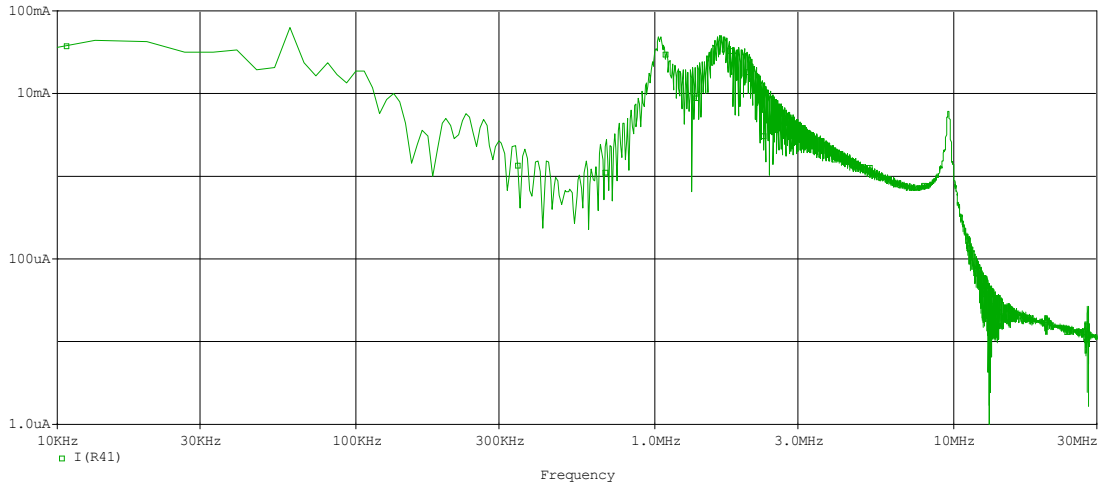


**Figure 6-5: Simulated CM emission spectrum with motor housing grounded**

We find six resonance frequencies in spectrum, which are 15kHz, 60kHz, 1.03MHz, 1.6MHz, 1.97MHz and 8.6MHz. We name them from $f_1$ to $f_6$ for convenience sake. The $f_2$, $f_3$, $f_5$ are formed in loop1, loop2, loop3 when we have relay closing, the $f_1$, $f_4$, $f_6$ are introduced by loop4, loop6, loop5 when the relay is opening.

The simulation result is validated by measurement. Figure 6-6 shows measured voltage on pin 1 and pin 4 of the relay, which is COM terminal and Normal Open terminal of one DPDT switch inside the relay. We find four resonant modes in measurement, with the frequency of 12.5kHz, 60kHz, 1.25MHz, 8MHz. They are corresponding to $f_1$, $f_2$, $f_3$ and $f_6$. The $f_4$, $f_5$ were not observed because they are CM current flowing through grounding wire. The agreement proves that our model is reliable and main resonant modes are included in simulation.

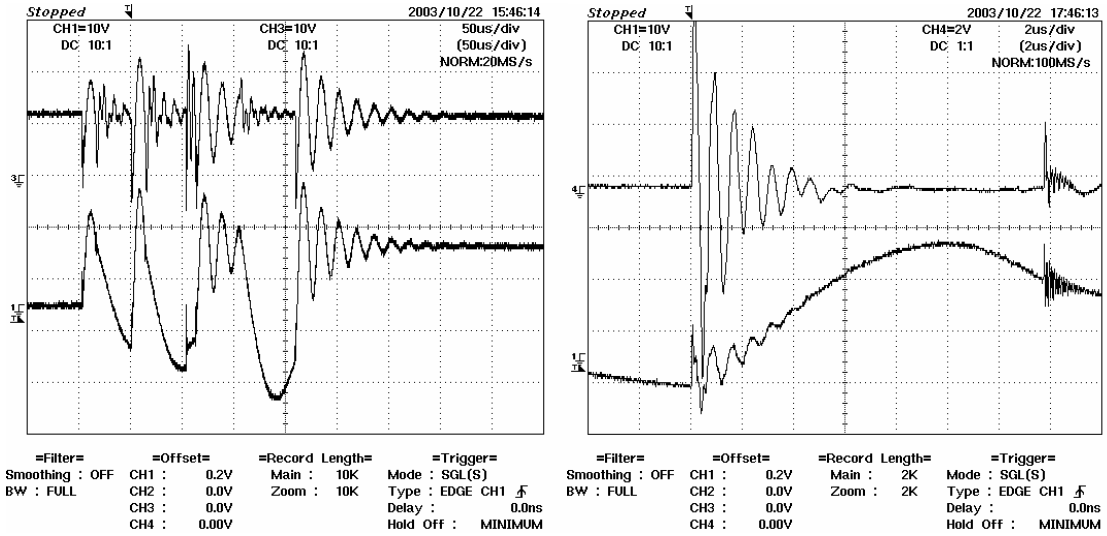


(a) (10V/div 50μs/div) (b) (2V/div 2μs/div)

**Figure 6-6: Measured voltage on pin1 and pin 4 of relay**

## 6.4 Factors related to transient specification

Some discussion is to be made to determine the influence of designable parameters,

1. The impedance between the motor housing and the ground.

If the motor case is insulated from the ground, CM currents are blocked. Therefore, the voltage drop in LISN is DM voltage only. Conducted emission spectrum achieved in the LISN is shown in Figure 6-7.

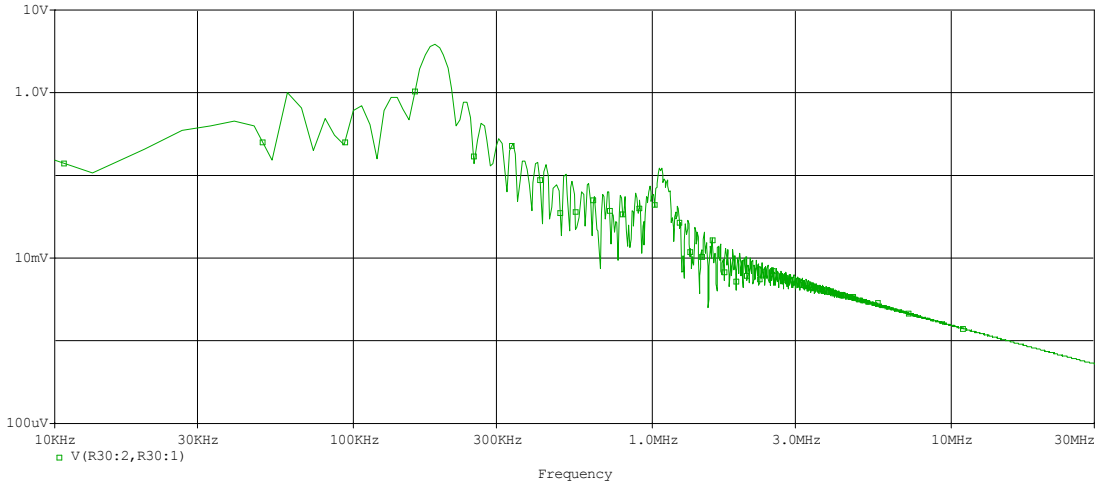


**Figure 6-7: Simulated emission spectrum without the motor housing grounded**

The only resonance frequency is 200kHz comes from resonant mode $f_3$. CM resonant mode $f_4$ , $f_5$ totally disappear. Therefore, by isolating the motor to the vehicle chassis, we will get a very low EMI level.

2. The inductance of the wire from motor housing to the ground.

If we increase the inductance of the ground wire for the motor to 1 μ H, the simulated CM emission spectrum is shown in Figure 6-8.

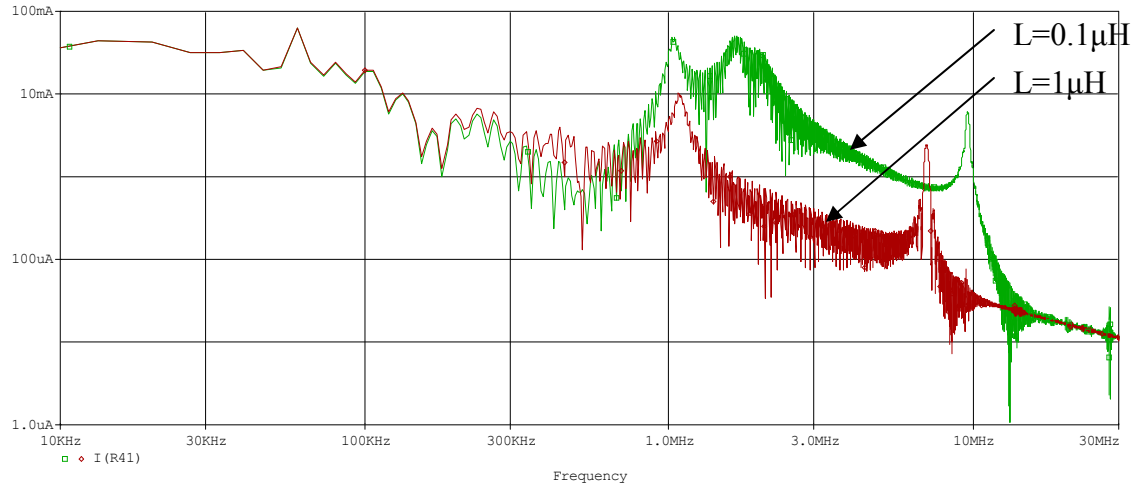


**Figure 6-8: Simulated CM emission spectrum with increased grounding wire inductance**

The resonance $f_4$, $f_5$ disappear and $f_6$ decrease to 6.8MHz. As shown in this figure, the inductance of the grounding wire of the motor affects only the common-mode resonance peak.

3. The resistance of the wire from the motor housing to the ground.

If we increase the resistance of the ground wire for the motor from 0.1Ω to 1 Ω, then to 10 Ω, the simulated CM emission spectrum is shown in Figure 6-9.

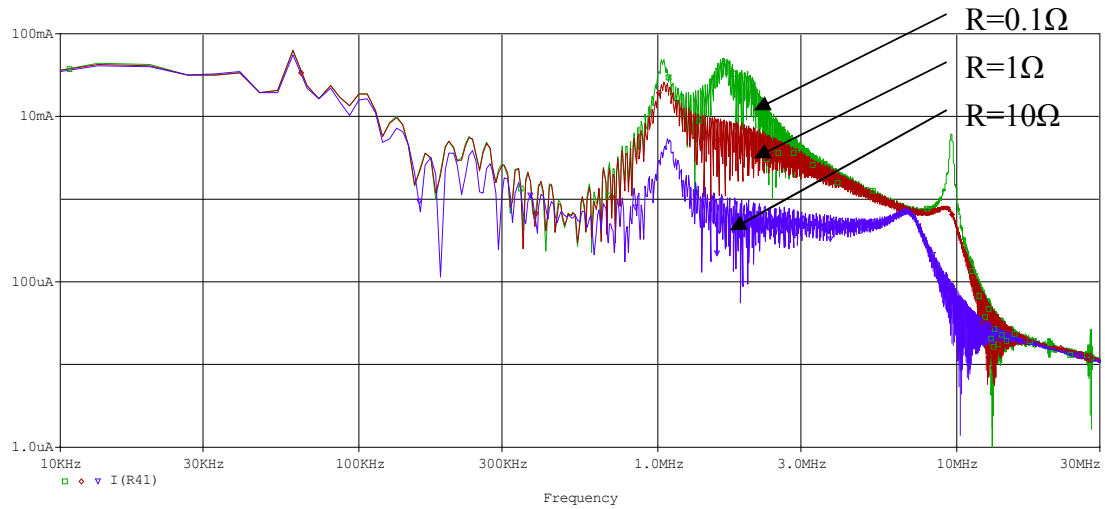


**Figure 6-9: Simulated CM emission spectrum with grounding wire impedance increased**

$f_4$, $f_5$ are decaying rapidly, so no oscillation is constructed, $f_6$ is also suppressed. In fact, wire resistance is in series connected in the loop3 and loop6, the amplitude of $f_4$, $f_5$ is decreased. CM current along the ground wire converted from potential difference in loop5 is also decreased by increased wire impedance.

4. The grounding suppression capacitor.

Replacing the grounding suppression capacitor with 47pF, the simulated CM emission spectrum is shown in Figure 6-10.

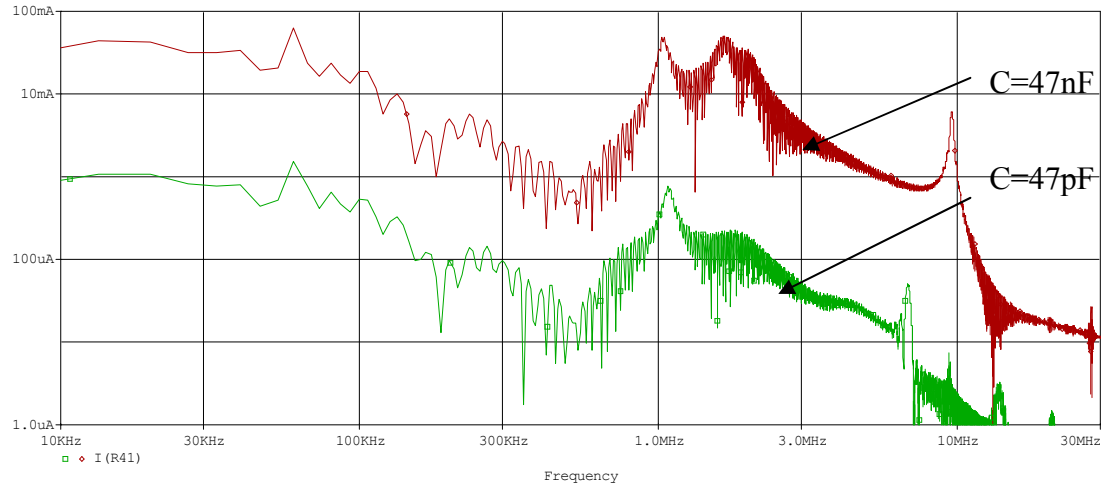


**Figure 6-10: Simulated CM emission spectrum with grounding suppression capacitor decreased**

The grounding suppression capacitors block the resonant mode in CM path.

5. The transient time of the switch.

We change the switch transient time from 1us to 10us. The simulated CM emission spectrum is shown in Figure 6-11.

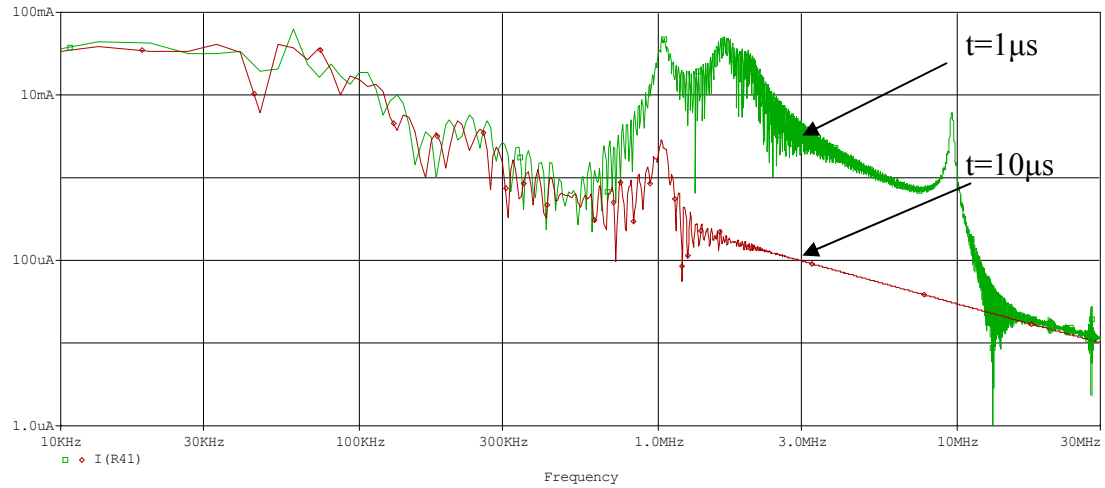


**Figure 6-11: Simulated CM emission spectrum with switching time increased**

The high frequency above 1MHz is drastically decayed. The Equation 4.8 shows that the resonance will decay effectively if switching time is in the same order of the resonance period, and the resonance can be ignored if a calculated resonance period is less then 1/25 of the switching time.

6. The shunt suppression capacitor

We change the shunt suppression capacitor from 470nF to 4700nF. The simulated CM emission spectrum is shown in Figure 6-12.

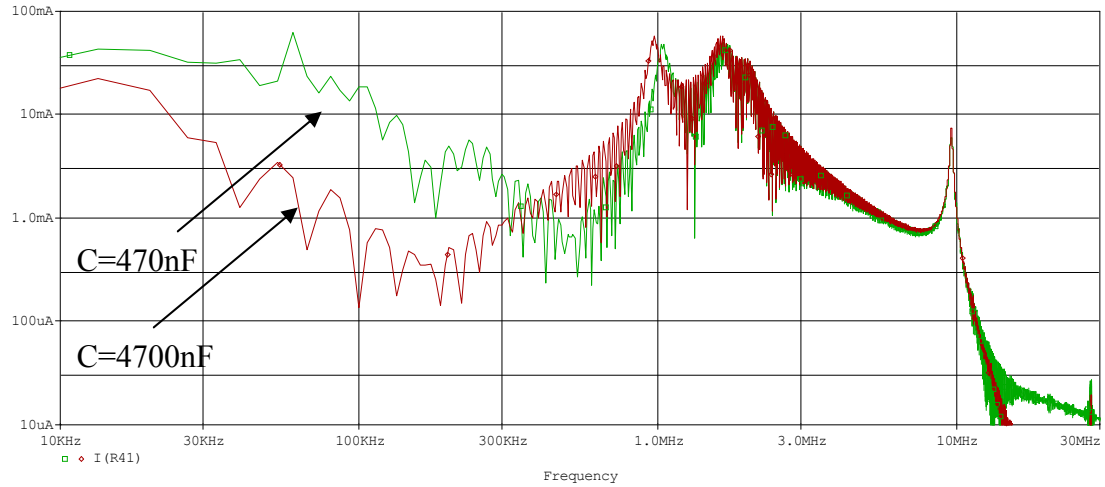


**Figure 6-12 Simulated CM emission spectrum with shunt suppression capacitor increased**

The shunt suppression capacitor strongly affects the resonant peak at low frequency. It decreases the resonant peak with 30dB below 300kHz, and has in practice no influence on the high resonant frequency, since it is always connected in series with varistor or battery input capacitor which has a much lower value.

7. The wire inductance of the motor cable.

By decreasing the wire inductance of the motor cable from 0.1μH to 10nH, the simulated CM emission spectrum changes a lot in high frequency as Figure 6-13 shows.

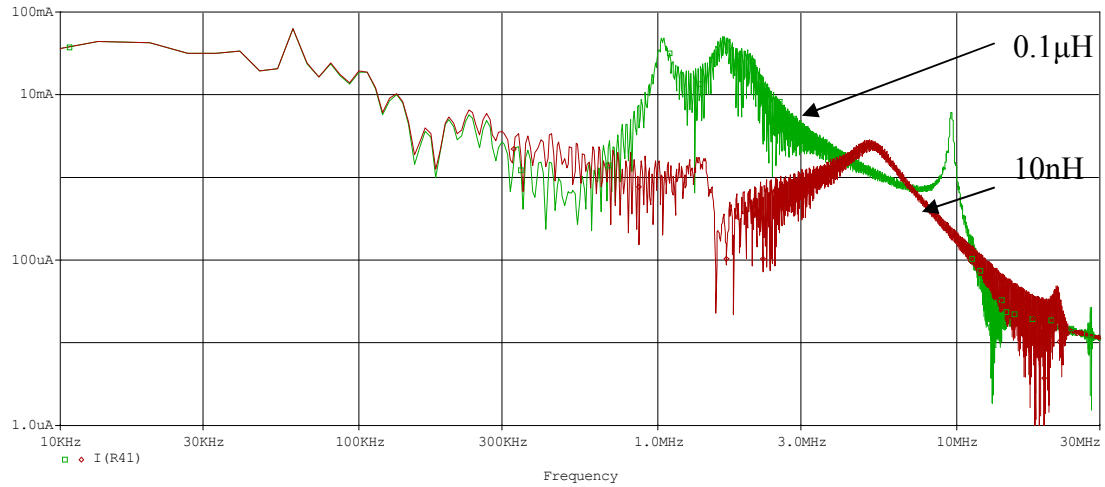


**Figure 6-13 Simulated CM emission spectrum with wire inductance of motor cable decreased**

We find that the $f_3$ resonant mode shifts to 4MHz and the $f_4$, $f_5$, $f_6$ resonant modes disappear. That is why we prefer having a short connection between SCU and the motor.

8. The varistor capacitance.

Replace MOV with another model whose capacitance is 65pF, we get predicted CM emission spectrum as Figure 6-14 shows.

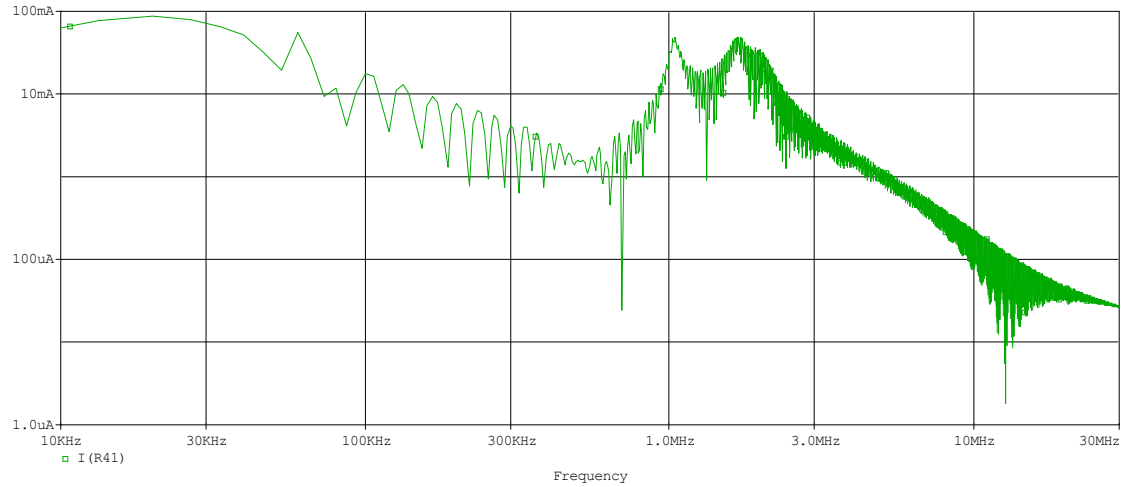


**Figure 6-14 Simulated CM emission spectrum with another varistor**

We find that $f_1$ to $f_5$ resonant modes are not changed, while $f_6$ disappear. Another possibility is by replacing the varistor with a diode, but then we have to change topology of this circuit.

9. The battery input capacitor.

By increasing the battery input capacitance from 14nF to 140nF, we get predicted CM emission spectrum as Figure 6-14 shows.

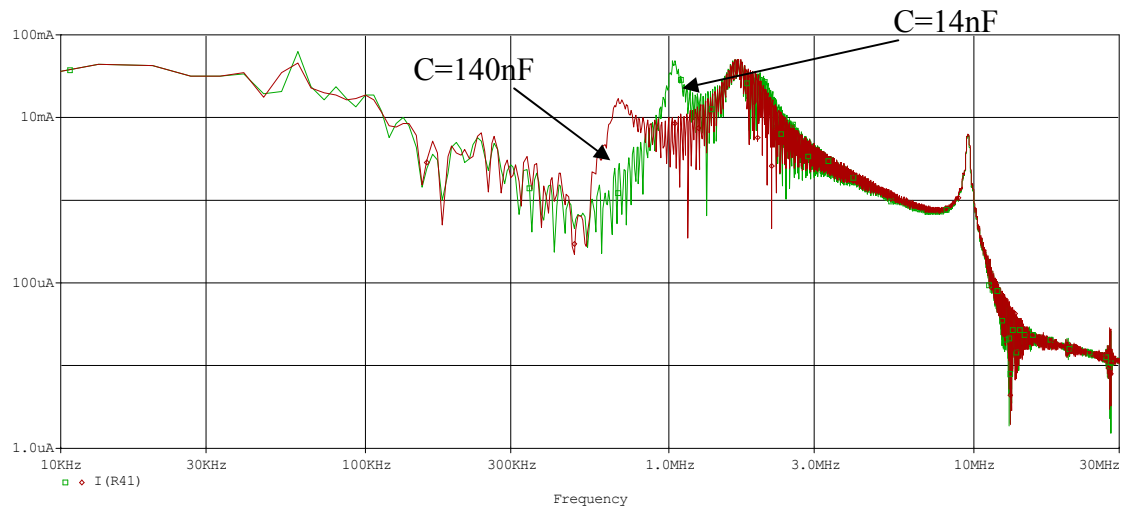


**Figure 6-15 Simulated CM emission spectrum with battery input capacitor increased**

We find that increasing the battery input capacitor shifts the resonant mode $f_3$ towards a lower frequency.

## 6.5 Conclusion

We found seven resonant modes from the spectrum of the EMI, four of them occur when relay is opening, and another three happen when the relay is closing. By comparison between different configurations, we got the following conclusion:

- The simplest way to suppress EMI is by isolating the motor from the vehicle chassis. In the viewpoint of transient noise caused by relay, isolating motor housing has benefit to suppress transient noise.
- If the above requirement is not satisfied, the impedance between motor housing and ground should keep at least 10Ω which leads 20dB suppression.
- Decreasing the grounding suppression capacitors will block resonant mode in CM path with decreased amplitude. By reducing grounding suppression capacitor to 1/1000 of primary value, the CM current can be suppressed 40dB.
- Switching time can affect resonance dramatically. Relay with longer contact time produces lower EMI in high frequency. But in order to change switching time, we need to replace this relay with MOSFET.
- The shunt suppression capacitor affects the resonant peak only at low frequency.
- The wire inductance of the motor cable affects the high resonant frequency effectively.
- The varistor capacitance strongly affects the peak of resonant mode $f_6$. Using varistor with smaller capacitance will move resonance towards a higher frequency even disappears.
- Increasing the battery input capacitor shifts the resonant modes $f_3$, $f_5$ towards a lower frequency.
- The suppression circuit of the motor, not the coils in motor, mainly determines the noise characteristic. This conclusion is also true for running noise produced by PWM. Motor coil parameters only have influence on the commutation noise.

# Chapter 7

# PWM

PWM (Pulse Width Modulation) signal is employed to get a variable speed control in the motor accelerating and decelerating. In some product, the EMI level goes beyond regulation due to the switched waveforms. Because EMC measurements are always done under "worst case", SCU is set to run in 50% PWM status in one measurement item, which makes it the toughest item to pass.

In this chapter, we will give the method to model SCU. Based on the previous models, we will point out resonant modes. Among them, some will be a dominant component in low frequency radiation emission, while others will produce a big trouble in high frequency range. We will conclude with some suggestions to suppress noise caused by this transient.

## 7.1 Modeling of MOSFET

The switching device, a MOSFET, was modeled in this study as a switch parallel with two capacitors, as shown in Figure 7-1. The junction capacitor $C_j$ involved in the reverse recovery current and the capacitance $C_k$, as the parasitic capacitance between drain and ground plane because drain has biggest voltage sudden change and soldering area. Both $C_j$ and $C_k$ can be obtained by measuring. The turn on/off time of the switch is set via parameter in the switch model which is measured in experiment.

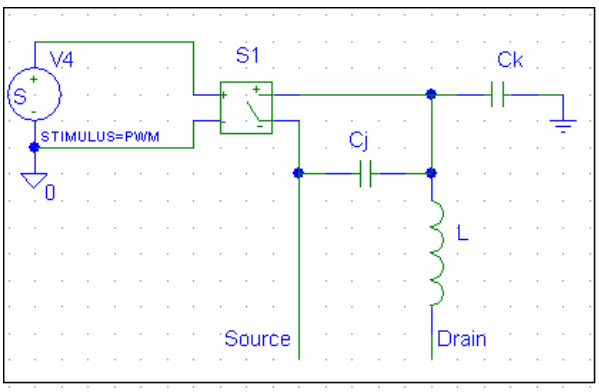


**Figure 7-1: Model of MOSFET for high frequency**

Of course, when more parasitic elements are used, the simulation becomes more realistic. There are many sophisticated MOSFET models available for simulation, they always use very complex topological which will result in excessively long run times. But we just want to find out what main source is for EMI here, we prefer a relative comparison not the exact value.

## 7.2 Running analysis

After transient of bouncing, the relay is in a stable state. All relays are now treated as low-impedance pass through. The MOSFET is a switch component that makes voltage and current suddenly changed. The main difference between this kind of transient and prior transient caused by relay and switch is that this one is periodic. We catalogue the noise caused by this periodic transient to running noise.

Because the MOSFET has a more stable switch parameter compared to commutation, for instance, the transient time, interval time, the noise caused by PWM wave is more like a narrowband noise.

In [6], [7], [9], [11], [12], [16], [17] and [19] EMI produced by AC motor running in PWM is discussed. Conducted emission produced by power electronic converters is dealt with at [8], [10], [18] and [20]. From these literatures, the running analysis approaches are referable, but the limitation of previous research still exists:

- No discussion about conversion from DM current to CM.
- Although wiring configuration is important for EMC performance, its influence is not investigated.
- How radiated emission is produced by conducted emission is not introduced.

In this section, we use a real product to simulate and validate our model over a complete PWM switching period.

The frequency of PWM is 100kHz, and this frequency cannot lower than 15kHz, otherwise the acoustic noise is generated. Another factor for the preference of high PWM frequency is therefore the size of filter can be kept small.

We use Figure 7-2 to illustrate the transient of PWM switch.

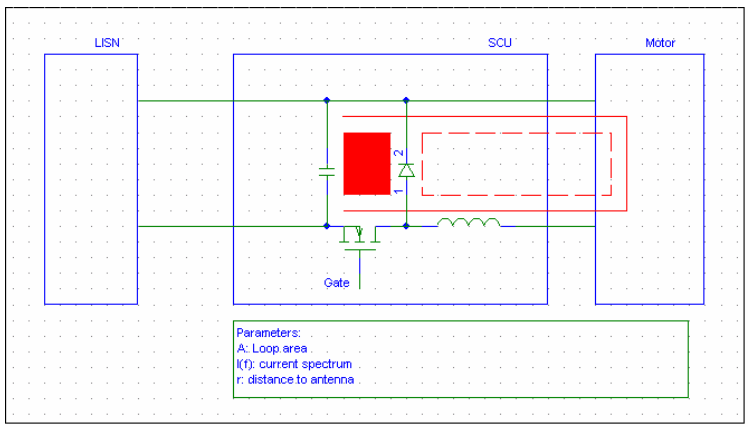


**Figure 7-2: Diode current loop**

In phase 1, MOSFET is switched on firstly. The current from the battery flows to the motor then through MOSFET and returns to the battery. In phase 2, the MOSFET is turned off, the current in the inductors cannot change instantaneously, the voltage polarity across the inductors will be reversed due to electromagnetic force when d*i*/d*t* <0, this voltage will forward bias diode, then the diode take the current loop cover. The block in Figure 7-2 is embrace with high d*i*/d*t* current, which emits radiation efficiently like a loop antenna. We call the current in this loop as diode current.

Besides diode current, current with ripple is produced between power supplier and SCU, between SCU and motor when motor is running at PWM mode. Their locations are illustrated in Figure 7-3.

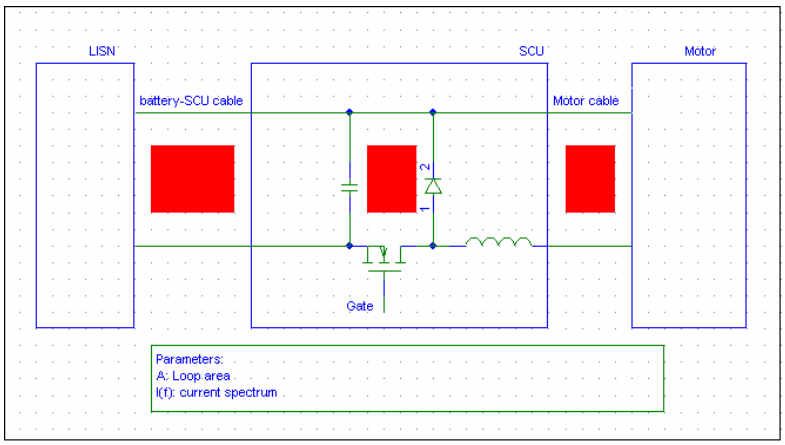


**Figure 7-3: Main DM current loops when SCU is working at PWM mode**

The measurement results in time domain of these three DM currents are shown in Figure 7-4.

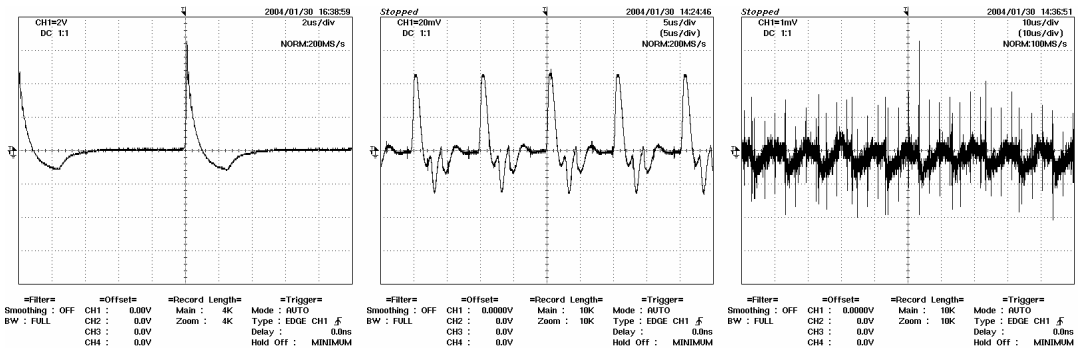

(a) Diode current (0.44A/div 2μs/div)

(b) DM at motor cable (4.4mA/div 5μs/div)

(c) DM at battery-SCU cable (0.22mA/div 10μs/div)

**Figure 7-4: The DM current waveform when motor running in PWM mode (measurement)**

We found a small ripple in the falling edge of the waveform of diode current. It is caused by a new resonant mode which does not exist in real product. This resonant mode is produced by an extend wire inserted into diode current loop to contain the clamp of current probe.

The spectra of these DM currents are also shown in Figure 7-5.

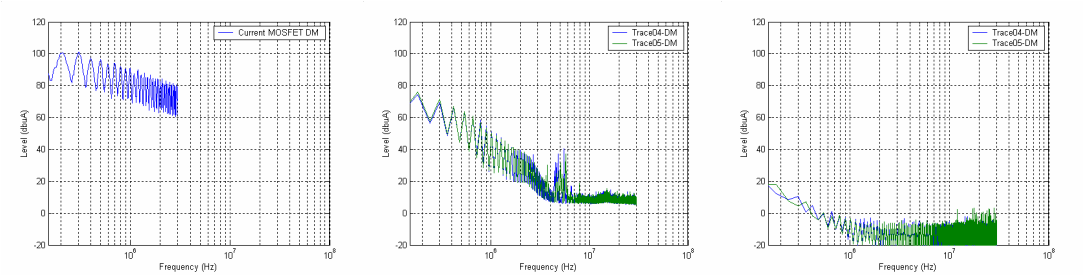


(a) Diode current (b) DM at motor cable (c) DM at battery-SCU cable

**Figure 7-5: The spectrum of DM current when motor running in PWM mode (measurement)**

The diode current has a highest level in these DM signals. It starts from 100dBμA at 400kHz and follows a slope of -20dB/dec. Due to the sharp rising edge of diode current about 100ns, the decay slope keeps -20dB/dec below 3MHz.

The DM current at motor cable is 70dBμA at 400kHz and follows a faster decay slope of -40dB/dec. The DM current at battery-motor cable is 20dBμA at 400kHz and also follows a decay slope of -40dB/dec.

Compared with diode current, the spectra of DM currents at motor cable and battery-SCU cable decrease much faster, which makes the diode current to be the main source of radiated emission below 3MHz.

In Figure 7-5 (a) and (b), there are two curves present measurement results with and without motor housing connected to a metal plane. It is important to realize that when changing the wiring configuration, the differential-mode current is not significantly changed. This is due to the fact that DM current is a functional current. The spectrum of DM current is related to topology of the circuit and components value in SCU and motor. We can also find from above figure that the DM current mostly concentrates at low frequency. This conclusion is useful to identify a noise source.

These DM current can be predicted by simulation as Figure 7-6 shows.

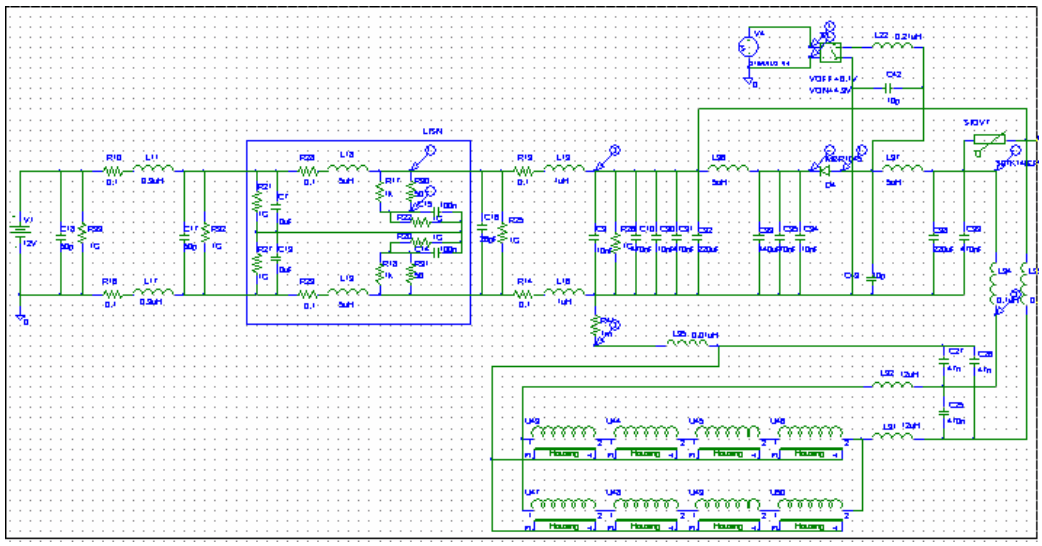

**Figure 7-6: Simulate SCU operates in PWM signal**

The simulation and measurement result of diode current are compared at Figure 7-7.

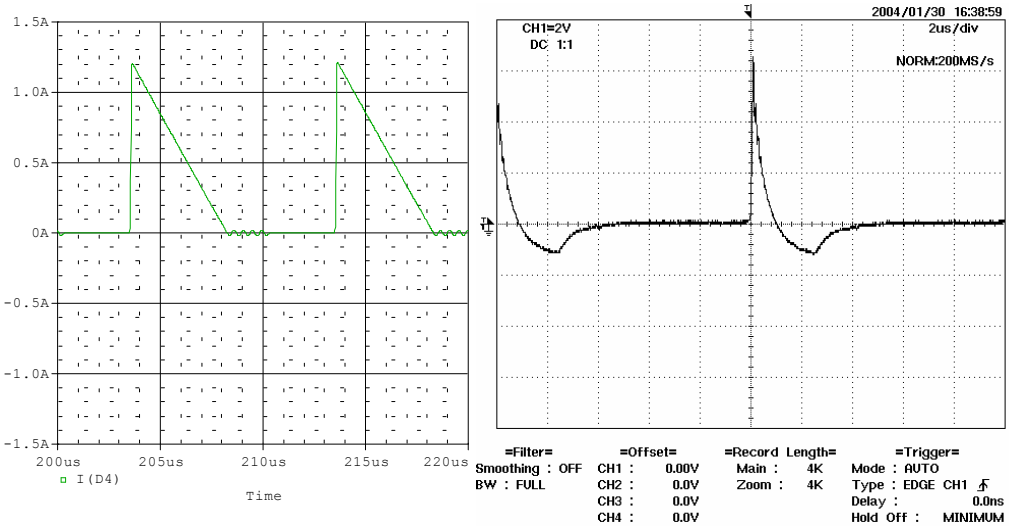


(a) Simulation result (0.1A/div 1μs/div) (b) Measurement result (0.44A/div 2μs/div)

**Figure 7-7: Diode current comparison between measurement and simulation**

The amplitudes of two waveforms are 1.36A and 1.2A. The shape is slightly different because current probe has less transfer impedance in low frequency. The decay time constants are 3us and 4.2us respectively which are still in the same order. Both waveforms have rise time about 100ns. The predicted diode current agrees well with the measurement result in the frequency range up to 3MHz. Therefore, the diode current is predictable.

Via the formula of Equation 3.17 and Equation 3.18, we can predict radiated emission based on the predicted diode current.

We assume the loop area of this current is 0.00001 $m^2$, which is 0.1cm×1cm. The predicted radiated emission is shown at Figure 7-8.

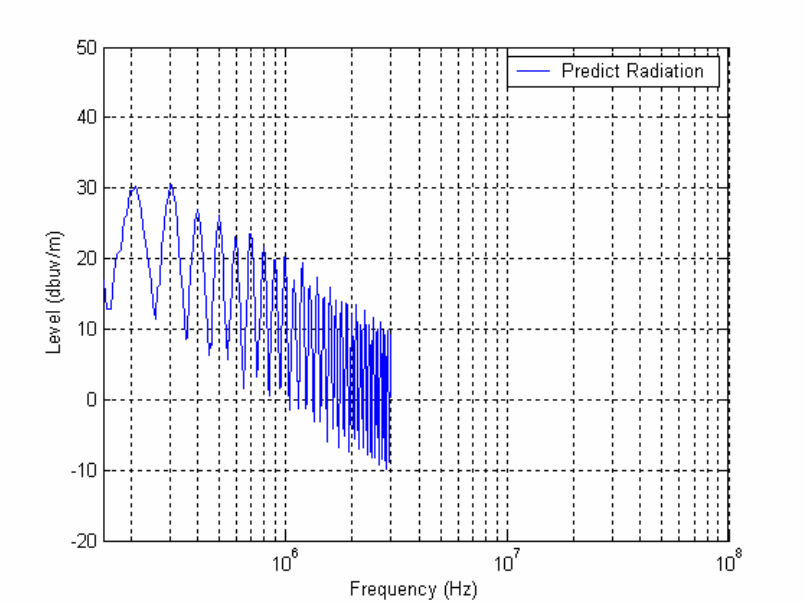


**Figure 7-8: Predicted radiated emission below 2MHz**

Compared to the measured radiated emission shown at Figure 7-9, the difference between then is within a range of 3dB. We conclude that the noise below 2MHz is predictable at the stage of design.

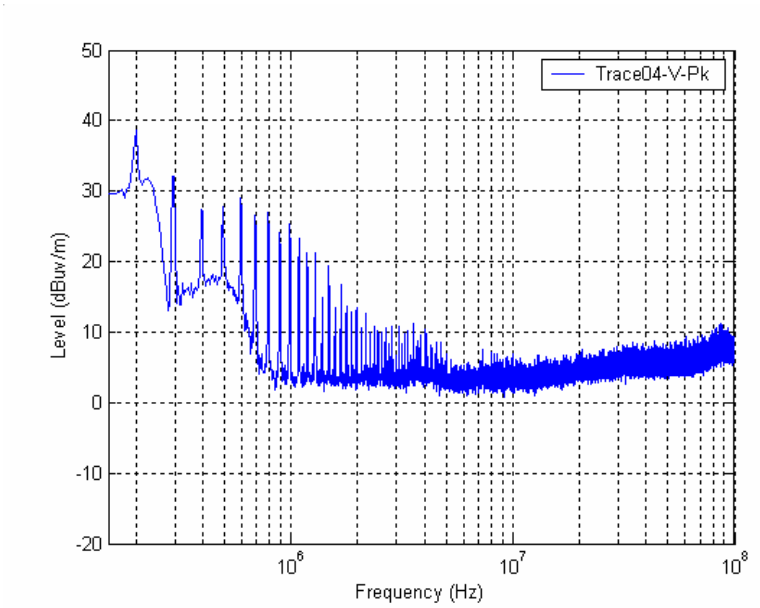


**Figure 7-9: Measured radiated emission with setup1**

Compare Figure 7-4 (b) to Figure 5-25 (b), the commutation of MOSFET aggravates ripple in the motor cable. Therefore the level of resonance caused by motor cable inductance, shunt suppression capacitor in motor and varistor in SCU increases as well. We show the mechanism of resonance in Figure 7-10.

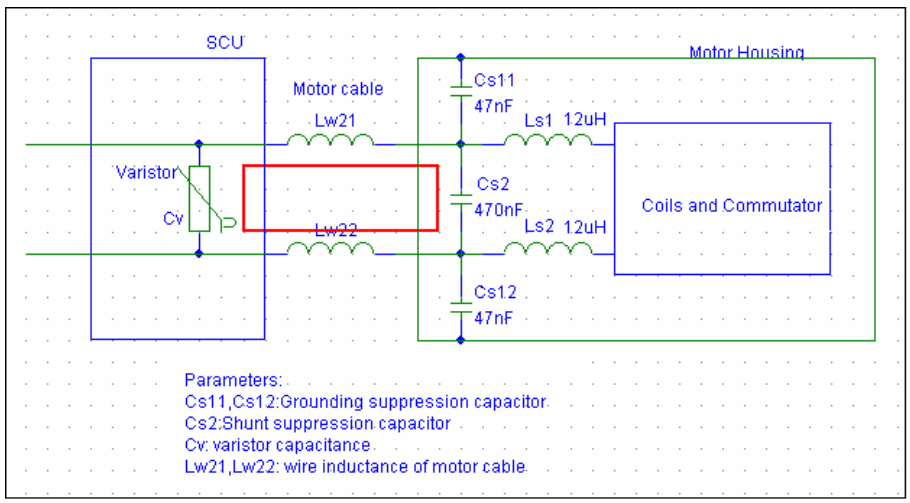


**Figure 7-10: Mechanism of resonance mode in motor cable**

The resonant peak can be calculated by this equation:

$$f = \frac{1}{2\pi\sqrt{LC}} \tag{7.1}$$

Here, $L=L_{w21}+L_{w22}$, $C= C_V \cap (C_{S2}+(C_{S11} \cap C_{S12}))$, operator $\cap$ represents: $A \cap B = \frac{A \times B}{A + B}$

We propose the value of these parasitic parameters for an estimation of resonance frequency:

$L_{w21}$=$L_{w21}$=0.06μH, $C_V$=2500pF.

The resonance peak should appear at 9.1MHz. It is consistent with the measurement result shown in Figure 7-5 (b). Slight difference in frequency is caused by the influence of current probe, which is explained in 3.2.2.

Although DM noise at motor cable does not make trouble alone, but DCM current which is converted from this DM current has significant effect. The conversion mechanism is shown at Figure 7-11 and 7-12.

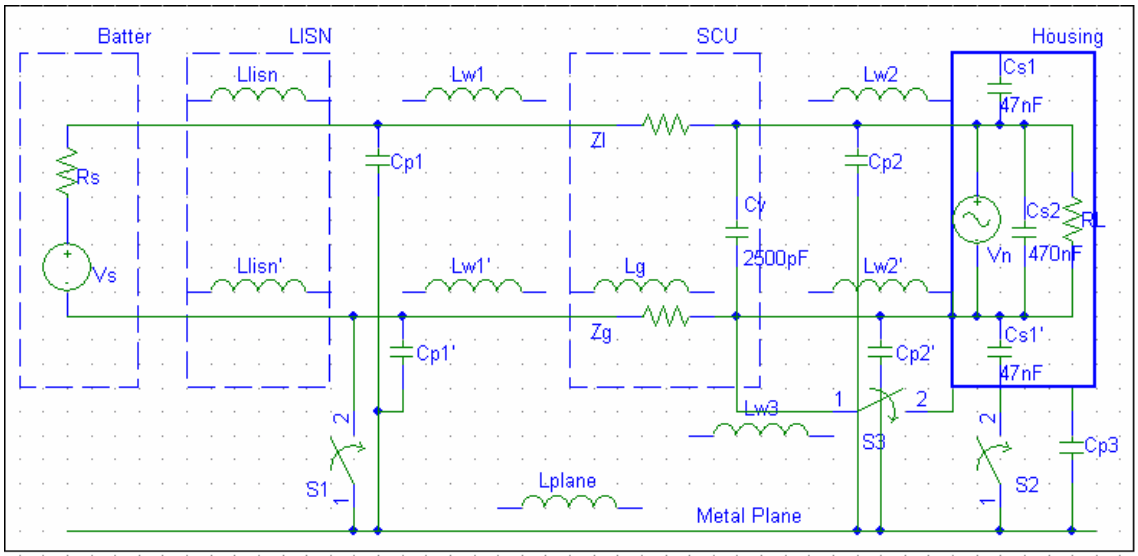


**Figure 7-11: Two Unbalance Wires carrying DM currents drive CM current**

In most situations, the biggest part of reference - car body will be placed nearby to the sunroof system. Therefore two wires of motor cable are unbalanced to reference. A voltage difference will drive a CM current.

When the motor housing is isolated to the reference. Although unbalance exists, there is a very weak CM current loop generated. The radiation is the smallest.

When motor housing is connected to reference, $C_{p2}$ is parallel to the suppression capacitor. The unbalance between $C_{p11}$ and $C_{p12}$ leads CM loop current; it passes through suppression capacitor and reference. The resonance frequency is around 9 MHz.

When both motor housing and battery negative pole are connected to reference, $C_{p11}$ is shortened. In this situation, the unbalance issue is most severe, and the low impedance in the CM current loop aggravates this situation. A lump in 9MHz will appear at radiated emission with highest level in all these wiring configurations.

Even without considering the difference between two suppression capacitors, the slightly different cable lead impedance and track impedance in PCB will result in CM current. Two suppression capacitors with different values aggravate the situation. This mechanism is quite similar to the former one.

The resonance mode in DM current is always there with a certain level, but with a particular wiring configuration or layout, CM current will be produced effectively. The

conversion efficiency is also related with the frequency. Conversion ratio above 3MHz is obviously higher than in low frequency.
However, the amplitude of resonance is decided by unbalance level which is difficult to be measured. It is defined in [4] and measured with LCL (Longitudinal Conversion Loss) which has a range up to of 40dB. It makes the prediction of CM current radiated emission level can only start with conducted measurement.

## 7.3 Conclusion

Transient of PWM signal causes two main noise sources because of its sharp increasing edge. To reduce the influence of these two noise source, the diode current and the DM current in motor cable, the below EMC design guides are concluded from this chapter,

1. The area embraced by high *di/dt* loops must be as small as possible. By decreasing the loop area to 1/10, the emission level will reduce 20dB more.
2. If possible, use 70 kHz as working frequency, because first and second harmonic components are below the lowest frequency required by CISPR-25.
3. If possible, modulate the switch frequency in 100Hz as [28] described. It will flat the EMI spectrum.
4. If the above provision cannot be satisfied, twisting the track in PCB is another solution by introducing mutual cancellation of the fluxes. It is shown in Figure 7-12.

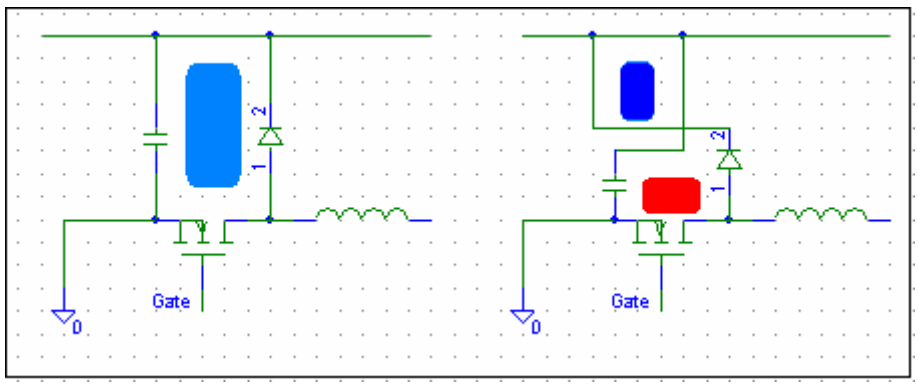


**Figure 7-12: A proposed noise reduction method by twisting tracks**

5. Using a metallised plastic SCU case will definitely reduce the EMI level below 2MHz, but it is costly.
6. To suppress radiated emission above 2MHz, the first technique is isolating the motor housing to the car body. If we use an insulated cover or plastic screw, the capacitance between motor housing and car body should be kept below 5pF. If this condition is satisfied, CM current emission is negligible.
7. If the above provision cannot be satisfied, make balance wires by twisting them.
8. If CM currents has been produced, but we can restrict them in a small area by adding a “third wire” between motor housing and SCU ground, keeping the wire

short and running along the other two wires. This proposal is most efficient when motor housing and battery negative pole are connected to car body.

9. The next provision is shifting resonance peaks out of important band. By reducing the wire length between motor and SCU or using the varistor with small capacitance or replacing varistor with diodes, the resonant frequency at motor cable will be extremely high or even will disappear.

# Chapter 8

# Comparison measurement and synthesis

We have done many measurements to validate our model as prior chapters described. In this chapter, we will do comparison measurement for EMI synthesis. We will describe the measurement equipment we used. We give setup and procedure of these measurements. We do many comparisons between measurement results. By this way, we confirm the influence of designable parameters.

## 8.1 Measurement Equipment

We arrange all the EUT (Equipment Under Test) on a table with a height of 80-90cm. The table is covered with a metal plane shown in Figure 8-1. The metal plane is introduced to include the influence of car body. This EUT is a real product.

**Figure 8-1: Layout of measurement**

We use current probe to measure the DM current. The voltage output of the current probe is connected to a spectrum analyzer (ADVANTEST R3131) or to an oscilloscope (YOKOGAWA DL1540). To monitor weak signals, a pre-amplifier (KALMUS 737LC) is used to amplify weak voltage signal. This amplifier owns a constant gain of 44dB up to 1GHz.

Because the calibration of current probe is normally done with a 50Ω terminator, if the output of current probe is connected to high impedance input port of oscilloscope, a 50Ω resistor and BNC-T connector are used to make measurement results reliable. The

BNC-T connector is not good for high frequency measurement but it is valid here because our interesting frequency range is 150kHz to 30MHz A self made LISN is inserted between the battery and SCU to make impedance stable, with its schematic diagram shown at Figure 8-2.

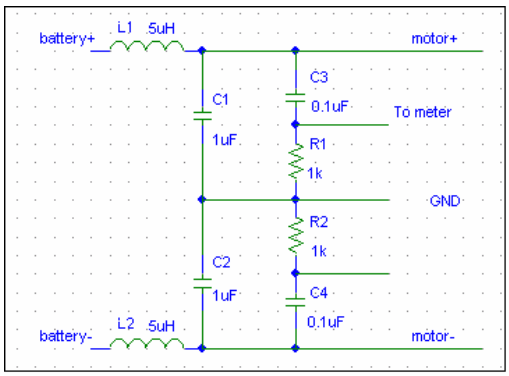


**Figure 8-2: Schematic of LISN**

To measure CM current, two wires must be put through current probe in one direction. On the contrary, to measure DM current, two wires should be put through current probe with opposite direction.

Each current probe has a characteristic curve representing the relationship between output voltage and the current under measuring, they are related with

$$Z_T = \frac{V}{I} \tag{10.1}$$

The Figure 8-3 shows a calibrated impedance curve of the current probe used in our measurement.

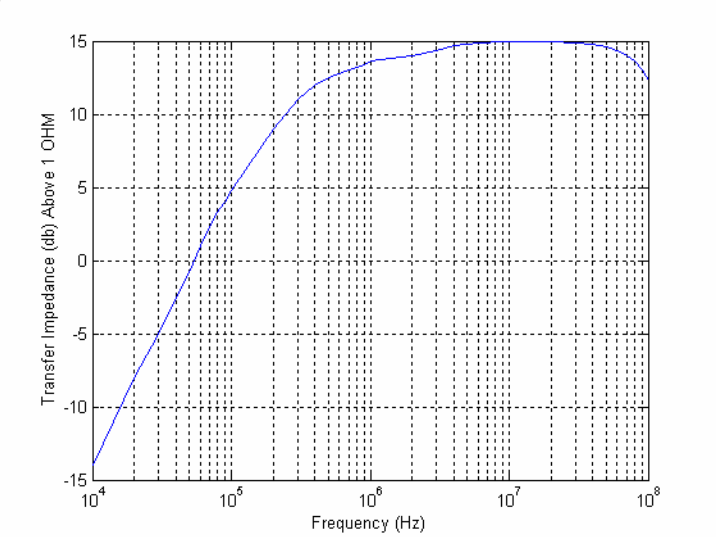


**Figure 8-3: Current probe transfer impedance**

In most case, this is given in dB as,

$$Z_{T\,dB\Omega} = V_{dB\mu V} - I_{dB\mu A} \tag{10.2}$$

With this calibration curve and measurement result of voltage, we know the current as,

$$I_{CM\ dB\mu A} = V_{dB\mu V} - Z_{TdB\Omega} \tag{10.3}$$

Some interference introduced by the instruments themselves needs to be mentioned here. We found that a monitor of oscilloscope causes a 324 kHz pulse, and a spectrum analyzer produces a narrowband noise around 20MHz.

In radiation measurement, the employed receiver is ESI 40 manufactured by Rohde & Schwarz, and the antenna model is SAS-2/A, which is an extremely broadband E-field receiving antenna made by ARA.

## 8.2 Measurement Setup

We use existed validation test setup proposed by [22], [23] and [24] for our comparison measurement. It is shown at figure 8-4.

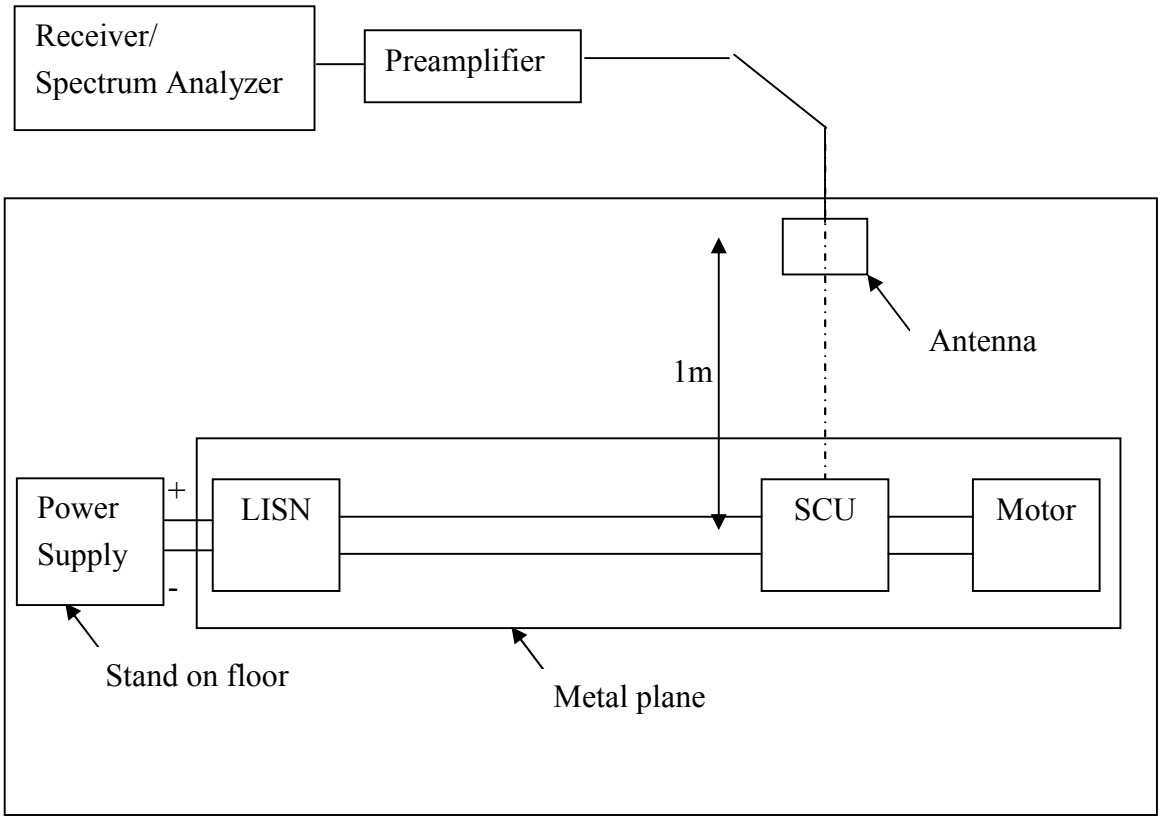


**Figure 8-4: Measurement setup**

This configuration is quite similar to a measurement setup proposed by CISPR-25, which is illustrated in Figure 8-5.

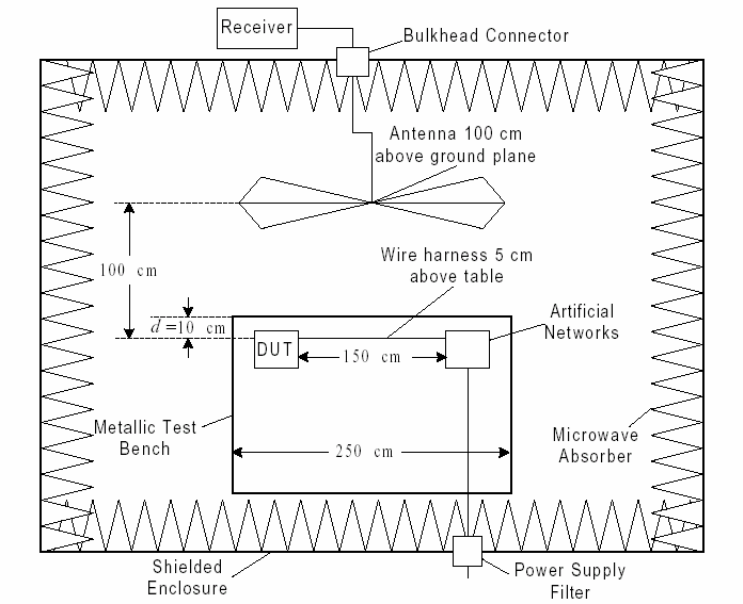


**Figure 8-5: Diagram of CISPR-25 radiated emission module testing setup**

During the measurement, the motor is operating in PWM or always-on state.

For the wire length and layout the cable, configuration follows this way without being specified:

- motor cable length: 0.06m
- motor cable height above metal plane: 0.05m
- battery-SCU cable length: 1m

Three more situations are tested. One is placing the motor cable on the surface of metal plane. Another is reducing the length of battery-SCU cable to 0.1m. The third is increasing the length of motor cable to 0.66m.

The next test variable is wiring configuration. By varying the connection between battery negative pole and metal plane, the connection between motor housing and metal plane and proposed "third wire" between SCU ground and motor housing, we have eight configurations. We name them from setup1 to setup8 as Table 8-1 lists.

**Table 8-1: Connections in different wiring configurations**

| | Connection | | | | | |
|---|---|---|---|---|---|---|
| | Battery Negative-Metal plane | | Motor housing-Metal plane | | Third Wire SCU ground-motor | |
| Setup | open | short | open | short | open | short |
| Setup1 | × | | × | | × | |
| Setup2 | × | | | × | × | |
| Setup3 | | × | × | | × | |
| Setup4 | | × | | × | × | |
| Setup5 | × | | × | | | × |
| Setup6 | × | | | × | | × |
| Setup7 | | × | × | | | × |
| Setup8 | | × | | × | | × |

In fact, wiring configuration is a key factor in our study, because it is the cheapest solution without additional components.
We also show these configurations via Figure 8-6.

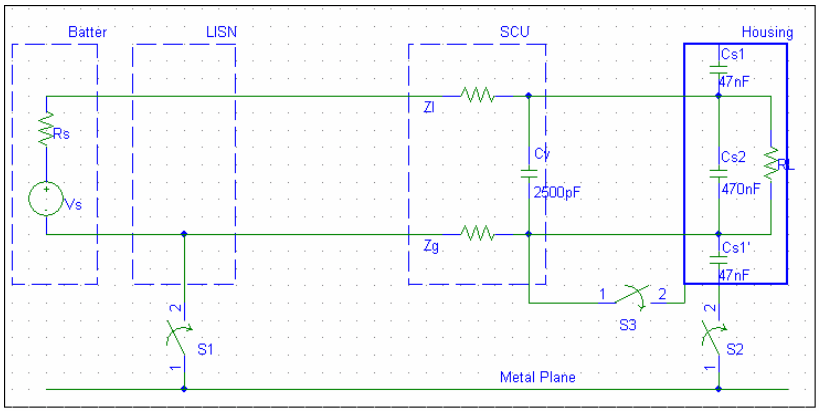


**Figure 8-6: Motor and SCU in different wiring configurations**

Here, the status of $S_1$, $S_2$ and $S3$ corresponds to three connections in Table 8-1.
Setup1 is an ideal situation. This configuration may only happen for a test. In this situation, common mode currents are only formed via capacitive coupling.
Setup 2 has commonly happened in a validation test, because the motor is installed in a metal sunroof structure, and the battery is kept standing on the floor. By knowing what influence a test setup will bring, we can leave more margins to limitation.
Setup 3 is more commonly in automotive. Because the correct function of a starter is a principal consideration in automotive electric system, the current return path for this device must exhibit low DC resistance from battery negative to the starter motor ground (in most case, the engine block) to ensure the best connection. In a practical wiring, the battery negative pole is connected to the car body. The SCU and sunroof motor are normally installed in the ceiling, it makes uncertain for the grounding of SCU and the motor, in setup 3, it is a situation SCU and the motor are isolated to the car body, they are installed via plastic screws or isolated rings.
Setup 4 is another possibility; in this configuration, the motor is fixed firmly in the sunroof structure, which is a metal part installed to the car body. By this way, the motor housing is grounded.
Setup5 to setup8 are proposed in this project, by adding a third wire between SCU and the motor; this wire is running along other two wires and made as short as possible; this configuration is the same as grounding the motor housing and SCU but with smaller CM “noise” current loop.
The last test variable is shield plan. We shield particular parts by wrapping it in aluminum foil, this foil is connected to metal plane and via the screen of a measurement cable to the wall of the EMC measurement chamber. We set three configurations below.

- Without shield at all.
- With motor and motor cable shielded.
- With SCU shielded.

We call these shield plans as shield 1, shield 2 and shield 3 respectively.

## 8.3 Measurement Procedures

The Table 8-2 below shows the configuration of each measurement. Four shadowed traces are proposed but not available due to time limitation.

**Table 8-2: Measurement configurations**

| | Cable length | | Cable length | | Cable height | | Connection | | | | | | Motor working state | | shield plan |
|---|---|---|---|---|---|---|---|---|---|---|---|---|---|---|---|
| | SCU-motor | | LISN-SCU | | LISN-SCU | | LISN-metal panel | | Motor-metal panel | | Third Wire SCU-motor | | | | |
| Trace | 0.06m | 0.66m | 1.0m | 0.10m | normal | surface | open | short | open | short | open | short | ON | PWM 50% | |
| trace01 | X | | X | | X | | X | | X | | X | | X | | 1 |
| trace02 | X | | X | | X | | X | | | X | X | | X | | 1 |
| trace03 | X | | X | | X | | | X | | X | X | | X | | 1 |
| trace04 | X | | X | | X | | X | | X | | X | | | X | 1 |
| trace05 | X | | X | | X | | X | | | X | X | | | X | 1 |
| trace06 | X | | X | | X | | | X | | X | X | | | X | 1 |
| trace11 | X | | X | | | X | X | | | X | X | | | X | 1 |
| trace12 | X | | X | | X | | X | | X | | | X | | X | 1 |
| trace13 | X | | X | | X | | X | | | X | | X | | X | 1 |
| trace14 | X | | X | | X | | | X | | X | | X | | X | 1 |
| trace15 | X | | X | | | X | X | | | X | | X | | X | 1 |
| trace21 | X | | X | | X | | X | | X | | X | | | X | 2 |
| trace22 | X | | X | | X | | X | | | X | X | | | X | 2 |
| trace23 | X | | X | | X | | | X | | X | X | | | X | 2 |
| trace24 | X | | X | | X | | X | | X | | X | | | X | 3 |
| trace25 | X | | X | | X | | X | | | X | X | | | X | 3 |
| trace26 | X | | X | | X | | | X | | X | X | | | X | 3 |
| trace27 | | X | X | | X | | | X | | X | X | | | X | 1 |
| trace28 | X | | | X | X | | X | | | X | X | | | X | 1 |
| trace31 | X | | X | | X | | | X | X | | X | | | X | 1 |
| trace32 | X | | X | | X | | | X | X | | X | | | X | 1 |
| trace33 | X | | X | | X | | | X | X | | | X | | X | 1 |
| trace34 | X | | X | | X | | | X | X | | | X | | X | 1 |

Because of the limitation of measurement equipment, the radiated emission measurements have been performed by Thales Nederlands B.V. Environment Competence Center.

In order to achieve these goals, the radiated emission is measured in the range from 150kHz to 100MHz, and in vertical and horizontal polarization. Measurement bandwidth is set to 9kHz.

To easily recall setup, we use pictograms next to measurement result to present wiring configuration and shield plan. Three green blocks represent battery, SCU and motor from left to right, and the black wire below blocks represents metal plane in measurement setup.

## 8.4 Radiated Emission Measurement Results

### 8.4.1 Measure with different polarity

The first comparison is done with different polarity. In the setup of the measurement, the antenna is placed perpendicular to the cable of the motor, which is the worst situation. Two measurements are done with vertical polarity and horizontal polarity. We draw the results into Figure 8-7.

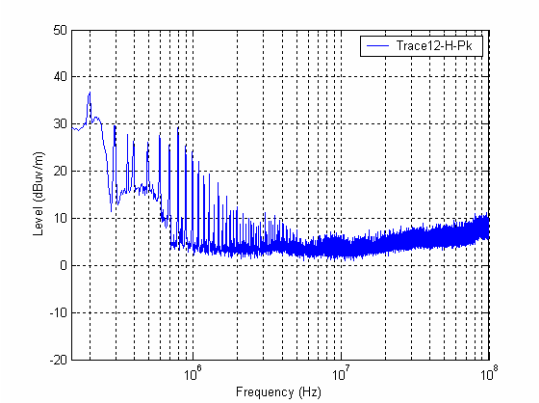


(a) Horizontal polarization result

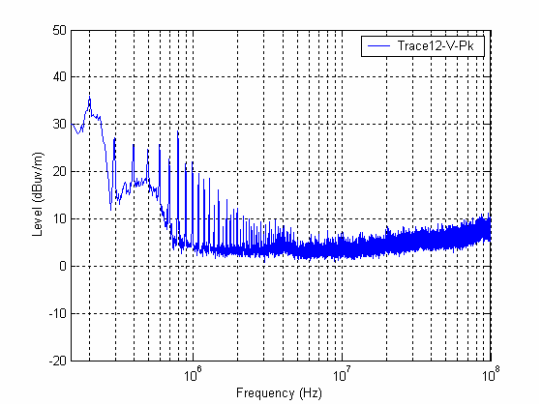


(b) Vertical polarization result

**Figure 8-7: Comparison between horizontal and vertical polarization measurement results when motor running in PWM and wiring configuration is setup5**

By comparing, the difference is less than 3dB. Therefore, we will only use vertical measurement results for comparison and synthesis, which makes no difference.

### 8.4.2 Comparison between different running modes of motor

This comparison is between the electric fields from a motor running in always-on mode and from a motor running in PWM mode.

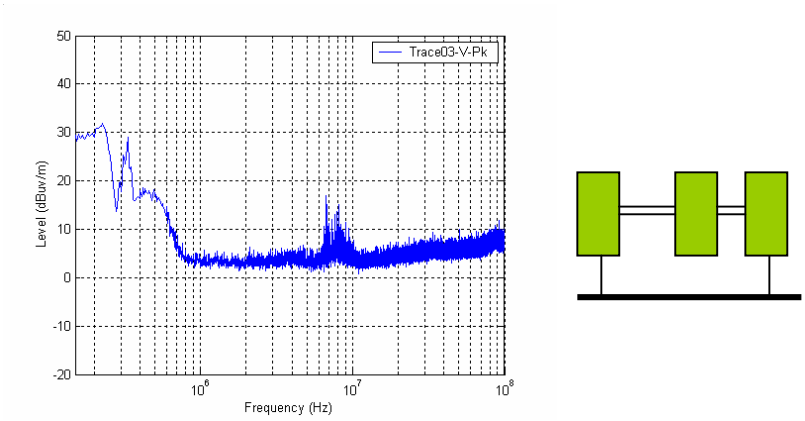


(a) Motor running in always-on mode

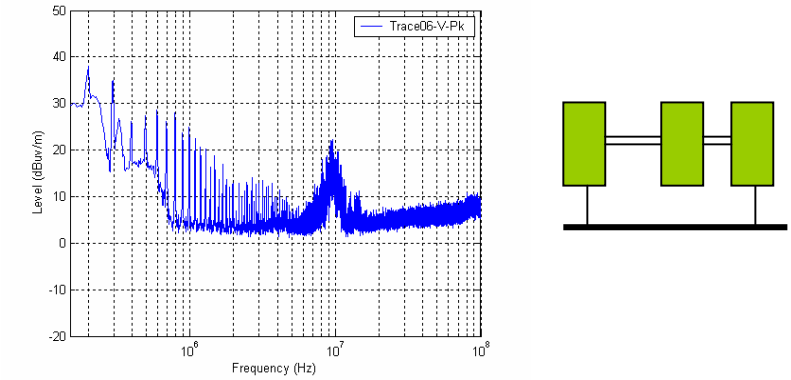


(b) Motor running in PWM mode

**Figure 8-8: Comparison of measurement results when motor is running in always-on mode and in PWM mode, while wiring configuration is setup4**

In this case, we can clearly see that the motor running in PWM mode radiates more than running in always-on mode and accompanied by distinguished peaks. By removing these peaks, there is no significant difference between the field intensities. This is consistent with the theory that two signals not relevant can be superposed. It is obvious that the motor running in PWM mode emits broadband noise from the motor commutation and narrow band noise from the PWM signal. The narrow band noise is at least 25dB above broadband noise.

A lump is observed around 9MHz in both modes, and this lump increases 7dB when motor is running in PWM mode. This is consistent with conclusion in Section 7.2 that transient of PWM signal aggravates the ripple in motor cable, and brings the EMI level higher.

In this comparison, we also find that the centre frequency of this lump is fixed. This measurement result confirms the mechanism of this noise, that it is converted from the DM noise in motor cable as Section 7.2 supposed.

### 8.4.3 Comparison between different wiring configurations

This comparison is the radiated emission between different wiring configurations.

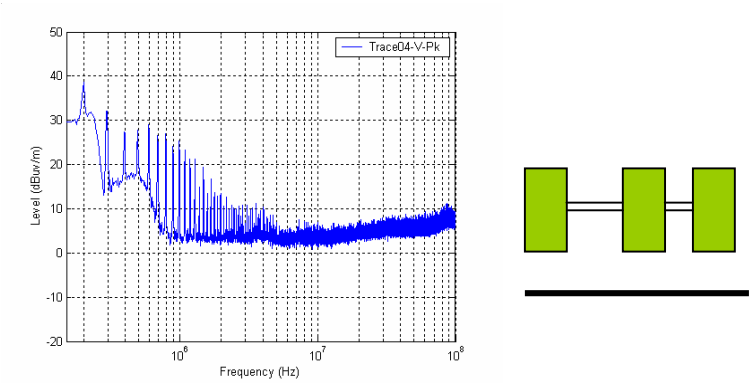


(a) Wiring configuration is setup1

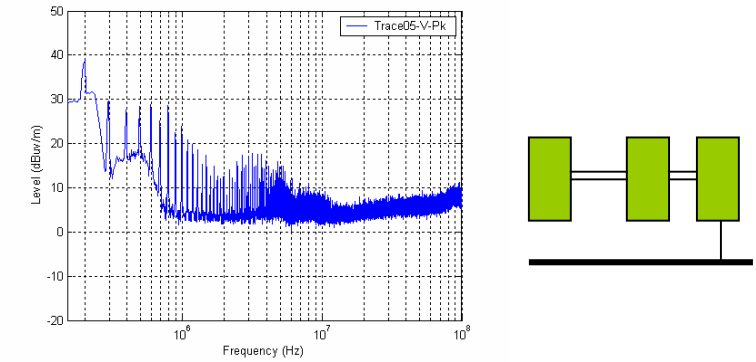


(b) Wiring configuration is setup2

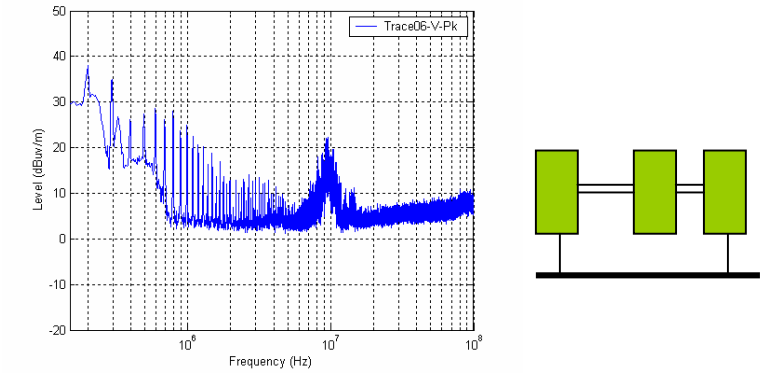


(c) Wiring configuration is setup4

**Figure 8-9: Comparison of radiated emission with different wiring configurations when motor is running in PWM mode**

In this comparison we can see that the difference between fields below 2MHz are negligible. One lump is found in setup1 around 9MHz, and setup2 comes out two lumps around 5MHz and 9MHz, while setup4 is accompanied by two lumps in 350kHz and 9MHz.

The lump of 9MHz fixes in frequency but varies in level, with setup2 its level is 4dB higher than with setup1, and with setup4 is about 15dB above which found in setup1.
The measurement result is consistent to analysis result in Section 7.2, the resonance mode in DM current is always there with a certain level, but with a particular wiring configuration or layout, CM current will be produced effectively.
The mechanism of lump of 5MHz is explained in Section 5.4. As predicted, this lump appears with setup2 and disappears with setup1 and setup3.
The peak in 350kHz is predicted at Section 5.4, which proves the model. With same mechanism, peak appears at 800kHz as Figure 8-10 shows. The resonant mode in 800kHz is excited by PWM signal and it lifts the level about 10dB higher.

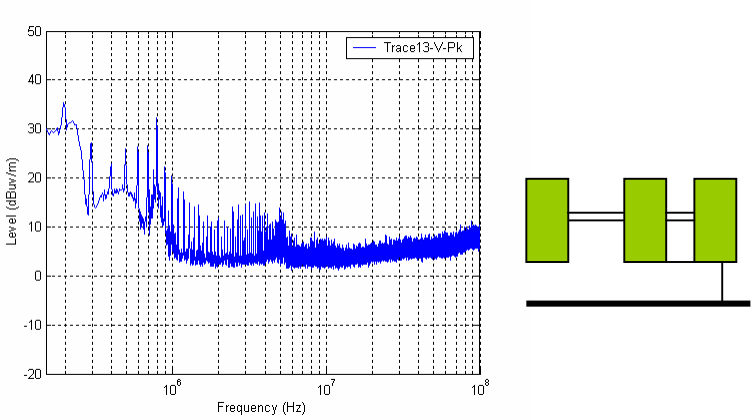


**Figure 8-10: Radiation measurement result with setup7**

## 8.4.4 Comparison of the effect of "third wire" for different wiring configurations

To see the improvement of the third wire, the following comparison, were made.

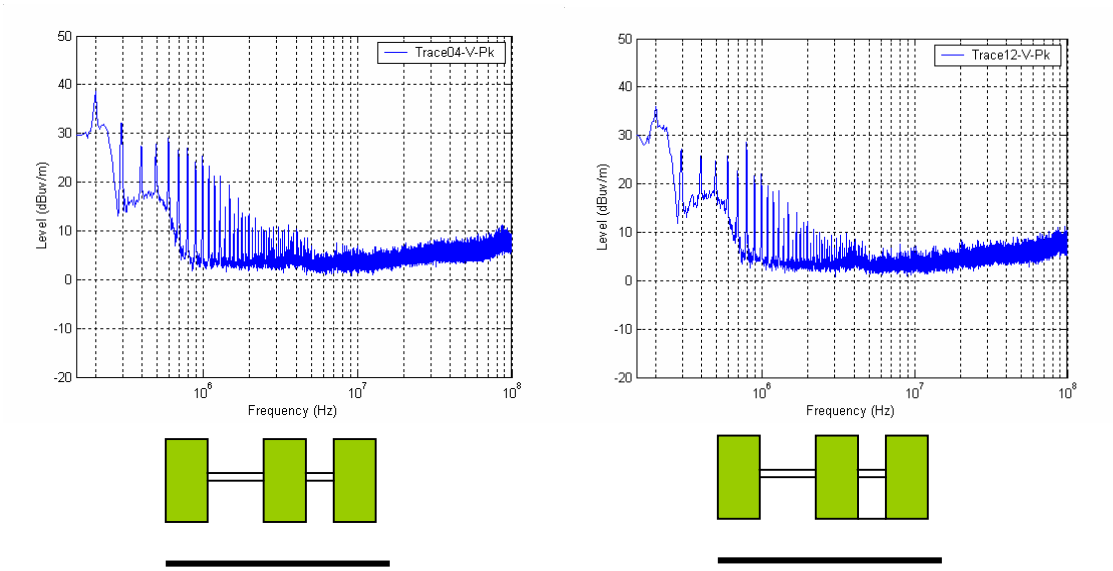


(a) setup1 (b) setup5

**Figure 8-11: Comparison between setup1 and setup5**

For setup1, the third wire does not make an obvious difference. This is due to the fact that CM current is blocked in setup1.

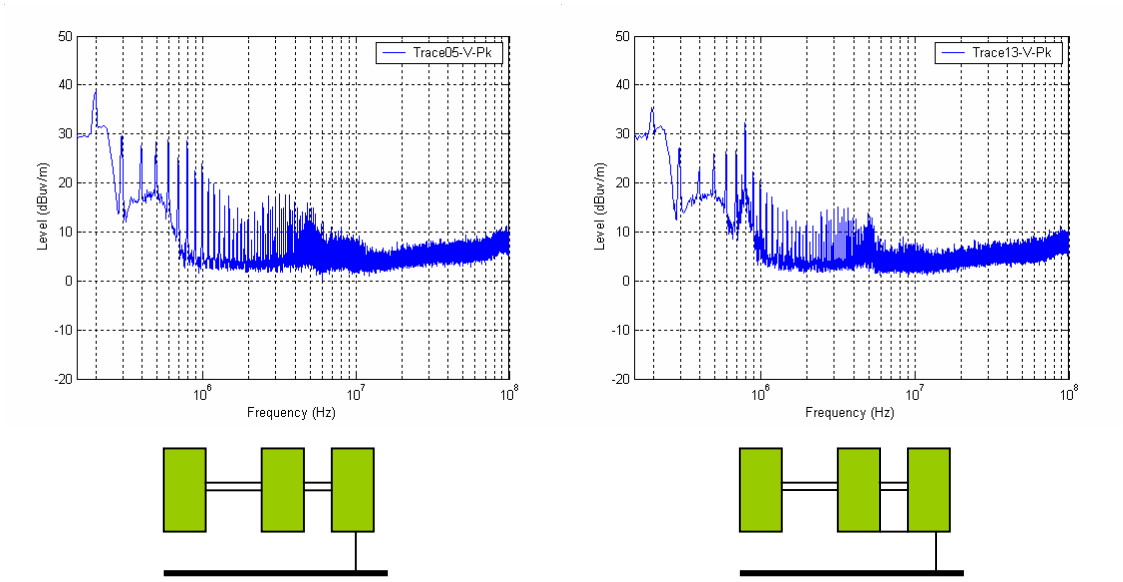


(a) setup2 (b) setup6

**Figure 8-12: Comparison between setup2 and setup6**

This comparison shows that for setup2, the third wire has 2dB suppression for a lump around 9MHz. The difference is clearer than the former one but the third wire produces another lump appearing in 800MHz and excited by PWM signal to 32dBμV/m.

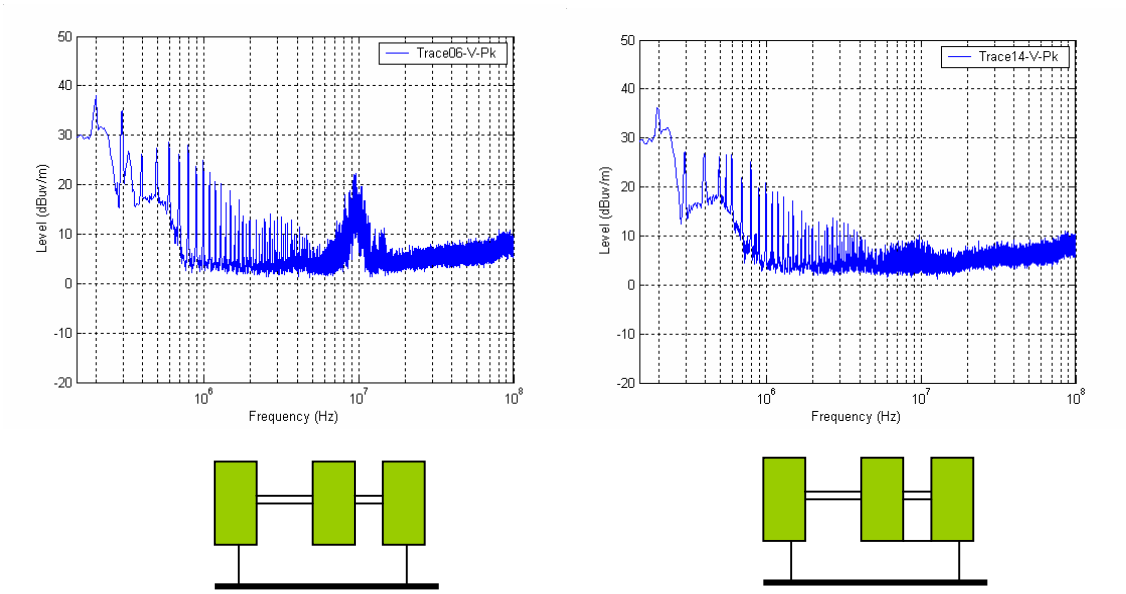


(a) setup4 (b) setup8

**Figure 8-13: Comparison between setup4 and setup8**

With the third wire added into setup4, the two lumps around 9MHz and 340kHz are effectively suppressed. The former one decayed almost 12dB, and the latter one is

totally disappear. The third wire is goal-directed in this situation. This experiment proves the discussion in Section 7.2

### 8.4.5 Comparison of the effect of shielding for different wiring configurations

By comparisons of radiated emission are done with and without SCU shielded, we confirm the location of the noise sources.

We find from Figure 8-14, by shielding SCU, the radiation emission from 150kHz to 2M is drastically suppressed at least 10dB. This comparison proves that the DM current inside SCU is the main source of EMI in low frequency.

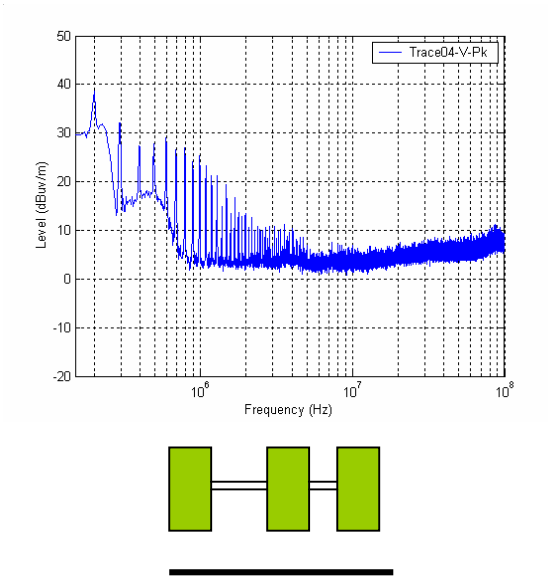


(a) setup1 without SCU shielded

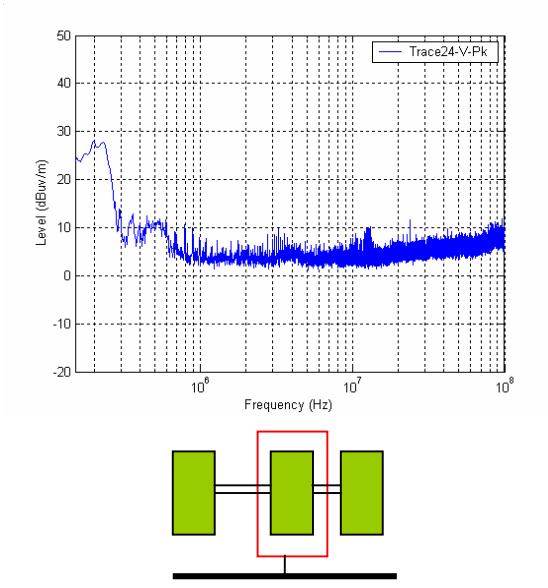


(b) setup1 with SCU shielded

**Figure 8-14: Comparison between with and without SCU shielded for setup1**

From Figure 8-15, we find distinguishing peaks are left with a low level if the wiring configuration is setup2. The reason is part DM current is converted into CM current flowing through metal plane. Therefore, the radiation produced by converted CM current is not shielded. This experiment confirms the mechanism CM current which is converted from DM current produce EMI.

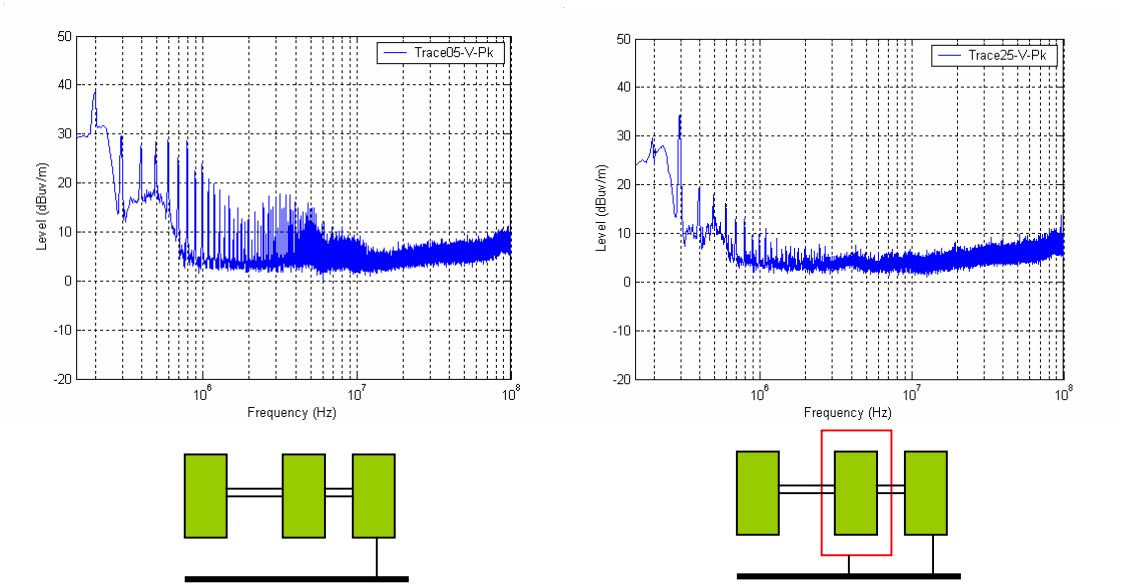


(a) setup2 without SCU shielded (b) setup2 with SCU shielded

**Figure 8-15: Comparison between with and without SCU shielded for setup2**

The fact that spectrum above 2MHz changes significantly may be caused by a casual contact between the shield foil and the motor housing which acts as third wire.

## 8.5 Synthesis

We have built circuit models for each element in SCU system respectively, but EMC study still needs focus on their relation, that is, which factor is designable, what progress can be made by tuning these parameters.

We treat transient as the root for everything. In an aspect of physics, transient in the electric world is the acceleration of electrons. The stable state will produce no EMI. In this project, four transient exists, that is, the opening and closure of a switch, bouncing of relay, switching of MOSFET by PWM signal and motor commutation.

A lot of models are built to illustrate how these transient generates noises. The level of a functional signal is first predicted, by annotation of the parasitic parameter, functional signal will convert to an unintentional signal, but this conversion is bi-direction, in some situations, unintentional signal will enforce functional signal conversely.

When the amount of conducted emission is predicted, radiation models are applied to predict radiation level. As a consequence, the radiated noise can couple with the circuit conductors, thus becoming conducted noise again.

In fact, all these conversions are equilibrium under stable status. Most times forward conversion dominates back conversion.

We classified the noise sources because designable parameters influent their contribution to EMI differently. Upon the former discussion, we built a routine to identify the catalogue of noise as Figure 8-16 shows.

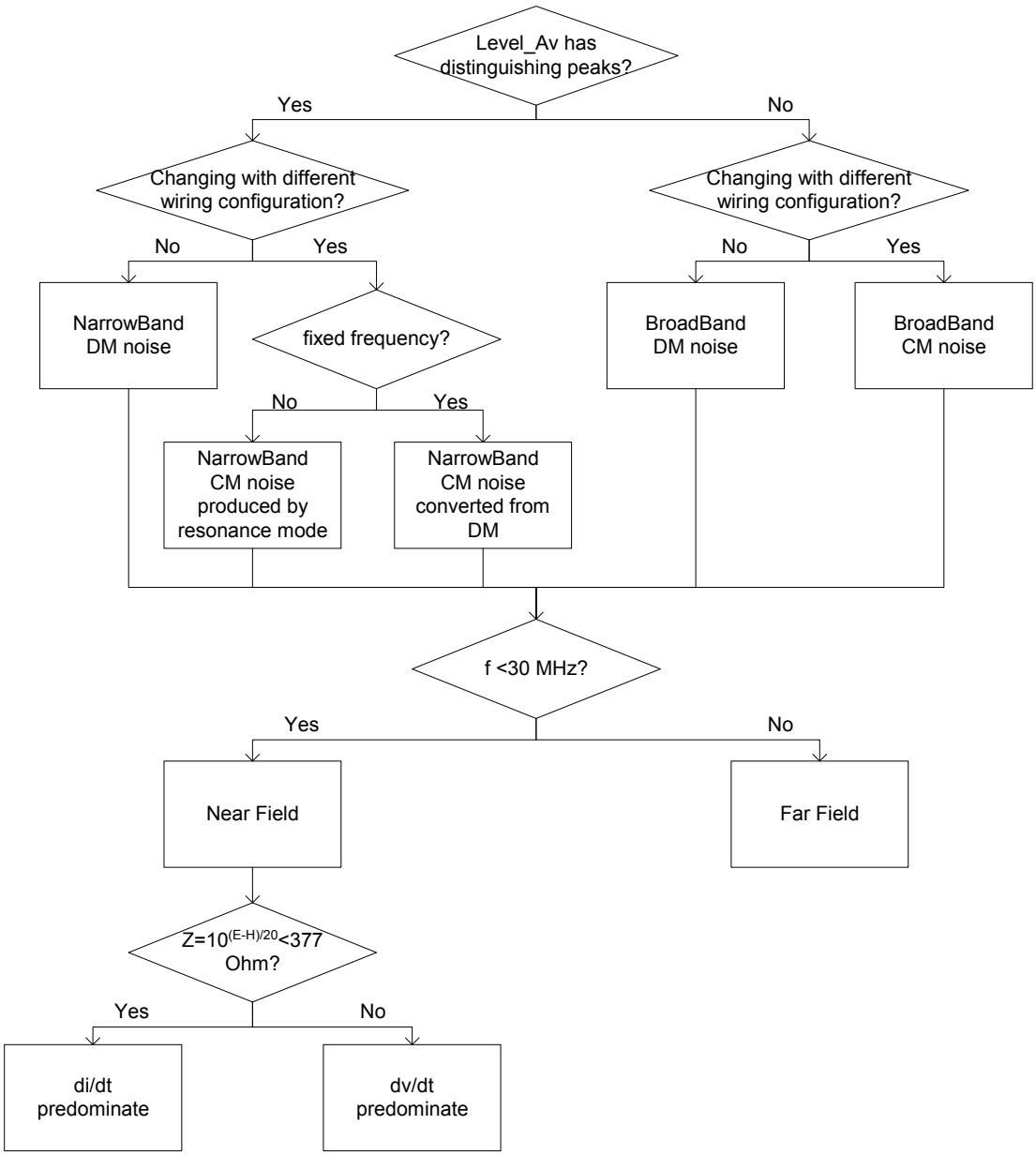


**Figure 8-16: Routine to identify characteristic of noise**

The simulation tool PSPICE appears as a good tool to use for tracing resonance mode. We use routine to classify resonance modes which we found. By synthesis, we find that transient noises caused by relay bouncing and running noise caused by PWM commutation have same mechanism. They are concluded in Appendix B. The only difference is transient noise has higher level due to larger current variation. This phenomenon proves that topology decides resonant mode, and transition provides excite source.

To propose an optimised configuration, we start with selecting the designable parameters which produce trouble and benefit simultaneously. That is why the wiring configuration is first parameter for our decision. Another reason is wiring configuration is most applicable because it is cost-efficiently solution.

Commutation noise is most beyond our control, because it is determined by motor parameter, for instance, geometry of winding, material, etc. Suppression circuit can suppress commutation noise but bring excessive components. By good connection at motor housing to car body and battery negative pole to car body, this noise can be effectively suppressed.

Commutation noise and PWM ripple cause the DM current in motor cable accompanies with a rapid varying current. It makes a resonance mode which determined by motor cable inductance. This DM current will convert to CM in surrounding as Section 7.2 described. For the proposed wiring configuration, the level is lifted about 7dB. But it is controllable, because the influence of this noise source can be suppressed by adding "third wire" or even be eliminated by a shorter motor cable or small capacitance varistor.

The transient noise caused when motor is switch off is hard to be reduced except by making motor cable shorter and making current variation change smoothly.

In a word, good connection at both sides and keep motor cable short is optimised configuration.

The secondary optimised configuration is isolating motor housing to car body. With this wiring configuration, transient noises which are built via car body disappear. The disadvantage this configuration brings is commutation noise is hard to be suppressed. Making battery-SCU cable shorter is a solution, but it is not realistic.

# Chapter 9

# Conclusions

This thesis deals with individual models for sunroof products in the frequency range of 150kHz to 100MHz. The work starts with parasitic parameters extraction using “back-annotation” method. Using the model we established, we present many discussions about what influence will make via the variation of parameters. We do transient analysis and running analysis respectively. We also use measurements result from an authorized test center to prove our hypothesis. The mechanisms of noise sources are clarified.

The objective of this report is to propose an optimized configuration for all the designable parameters. The reason why we use the word “optimized” instead of “best” is some designable parameters produce troubles and benefits simultaneously.

The wiring configuration is first parameter for our choice. The reason is that it has dominant influence to CM current which becomes main noise source above 2MHz, and wiring configuration is most applicable for price factor. The connection from car body to motor housing and the connection from car body to battery negative pole provide four wiring configurations. Synthesis shows that good connection at both sides is optimised selection. The commutation noise has least influence for this configuration. The CM noise converted from DM current in motor cable can be suppressed by adding “third wire” or even be eliminated by a shorter motor cable or small capacitance varistor. The transient noise caused when motor is switch off is hard to be reduced except by making motor cable shorter and making current variation change smoothly.

In a word, good connection at both sides and keep motor cable short is optimised configuration.

The secondary optimised configuration is isolating motor housing to car body. The reason is given at Section 8.5.

Besides that, some more designable parameters are available for reducing EMI further. We list them below because they has benefit and no disadvantage.

1. Topology in SCU plays a crucial role in the EMI performance. To suppress its influence, we can make the area embraced by hight di/dt smaller and current variation smoother. Section 7.3 describes the detail.

2. Removing switch input capacitor eliminates noise caused by switch as Section 4.4 described.
3. Make the grounding suppression capacitance and shunt suppression capacitance as large as possible or plan another form of suppression circuit as Section 4.3 concludes.
4. To avoid resonant modes falling in radio band, we can solve it by shifting the resonant frequency, which can be estimated by the procedure shown in appendix B.

# Appendix A

# Radiated emission measurement results

This appendix summarizes in short form the effects of most designable parameters, which include the wiring configuration, wire length, shield configuration, etc. We use a SCU product named P174, a 12-volt DC motor, a battery and a metal plane to do these radiated emission measurements. Metal plane is employed to evaluate the influence of car body in real life.
Full text will be furnished on request.

# Appendix B

# Potential noise sources list

This appendix summarizes in short form the potential noise sources of sunroof system. We present the mechanism of noise sources firstly with diagrams. We give some examples to illustrate how to predict resonance frequency or level. These examples are correspondent to real configurations. The component values in examples are from estimation or measurement. Part prediction results are validated. We also give some introduction of the influence of designable parameters. We use two SCU products named P138 and P174, a 12-volt DC motor, a battery and a metal plane to do these analyses.

Full text will be furnished on request.

# Acknowledge

First of all, I want to thank Prof. Frank Leferink for being my supervisor and the opportunity I got to do my master thesis at NEDAP. His vast experience, instruction, arrangement for measurement have been an invaluable resource to me. Besides, I would like to thank Prof. W.C. van Etten for his supervision and comments on this project.
I would like to express my deep appreciation and gratitude to my research supervisor Jos van Duijn for his constant encouragement and guidance during the course of this research and discussions on my research work. He gave me valuable suggestions on numerous occasions.
I am grateful to Fons Sogtoen and Arthur Oosterveen in THALES ECC for doing EMC measurements.
I am so indebted to all colleagues at NEDAP as well as the Telecommunication engineering group, without mentioning names, for the period we have spent together.
And I would like to express my sincere appreciation to Jan van Breemen and Edith Klinkhamer, for their kind help, correcting spelling errors for me, and so on.
No words can express my feelings towards my parents who have devoted almost everything to support my education, and to encourage and help me in every possible way they can.
Finally my thanks go to my wife Ran Yang. This project started almost simultaneously with the birth of our son, Chengji Riemer Zhao. Fortunately, both of them are growing well. I would like to thank her for her patience, understanding, encouragement during the last, but very important phase of research and thesis writing.

# References


[1] Paul Horowitz, Winfield Hill, "*The art of electronics*," second edition, Cambridge University Press, 1989

[2] Simon R. Saunders, "*Antennas and propagation for wireless communication systems*", John Wiley & Sons Ltd, 1999

[3] C.R.Paul, "*Introduction to Electromagnetic Compatibility*", Wiley, 1992

[4] ITU-T Recommendation G.117, "*Transmission Aspects of Unbalance About Earth (Definitions and Methods)*", 1988

[5] Bernhard E. Keiser, "*Principles of electromagnetic compatibility*", 3rd edition, Artech House, 1987

[6] Erkuan Zhong, Thomas A. Lipo, "Imptovements in EMC Performance of Inverter-Fed Motor Drives", *IEEE Transactions on Industry applications*, Vol. 31 No. 6, Nov/Dec 1995, pp.1247-1256

[7] C.Y Won, Y.C Kim, J.H Lee, J.J Ahn, "The Prediction of Conducted EMI in PWM Motor Drive System", *14th International Symposium on EMC*, Zurich, Switzerland, 2001

[8] D.Y.Lee, J.H.Lee, S.H.Min and B.H.Cho, "Exact Simulation of Conducted EMI in Switched Mode Power Supplies", IECEC, No.01-2598, 1999

[9] Kempski A., Smolenski R., Strzelecki R, "Common Mode Current Paths and Their Modeling in PWM Inverter Fed Drives", *IEEE 33rd PESC*, Cairns, Australia, 2002

[10] Leopoldo Rossetto, Giorgio Spiazzi, "Conducted EMI Issues in a 600-W Single-Phase Boost PFC Design", *IEEE Transactions on industry application*, VOL.36, No.2, March/April 2000

[11] Li Ran, Jon Clare, Keith John Bradley, and Christos Christopoulos, "Conducted Electromagnetic Emissions in induction Motor Drive Systems Part I: Time Domain Analysis and Identification of Dominant Modes," *IEEE Transactions on Power Electronics*, Vol. No. 4, July 1998, pp. 757-767

[12] Li Ran, Jon Clare, Keith John Bradley, and Christos Christopoulos, "Conducted Electromagnetic Emissions in induction Motor Drive Systems Part II: Frequency Domain Models," *IEEE Transactions on Power Electronics*, Vol. No. 4, July 1998, pp. 768-776

[13] C. R. Suriano, J. R. Suriano, G. Thiele, T. W. Holmes, "Prediction of Radiated Emissions From DC Motors," *IEEE - EMC Society, Symposia Records 1996 to 1999*, CD-ROM Database 1999

[14] G. Grandi, D. Casadei, A. Massarini, "High Frequency Lumped Parameter Model for AC Motor Windings," *European Conference on Power Electronics and Applications*, Trondheim, Norway, September 8-10, 1997

[15] G. Grandi, A. Massarini, U. Reggiani, G.Sancineto, "Laminated Iron-Core Inductor Model for Time-Domain Analysis," *4th IEEE International Conference on Power Electronics and Drive Systems, IEEE-PEDS'01 Conference*, Bali, Indonesia, October 22-25, 2001

[16] G. Skibinski, R. J. Kerkman, D. Schlegel, "EMI Emission of Modern PWM AC Drives", *IEEE Industry Applications Magazine*, November/December 1999, pp.47-79.

[17] G. Skibinski, J. Pankau, R. Sladky, and J. Campbell, "Generation, Control and Regulation of EMI from AC Drives*", IEEE Industry Application Society Conference*, New Orleans, LA, October 2-6, 1997, pp. 1571-1583.

[18] G. Grandi, U. Reggiani, D. Casadei, "Modelling, simulation and experimental analysis of conducted EMI for a switching cell", *Optimization of Electric and Electronic Equipment*, OPTIM '96, Brashov, Romania, May 15-17, 1996

[19] G. Grandi, D. Casadei, U. Reggiani, "Analysis of Common Mode and Differential Mode HF Current Components in PWM Inverter FED AC Motors," *IEEE PESC'98 Conference*, Fukuoka, Japan, May 17-22, 1998, pp. 1146-1151

[20] M. Nave, "Prediction of conducted emissions in switch mode power supplies," *IEEE - EMC Society, Symposia Records 1955 to 1995*, CD-ROM Database 1996

[21] G. Grandi, D. Casadei, U. Reggiani, "Equivalent Circuit of Mush Wound AC Windings for High Frequency Analysis", *IEEE International Symposium on Industrial Electronics*, ISIE, Guimaraes, Portugal, July 7-11, 1997

[22] GMW3097, "*General Specification for Electrical/Electronic Components and Subsystems; Electromagnetic Compatibility. Requirement Part*", GM Worldwide Engineering Standards

[23] GMW3100, "*General Specification for Electrical/Electronic Components and Subsystems; Electromagnetic Compatibility. Verification Part*", GM Worldwide Engineering Standards

[24] *Automotive Test Specification*, NEDAP

[25] W. L. Weeks, *Antenna Engineering*, McGraw-Hill Book Co., New York, 1968

[26] M. R. Feusse, "*Modeling Conducted Emission Transient due to DC Motor Switching in Automotive Application*", Master Thesis, Michigan State University, 2001

[27] P. A. Chatterton, M. A. Houlden, "*EMC Electromagnetic Theory to Practical Design*", Wiley, Chichester, England, 1992

[28] D. A. Stone, B. Chambers, and D. Howe, "*Erasing EMC problems in switching mode power converters by random modulation of the PWM carrier frequency*," in Proc. IEEE APEC'96, San Jose, CA, 1996, pp. 327-332.